OPTICS ALIGNMENT PANEL - FINAL REPORT

Daniel J. Schroeder
30 December 1991

ABSTRACT

The Optics Alignment Panel (OAP) was commissioned by the HST Science Working Group to determine the optimum alignment of the OTA optics. The general goal and plan for achieving this end is given in the "Charge to OAP", included as Attachment 1. In essence, our job was to find the position of the secondary mirror (SM) for which there is no coma or astigmatism in the camera images due to misaligned optics, either tilt or decenter. We also took on the task of reviewing the despace position of the SM and finding the optimum focus. The outcome of this effort is as follows: (1) the best estimate of the aligned position of the SM in the notation of HDOS is (DZ,DY,TZ,TY) = (+248 microns, +8 microns, +53 arcsec, -79 arcsec), (2) the best focus, defined to be that despace which maximizes the fractional energy at 486 nm in a 0.1 arcsec radius of a stellar image, is 12.2 mm beyond paraxial focus. The data leading to these conclusions, and the estimated uncertainties in the final results, follow later in this report.

BACKGROUND

Following the action of the HST SWG in mid-April 1991 establishing the OAP, the persons listed in Table 1 agreed to serve on the panel. Meetings were held in May and June to assess existing data and propose plans for collimating the OTA. As a result of these discussions, three proposals were prepared and forwarded to the Telescope Time Steering Committee; copies of these proposals (coma, focus, and astigmatism sweeps) are included as Attachments 2A - 2C. After some modifications, these proposals were approved by the TTSC and the observations were made in September and October. Analyses of the data were carried out following the observations, and the recommendations of the OAP were presented on 6 November (see Appendix 2).

Table 1. OAP Membership

Dan Schroeder, Chair	Beloit College
Pierre Bely	STScI
Chris Burrows	STScI
Chris Ftaclas	HDOS
Ed Groth	Princeton University
Robert Jedrzejewski	STScI/ESA
Keith Kalinowski	GSFC
Ed Nelan	University of Texas
John Wood	GSFC
Bob Woodruff	Ball Aerospace

(NASA-CR-190139) OPTICS ALIGNMENT PANEL Final Report, 1 Jun. 1991 - 29 Feb. 1992 (Beloit Coll.) 88 p
N92-24796
CSCL 20F
Unclas
G3/74 0078291

SM ALIGNMENT

The history of the motions of the SM made to try and understand and improve FGS performance is long and involved, and will be not be discussed here. For our purposes it is sufficient to note the SM move history in decenter and tilt, Figs. 1 and 2, respectively. The starting position for the coma sweep, the first step in the alignment process, is Day 90323, with the nominal values relative to launch of (DZ,DY,TZ,TY) = (+281 microns, -109 microns, +53 arcsec, -79 arcsec). This position was one for which astigmatism due to alignment errors was small, less than 0.02 waves rms at 633 nm at the FGSs. Analysis of FOC f/96 images indicated about 1/15 wave of residual coma.

The aberrations introduced when the OTA SM is tilted and/or decentered are summarized in Table 2. This table, courtesy of Chris Burrows, shows the focus, coma, and astigmatism at various field points for several values of tilt or decenter. All of the aberrations are given in microns rms; to convert to waves rms at a specific wavelength, divide the number in the table by the wavelength in microns.

NOTE: Results in this document are generally given in microns rms, but are translated to waves rms at 633 nm when appropriate.

Two things in Table 2 are worth noting, (1) decenter only will significantly change coma but affect astigmatism very little, (2) astigmatism is changed significantly, but coma not at all, with the right combination of tilt and decenter. The first of these was the basis for the coma sweep; the second was used in setting up the astigmatism sweep.

COMA SWEEP

FOC images taken for desorption monitoring purposes during late 1990 and early 1991 served as the basis for defining the coma sweep. Measures of coma on these images, one at the Day 91066 position and the others at the Day 90323 position, indicated zero coma at (DZ,DY) = (+240, +20 microns), with no change in tilts. Images taken at this position, denoted by P1, were followed by images at (DZ,DY) = (+150, -70 microns), denoted by P2. Differences between these positions correspond to 0.027 microns or 0.043 waves rms on each axis.

The FOC segment of the coma sweep was successful, but the WFPC segment failed. Analysis of the FOC images was done by three different groups. Schroeder used the positions of the pads relative to the image peak (see attached report titled Desorption Monitoring for specifics on this method). Grusczak and colleagues at HDOS used phase retrieval software developed by HDOS, and applied to images with the saturated core removed. Burrows used his phase retrieval software on the entire image. All three methods gave similar results; the data are tabulated in Table 3 and plotted in Fig. 3. Note that the coma values derived from images at P2 are adjusted by 0.027 microns to give the values labeled C2.

Table 2 - SM Misalignments and Aberrations

Aberrations, expressed in microns rms, are shown for selected decenters and tilts of the OTA secondary mirror. Aberration results are given for focus (Z4), astigmatism (Z5, Z6), and coma (Z7, Z8) at three field points: on-axis and 10.97 arcmin in either the +V2 or +V3 directions. This angle is at the inner radius of the FGS FOV, the location of the wavefront sensors.

The alignment errors are defined as follows:

DY = decenter in +V3 direction of 100 microns
DZ = decenter in +V2 direction of 100 microns
TY = tilt of V3 axis by 50 arcsec (ccw rotation around V2)
TZ = tilt of V2 axis by -50 arcsec (cw rotation around V3, as seen looking toward origin from +V3 direction).

Error	Position	Z4	Z5	Z6	Z7	Z8
DY	on-axis				-0.0304	
	10.97 +V3	-0.0014	0.0015		-0.0304	
	10.97 +V2			0.0015	-0.0304	
DZ	on-axis					-0.0304
	10.97 +V3			0.0015		-0.0304
	10.97 +V2	-0.0014	-0.0015			-0.0304
TY	on-axis				0.0448	
	10.97 +V3	-0.0232	-0.0284		0.0448	
	10.97 +V2			-0.0284	0.0448	
TZ	on-axis					0.0448
	10.97 +V3			-0.0284		0.0448
	10.97 +V2	-0.0232	0.0284			0.0448

Coma introduced by tilt/decenter is field-independent; astigmatism is proportional to the field angle.

The aberration values for astigmatism include the effect of repointing the HST to keep an image at the same position on the focal surface.

These results indicate residual coma at the nominal zero-coma (ZC) position. Combined with data from Table 2, these residuals are used to find the true ZC location, as given in Table 4 and plotted in Fig. 4.

The significant digits carried in the numbers in Table 4 are based on the SM encoder readings and are not a measure of the accuracy with which the ZC position is known. Given the error in the mean in Table 3, and the average deviation of 0.006 and 0.005 microns for Z7 and Z8, respectively, it is not unreasonable to take +/- 0.006 microns or +/- 0.01 waves rms at 633 nm as the uncertainty in the location of the ZC position. Given 0.030 microns rms coma per 100 microns decenter from Table 2, we find that the uncertainty in the ZC position is approximately +/- 20 microns.

One final note: Although the WFPC part of the coma sweep was unsuccessful, one PC image taken during the focus sweep was at P2 with the others taken at P1. Measures by Schroeder on the pad positions give coma values which are consistent with those in Table 3, within the stated uncertainties. Because PC pixels are about two times larger than FOC f/96 pixels in angular size, the uncertainty in coma derived from PC images is also twice as large and therefore no attempt was made to combine the PC and FOC data.

ASTIGMATISM SWEEP

The starting point for the astigmatism sweep was the nominal zero-coma position P1. A series of four SM moves along the +/- V2 and +/- V3 axes, with decenter/tilt combinations of 300 microns/102 arcsec, introduced known amounts of astigmatism but no coma at the FOC. This set of four moves is shown in Figs. 1 and 2 as positions K1 through K4. The predicted astigmatism, and the measured results using phase retrieval, are shown in Table 5. These measures confirm earlier results from analysis of FGS data that astigmatism at the Day 90323 (and P1) positions was less than 1/50 wave rms at 633 nm.

FOCUS SWEEP

A focus sweep for each camera was defined to ensure that the maximum of the fractional encircled energy (EE) curve for each wavelength would be covered. Defining the initial axial position of the SM as zero, the FOC sweep went from -32 microns to +37 microns SM motion, where (-) means moving the SM toward the primary mirror. For the PC sweep the range of SM motion was -14 microns to +100 microns. Given a despace magnification factor of 110, the corresponding ranges in paraxial focus were 7.6 and 12.5 mm for the FOC and PC sweeps, respectively.

Details for the WFPC sweep are found in Attachment 3, Report on the PC Focus Sweep of October, 1991, by Ed Groth. Details for the FOC sweep are found in Attachment 4 by Robert Jedrzejewski. The chosen despace setting for the SM is its initial position for the week in mid-October when the focus sweep data was taken. Analysis of the FOC sweep data indicates this position corresponds to a distance of 12.2 +/- 0.3 mm from paraxial focus to the OTA focal surface.

Table 3

MEASURED ZERO COMA POSITION

SOURCE	P2 COMA		P1 COMA	
	Z7	Z8	Z7	Z8
HDOS, P2	0.012	0.028		
HDOS, C2			-0.015	0.001
HDOS, P1			-0.005	0.002
SCHROEDER, P2	0.019	0.022		
SCHROEDER, C2			-0.008	-0.005
SCHROEDER, P1			-0.002	-0.004
BURROWS, P2	0.033	0.041		
BURROWS, C2			0.006	0.014
BURROWS, P1			0.003	0.003
AVERAGE			**-0.004**	**0.002**
ERROR IN MEAN			0.008	0.007

NOTES: 1. Coordinate system as defined by HDOS
2. Units are um rms
3. P1 is first position of Coma Sweep
P2 is second position of Coma Sweep
Change from P1 to P2 was dZ7=dZ8=+0.027
C2 is estimate of P1 using P2 and delta Zs
4. All results are from FOC images

Table 4

SM POSITION FOR ZERO COMA

	dV2	dV3
LOCATION OF D323 POSN	281.24	-109.22
LOCATION OF COMA SWEEP P1	241.15	20.67
DIFFERENCE, MEASURED-P1	-6.57	13.16
LOCATION OF MEASURED ZERO	247.72	7.51

1. Coordinate system as defined by HDOS
2. Units are um of SM decenter position
3. Conversion from coma aberration to mirror position is:
100 um decenter = -0.0304 um rms coma

Table 5

ASTIGMATISM SWEEP - PHASE RETRIEVAL RESULTS
ACCURACY OF ASTIGMATISM ESTIMATE

	PREDICTION		MEASUREMENT		DIFFERENCE	
POSITION	Z5	Z6	Z5	Z6	dZ5	dZ6
D323	0.000	0.000				
1	-0.029	0.015	-0.036	0.022	0.007	-0.007
2	0.016	0.027	0.015	0.026	0.001	0.001
3	0.027	-0.017	0.017	-0.024	0.010	0.007
4	-0.023	-0.024	-0.025	-0.028	0.002	0.004
MEAN			-0.007	-0.001	0.005	0.001

Units of Zernike aberrations are um rms

ERROR IN PHASE RETRIEVAL ESTIMATE OF ASTIGMATISM < 0.005 um rms

The method used to determine the distance from paraxial focus to the OTA focal surface is outlined in Fig. 5. Each pad in the OTA pupil is seen in the image as a "bright" spot whose center is measured with respect to the image peak. The average distance, denoted by $\langle r \rangle$, is a measure of the position of the SM with respect to its nominal position. Analysis shows that $\langle r \rangle$ depends only on focus for a given amount of spherical aberration and is unaffected by the presence of coma or astigmatism. NOTE: See attached report on desorption monitoring for specifics on this method.

Results for measures on the FOC focus sweep images are shown in Fig. 6, with the SM position at the start of the sweep defined as zero. Although no image was taken at del SM = 0 during the focus sweep, an FOC image was taken at this position during the coma sweep one month earlier; this value, after adjustment for desorption, is included in Fig. 6. The best-fit straight line through the data gives del SM = 0 equivalent to dPF = 12.2 mm, with an uncertainty of +/- 0.3 mm based on an estimated uncertainty in $\langle r \rangle$ of +/- 0.8 pixels.

The pad circle radius method has been checked against measures of dPF based on phase retrieval for six FOC images taken during the coma and astigmatism sweeps. For each of these images the values of dPF derived by the two methods differ by 0.1 or 0.2 mm, well within the uncertainty of each method.

The pad method was also applied to images taken during the PC focus sweep, at least those images for which the pads were easily seen. These measures are plotted in Fig. 7 with the best-fit line from the FOC data, adjusted for the difference in pixel size, also shown. Within the uncertainty of the measures of $\langle r \rangle$, the line derived from the FOC data passes through the PC points.

DESORPTION

NOTE: The following two paragraphs are a summary of a more extensive report on desorption monitoring included as an attachment.

Desorption of the OTA structure has been a continuing effort since August 1990, with the pad method used to give measures of the SM position. FOC images, exposed to bring out the pad features, have been used since early 1991. The results of this program are shown in Fig. 8. The best-fit exponential curve, supplied by Chris Burrows, was based on data available through September 1991.

Periodic offsets of the SM made to counteract the desorption are as follows: 20 microns (26 Oct 90), 25 microns (22 Feb 91), and 15 microns (11 April 91). Since the final corrective move in early April, the SM position has steadily approached the August 90 setting of approximately 12.1 mm from paraxial focus. Measures during the fall of 1991 indicate a rate of desorption of about 1.5 microns/month during that time period, with approximately 5 microns total additional shrinkage remaining according to Burrows' curve.

CONCLUSIONS/RECOMMENDATIONS

The conclusions reached by the OAP, and the recommendations carried by the OAP to the HST Project Decision Meeting on 6 November, are summarized below.

Despace:

Measures of encircled energy during the camera focus sweeps gave the following distances for which EE is a maximum within an 0.1 arcsec radius:

Camera	Wavelength	Distance from PF
WF/PC	889 nm	14.5 mm
	487	12.2
FOC	487	12.2
	120	11.0

The best choice of focus is obviously wavelength dependent, but a compromise position of 12.2 mm from paraxial focus is acceptable to the camera teams and was recommended to the Project.

Desorption:

The rate of desorption during the fall of 1991 was about 1.5 microns/month, with a total additional shrinkage of about 5 microns projected by the exponential curve fit to the data. The recommendation is for continued monitoring at approximately 3-month intervals, with adjustment as needed, to keep the focus at the proper position.

Tilt/Decenter:

Analysis of the coma sweep data gives the following best estimate of the zero-coma position: (DZ,DY,TZ,TY) = (+248 microns, +8 microns, +53 arcsec, -79 arcsec). The Day 90323 coordinates (and the current ones) are (+281, -109, +53, -79). The OAP was divided on the question of whether to recommend a move to the zero-coma position or maintain the current SM location, and no specific recommendation was made to the Project.

The data indicates that the coma at the nominal zero-coma position is less than 0.01 waves rms and the astigmatism is less than 0.02 waves rms at 633 nm.

Figure 1

SM MOVE HISTORY - DECENTER

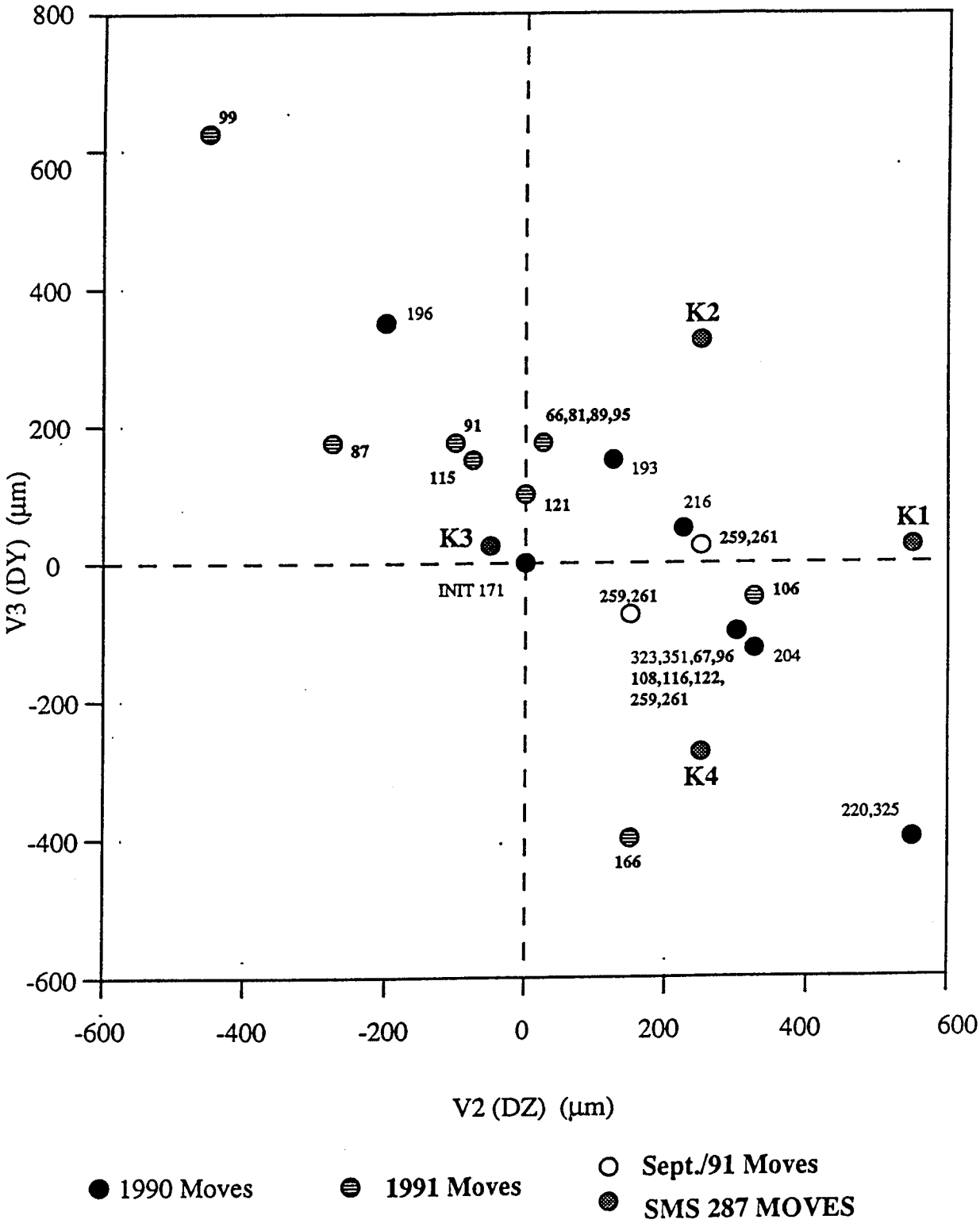

Figure 2

SM MOVE HISTORY - TILT

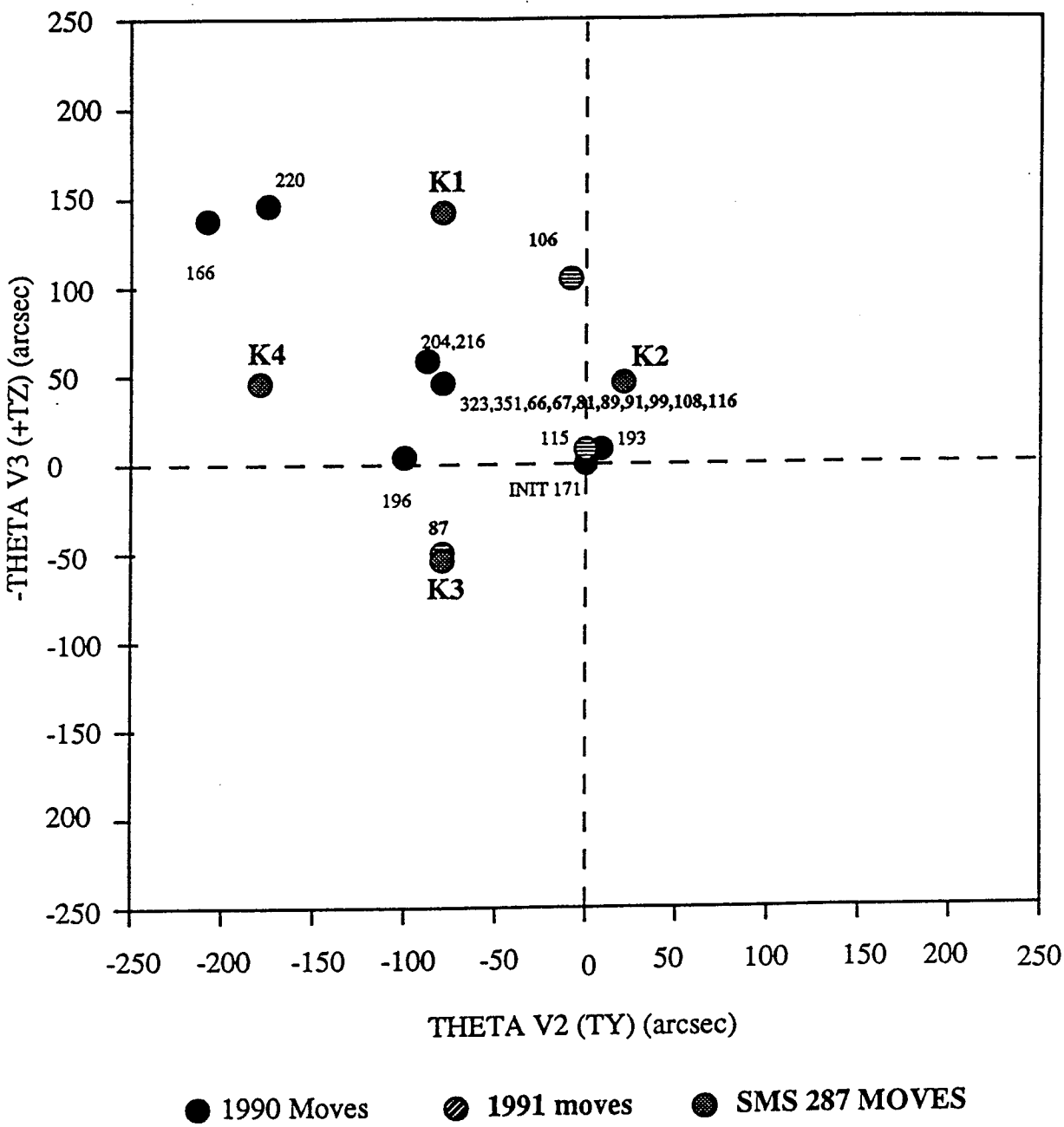

Figure 3

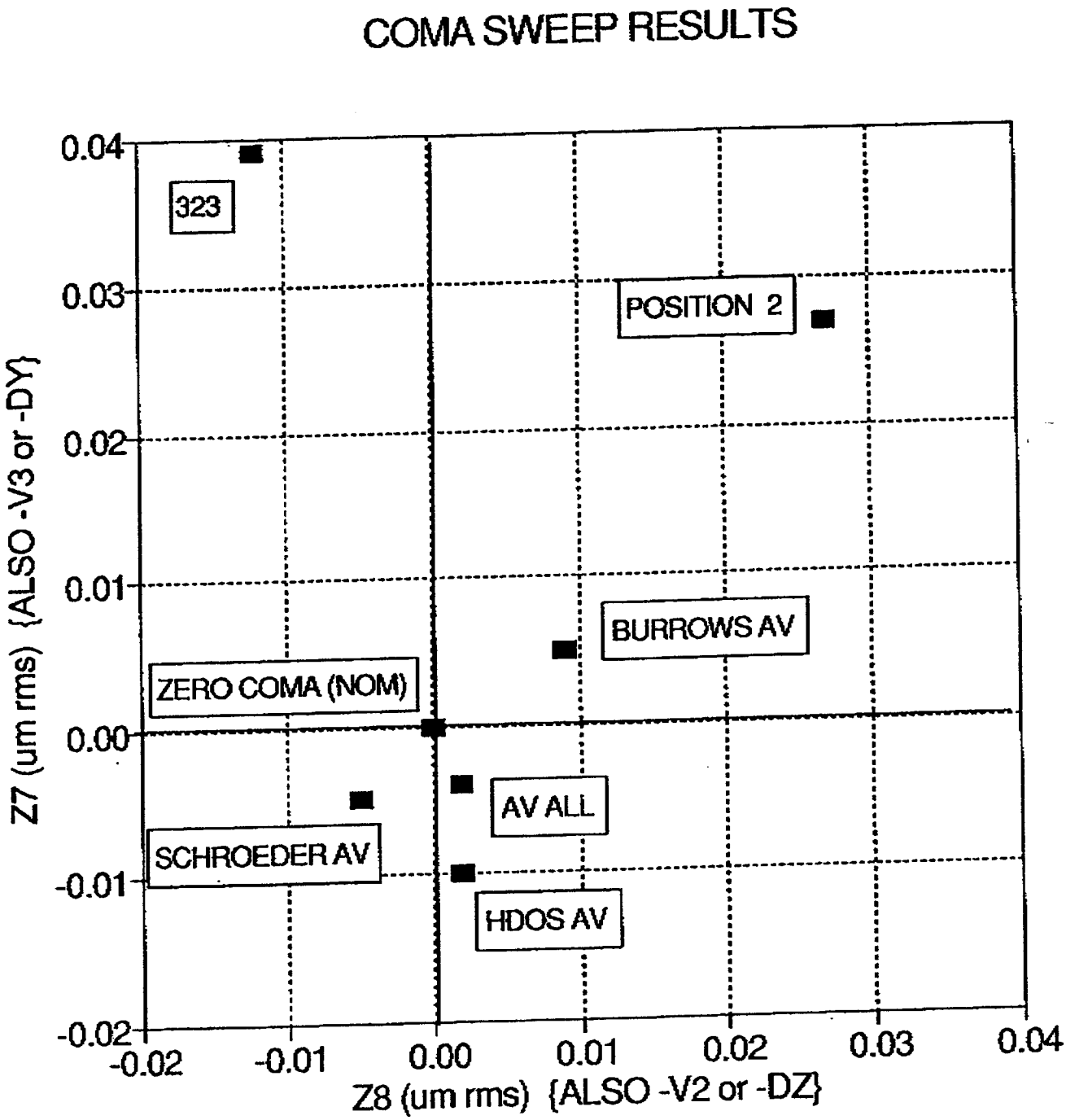
COMA SWEEP RESULTS
323
POSITION 2
BURROWS AV
ZERO COMA (NOM)
AV ALL
SCHROEDER AV
HDOS AV
0.04
0.03
0.02
0.01
0.00
-0.01
-0.02
-0.02
-0.01
0.00
0.01
0.02
0.03
0.04
Z7 (um rms) {ALSO -V3 or -DY}
Z8 (um rms) {ALSO -V2 or -DZ}

Figure 4

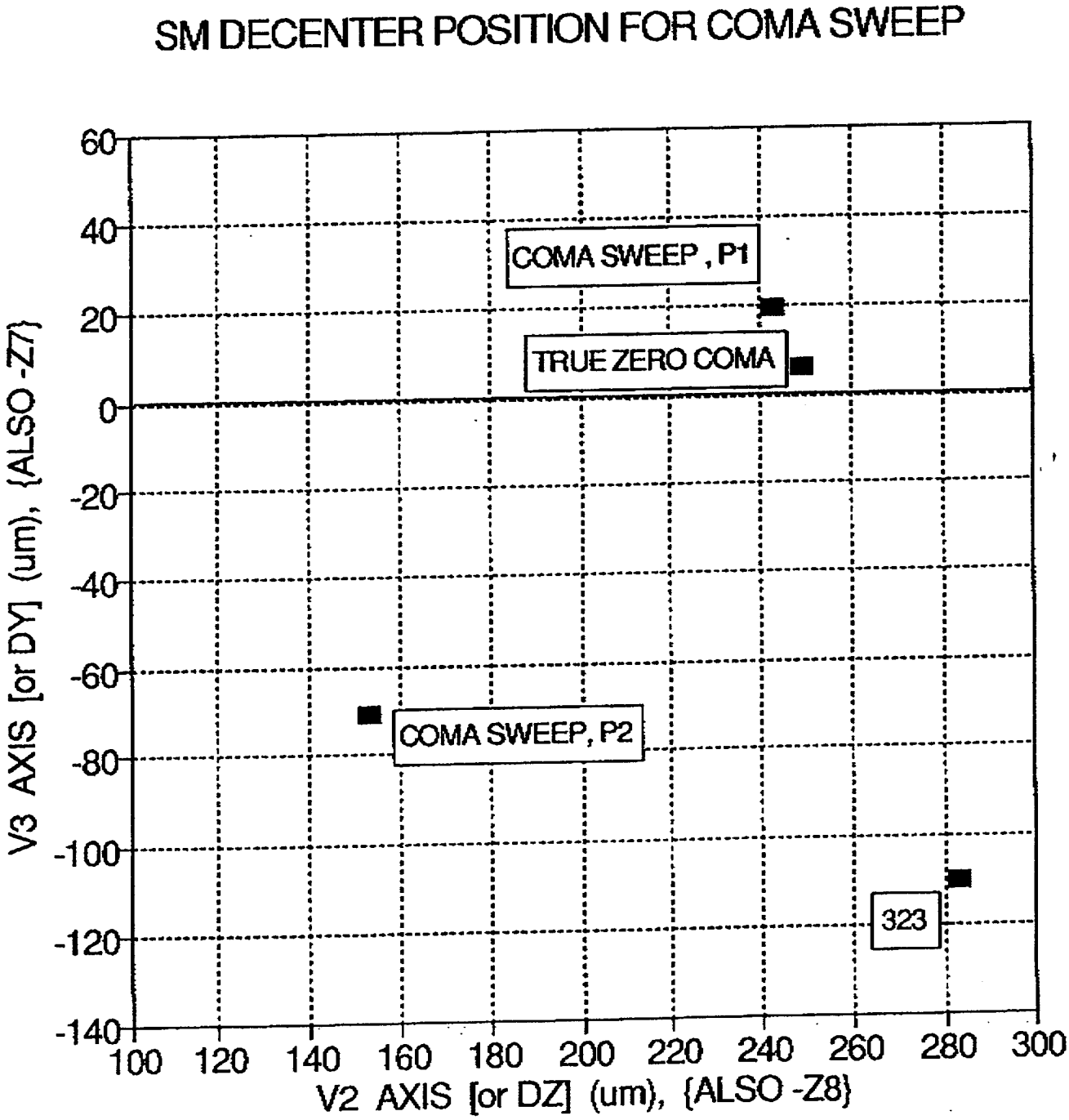
SM DECENTER POSITION FOR COMA SWEEP
60
40
20
0
-20
-40
-60
-80
-100
-120
-140
100
120
140
160
180
200
220
240
260
280
300
V3 AXIS [or DY] (um), {ALSO -Z7}
V2 AXIS [or DZ] (um), {ALSO -Z8}
COMA SWEEP , P1
TRUE ZERO COMA
COMA SWEEP, P2
323

Fig. 5. Pad images

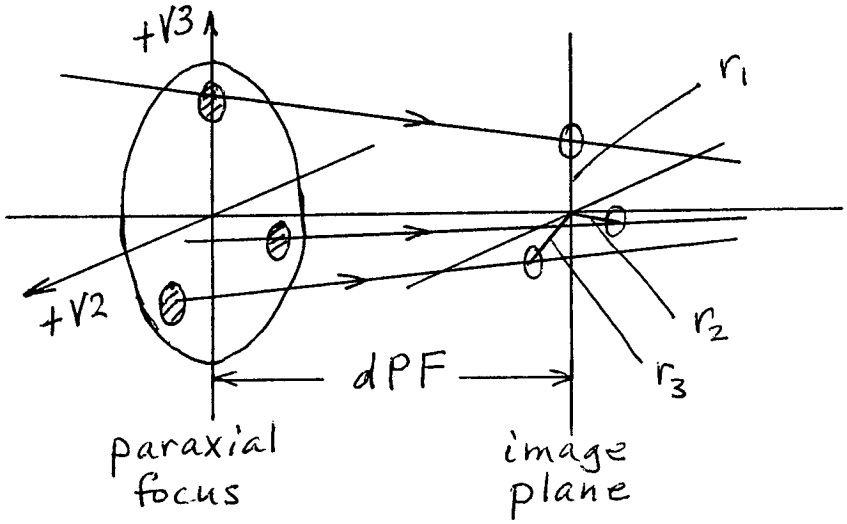

Define ⟨r⟩ = average distance from pad centers to image peak.

Given K = -1.0139 for primary mirror, ray trace analysis of rays from the pad centers gives the following relation:

$$\langle r\rangle(\text{microns}) = 596.5 - 1.998\ \text{dSM(microns)}$$

where dSM is the distance of the secondary mirror from its nominal position which places paraxial focus (PF) at the OTA focal surface.

For the cameras, in pixels, we get

$$\langle r\rangle = 87.57 - 0.2933\ \text{dSM(microns)} = 87.57 - 2.677\ \text{dPF(mm)} \qquad \text{FOC f/96}$$

$$\langle r\rangle = 49.69 - 0.1644\ \text{dSM(microns)} = 49.69 - 1.519\ \text{dPF(mm)} \qquad \text{PC f/30}$$

Fig. 6

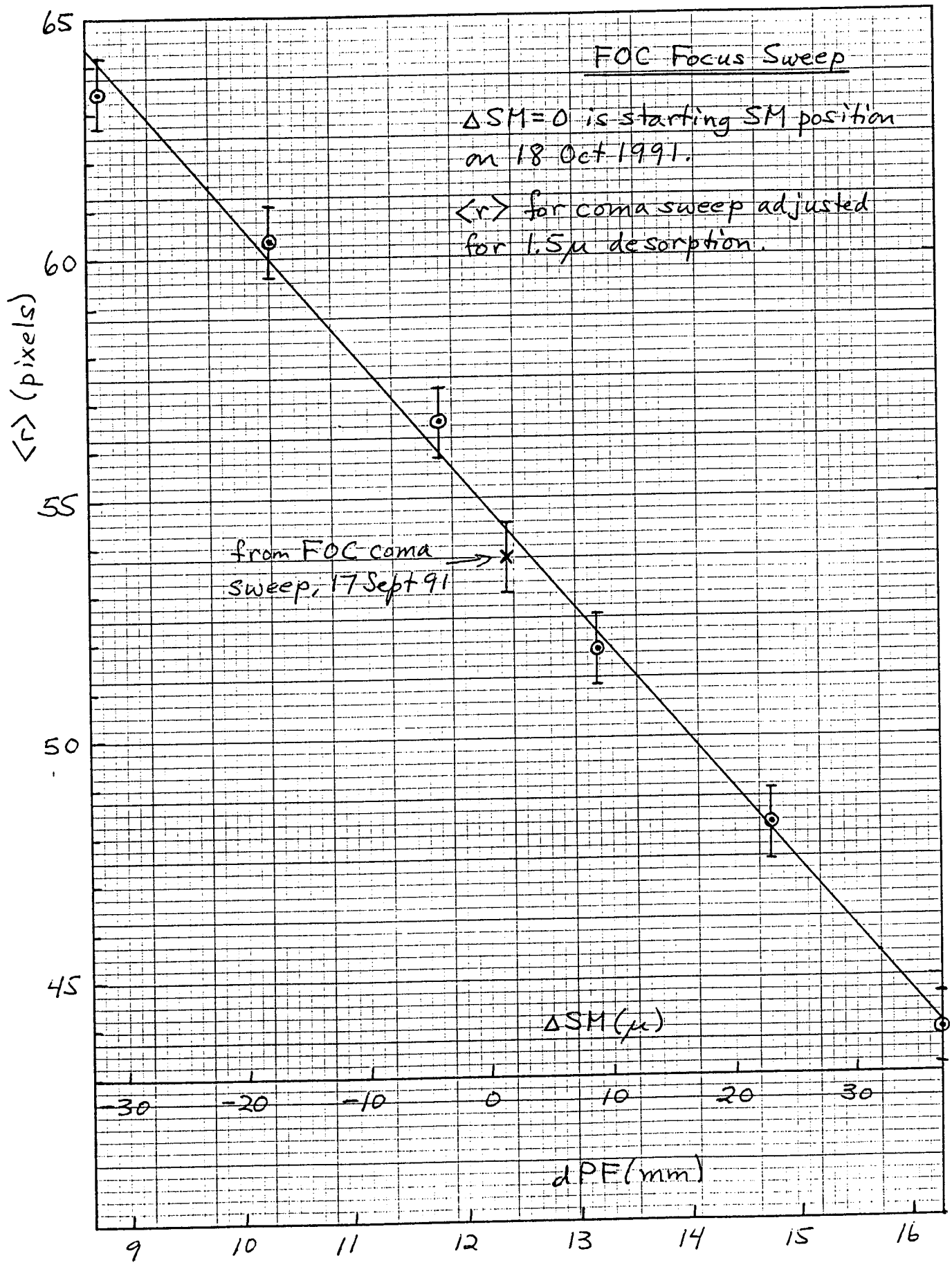
FOC Focus Sweep
ΔSM=0 is starting SM position on 18 Oct 1991.
<r> for coma sweep adjusted for 1.5μ desorption.
from FOC coma sweep, 17 Sept 91
<r> (pixels)
65
60
55
50
45
ΔSM(μ)
-30
-20
-10
0
10
20
30
dPF(mm)
9
10
11
12
13
14
15
16

Fig. 7

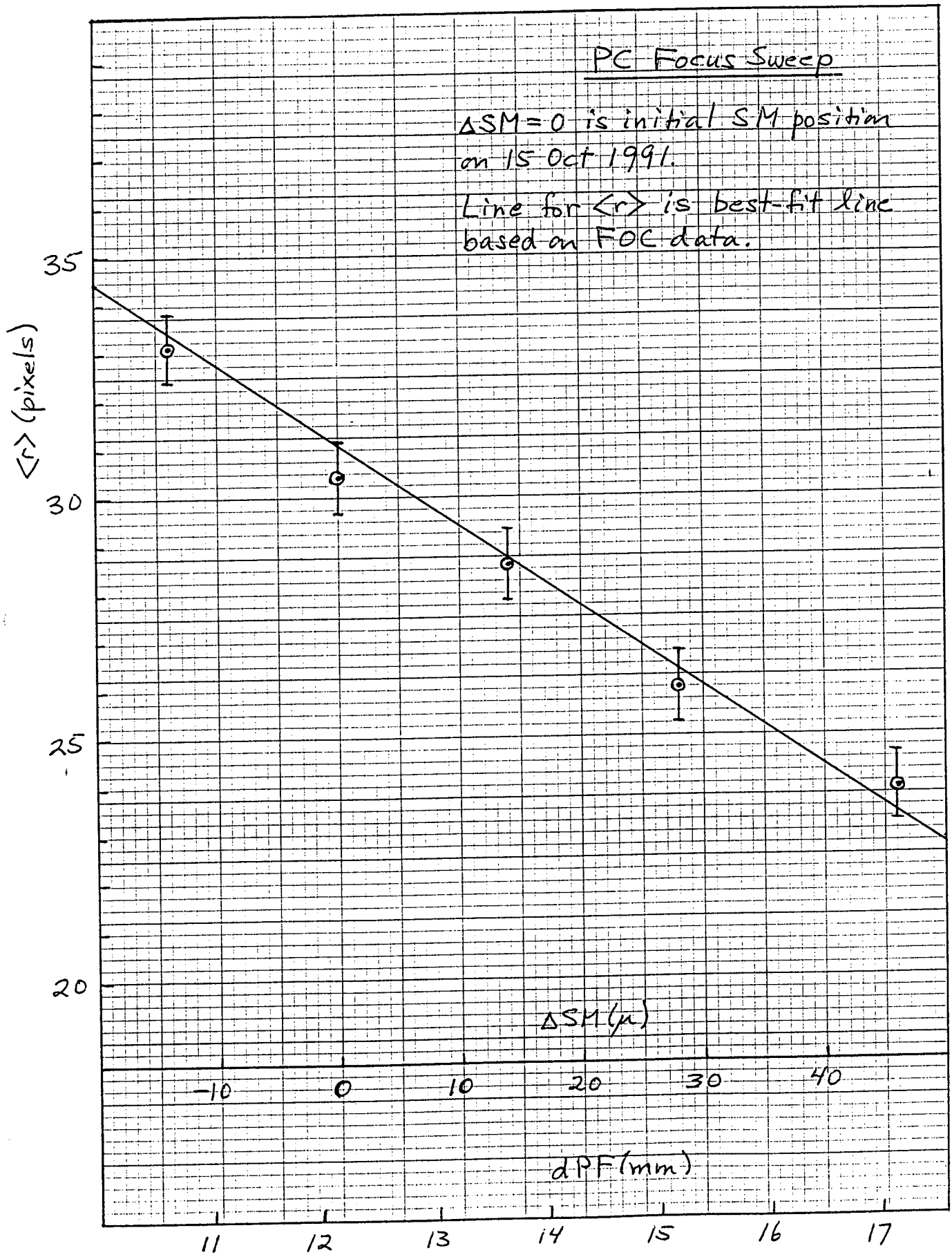
PC Focus Sweep
ΔSM = 0 is initial SM position on 15 Oct 1991.
Line for <r> is best-fit line based on FOC data.
<r> (pixels)
35
30
25
20
ΔSM (μ)
-10
0
10
20
30
40
dPF (mm)
11
12
13
14
15
16
17

Fig. 8

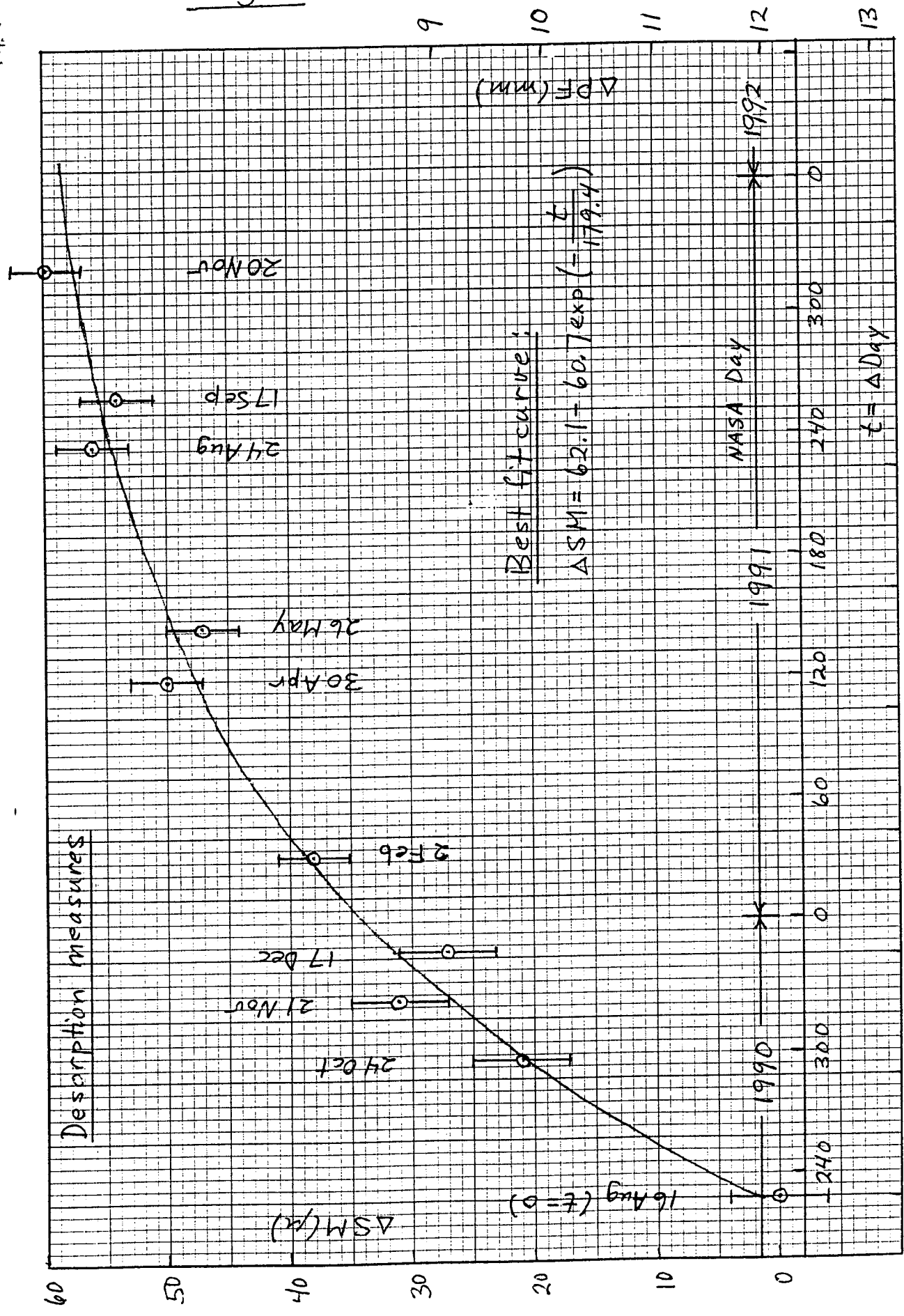
ΔSM (%)
ΔDF (mm)
t = ΔDay
Description measures
16 Aug (t = 0)
24 Oct
21 Nov
17 Dec
9 Feb
30 Apr
26 May
21 Aug
17 Sep
20 Nov
Best fit curve:
ΔSM = 62.1 + 60.7 exp(−t/179.4)
NASA Day
1990
1991
1992

Attachment 1

CHARGE TO OPTICS ALIGNMENT PANEL

The goal of the OAP is to define a strategy for achieving the best possible alignment of the OTA optics, both for the near-term using the current suite of instruments and for the longer term with WF/PC II, COSTAR, and future instruments. Optimum alignment is defined as that which, in the Panel's view, will result in a maximum of scientific productivity within the constraints set by FGS performance.

The plan for achieving this goal will include a review of the history of collimation settings and the performance of the FGSs and cameras at these settings, an assessment of possible strategies for optimizing the collimation of the OTA, and a study of tradeoffs between FGS performance and optimization of camera images. On the basis of their findings, the Panel will formulate a set of conclusions and recommendations.

The Panel is set up at the request of the SWG and will present its findings to the HST Project Scientist. During the course of its work the Panel may request STScI or GSFC support for studies of specific technical issues that may arise.

Daniel J. Schroeder
April 1991

Attachment 2A

14 June 1991

To: Telescope Time Steering Committee

From: Dan Schroeder
Optics Alignment Panel

Title: Collimation of OTA

PIs: Dan Schroeder, Chris Burrows,
Ed Groth, Robert Jedrzejewski

Description of Technical Problem:

Since the setting of the SM at its nominal position following the Aug 90 focus sweep, the HST has been plagued with marginal performance of the FGSs. In an attempt to understand their behavior and to improve their performance, a program was instituted to explore tilt/decenter space of the SM. During this exploration the emphasis was on getting S-curve data at various SM settings. A location was found, the so-called Day 66 setting, at which FGS's 1 and 3 gave excellent performance. The camera images, however, showed significant coma at this SM position and it was returned to its Day 323 setting where the FGS performance is less good.

Analysis of camera images at these two SM settings showed large coma for Day 66, about 0.15 waves rms at 633 nm, and moderate coma for Day 323, about 0.05-0.06 waves rms. In addition, the coma has opposite signs so that between these two settings is a point of "zero coma", hereafter called the ZC-point.

The aim of this proposal is to request that the SM be set at the computed ZC-point with camera images, both PC and FOC f/96, taken for verification. A second setting of the SM on the other side of the ZC-point re the current SM position is also requested. Following acquisition of the data the SM would be reset to its current Day 323 setting and the images would be analyzed for the presence of coma.

Knowledge of the ZC-point is important for several reasons: (1) it provides a reference setting for further exploration of tilt/decenter space while keeping coma zero, with the aim of reducing astigmatism and improving performance of the cameras and the FGSs, (2) the 2nd-generation SI teams can do a better job of designing their optical systems if the aberration limits set by the SM position are well-known, and (3) the current cameras can more easily do the required image retrieval if a final setting of the SM at an optimum ZC-point is chosen. The choice of an optimum SM setting depends, of course, on verifying that FGS performance is satisfactory and hopefully better than currently.

Test Results Needed:

PC: Stellar images with F486N filter.

FOC f/96 Stellar images with F486N filter and UV filter (to be selected).

Repeat the above at each of two SM settings.

Images taken with both cameras should be exposed to a depth which allows the positions of the pad centers to be determined. The pad positions are a sensitive indicator of the amount of coma present in an image.

Changes to Flight or Ground System:

No changes are necessary, pending evaluation of test results. Work is in progress defining the parameters of an "astigmatism sweep".

Existing Data or Already Planned Test:

The SM has not been set at the tilt/decenter position which preliminary analysis indicates is coma-free and no test is currently planned for moving to this position.

Desired Time for Execution:

If this request is approved, it is expected that a specific plan can be prepared within 10 days for submission to STScI. We anticipate that the plan could be executed by 1 Sept 1991.

Prerequisites to Execution:

Refinement of the location of the ZC-point based on analysis of existing PC and FOC images.

Estimate of Time Required:

It is estimated that 8 orbits will be needed to take the desired images.

Proposal Status:

As noted above, a specific proposal can be ready within 10 days of approval of this request. The SMS defining the FOC images taken for desorption monitoring purposes can serve as a starting point for this proposal. Appropriate targets and exposure times for PC images can be selected from those used in the Aug 90 focus sweep.

Analysis of Results:

The images taken will be analyzed by Chris Burrows and independently by Dan Schroeder. Chris will use his image retrieval software to determine the aberrations present in the images; Dan will measure pad locations in the FOC images and apply his algorithm to find the residual coma. These analyses and the comparison of the results should be completed within two weeks after the images are obtained.

Attachment 2B

17 June 1991

To: Telescope Time Steering Committee

From: Dan Schroeder
Optics Alignment Panel

Title: Mini Focus Sweep

PIs: Dan Schroeder, Chris Burrows,
Ed Groth, Robert Jedrzejewski

Description of Technical Problem:

The OTA SM was set at its nominal position following the Aug 90 focus sweep. The choice of this position was based primarily on measures of the encircled energy (EE) in a 0.1 arcsec radius circle for the FOC f/96 and WF/PC with F486N filters. Based on the now accepted conic constant for the OTA PM, K = -1.0135, this put paraxial focus (PF) about 14 mm from the nominal OTA focal surface. Denoting this distance by del-PF, modeling indicates that maximum EE for the WF/PC in the V-band occurs when del-PF is about 15 mm, while the peak in the EE curve for the FOC at 486 nm is at del-PF near 13 mm. The camera teams agreed at a meeting early this year on a setting of PF at the FOC peak in the EE curve. This was based on the fact that the EE peak shifts toward smaller del-PF at shorter wavelengths.

Since Aug 90 periodic adjustments to the SM position have been made to compensate for desorption. The sizes of these adjustments have been based on measures of the average radius of the circle on which the centers of the pads in the diffraction image are located. Denoting this average radius by r-bar, analysis shows that r-bar provides an absolute measure of del-PF. Measures of r-bar from all of the images taken for desorption monitoring purposes since Aug 90 show that del-PF has been almost entirely in the range of 9 - 12 mm, hence the cameras have not been getting as much energy in the image core as expected. This result derived from measures of r-bar is supported by measures of EE at various times during the past few months, all of which indicate that we are operating on the slope of the EE-curves and not at the peak.

The aim of this proposal is to request that a new mini focus sweep be carried out to establish definitively the relation between del-PF and EE in both the visible and UV, to set the SM appropriately, and to hold its position within tighter limits than heretofore, given what we now know about desorption. Knowledge of the relation between del-PF and EE in the UV is especially important for the GHRS when the small science aperture is used.

Knowledge of the relation between del-PF and EE, resetting the SM to near the EE peak, and holding it there, is important for several reasons: (1) the present cameras will operate with efficiency close to

maximum in terms of resolution, (2) the 2nd-generation SI teams can optimally design their optical systems for a given SM position, and (3) the constant need to take PSFs for reduction of science data may be lessened.

Presumably the mini-sweep data from Aug 90 could be used to reestablish the SM position, and a revisit to this data is in progress. However, we want to point out that this data is flawed in several ways. (1) The FOC images were not exposed to a depth which shows clearly the pads, hence measuring r-bar is difficult, at best, and probably impossible. (2) The sweep was interrupted by SAO observations and some of the data are separated by several weeks from the rest. During this time del-PF was changing at a rate of about 1 mm/month. (3) The HST was experiencing significant problems with jitter and loss of lock, hence image quality is suspect. Because the system is operating much more reliably, and because we have a better idea of what data is needed, a new focus sweep should be carried out.

Reanalysis of the PC6 data from the Aug sweep has been done by Ed Groth. His graphical results and commentary on them are attached, as are model EE calculations for both FOC and WF/PC at 230 and 486 nm. Overlay of the PC6 data and the model WF/PC curves supports his conclusion that " ... we don't really have enough data to make a consistent story."

Test Results Needed:

WF/PC: Stellar images with F486N and F230W filters, two or three images per filter.

FOC f/96: Stellar images with F486N and F230W filters, two or three images per filter.

(It may be desireable to use an F336W filter instead of F230W for the WF/PC, if contamination at 230 nm is a problem. For the FOC a filter at a wavelength shorter than 230 nm may be desireable, depending on where the science emphasis is for FOC, FOS, and GHRS.)

Repeat the above at each of six (6) SM positions corresponding to del-PF in the range of 9 - 15 mm, inclusive.

Images taken with both cameras should be exposed to a depth which allows both the EE and the positions of the pad centers to be determined.

Changes to Flight or Ground System:

No changes are necessary, pending evaluation of test results. The SM would be reset to its new position after the data are analyzed.

Existing Data or Already Planned Test:

The data from the previous mini-sweep is being reevaluated, as noted above. (Reanalysis of the FOC data is in progress.)

Desired Time for Execution:

If this request is approved, it is expected that a specific plan can be

prepared within 10 days for submission to STScI. We anticipate that the plan could be executed by 1 Sept 1991. Because the focus sweep would occur at about the same time of year, the SMS for the earlier sweep can be adapted for this sweep.

Prerequisites to Execution:

Reevaluation of all the earlier focus sweep data.

Estimate of Time Required:

It is estimated that 24 orbits will be needed to take the desired images at the selected settings of the SM. This is based on 3 orbits for the FOC images and 1 orbit for the WF/PC images at each SM setting. STR management limitations may require additional orbits.

Proposal Status:

As noted above, a specific proposal can be ready within 10 days of approval of this request and the SMS for the earlier focus sweep can serve as a starting point for this proposal. Appropriate targets and exposure times for images can be selected from those used in Aug 90.

Analysis of Results:

The images taken will be analyzed by the camera teams; measures of r-bar for the FOC images will be made by Dan Schroeder. These analyses and the determination of the proper location of the SM should be completed within three weeks after the images are obtained.

Attachment 2C

5 July 1991

To: Telescope Time Steering Committee

From: Dan Schroeder
Optics Alignment Panel

Title: Collimation of OTA - Astigmatism Sweep

PIs: Dan Schroeder, Chris Burrows,
Ed Groth, Robert Jedrzejewski

Description of Technical Problem:

At its 19 June meeting the TTSC approved a request from the Optics Alignment Panel for a 2-point "coma sweep". This involves decenters of the SM to two positions, with FOC and WF/PC images taken at each. One of the positions is the so-called "zero-coma" location based on analysis of images already available; the other is a non-ZC point in the general direction of the Day 066 SM setting.

Following analysis of these additional images, we expect that a ZC position of the SM can be specified with an uncertainty of the order of 0.01 waves rms at 633 nm. This does not mean, however, that the OTA is collimated. It only means that

$$\text{dec(microns)} = 2.95 \times \text{tilt(")} \qquad (1)$$

is satisfied in each of two orthogonal directions, with neither tilt nor decenter known.

To find the actual values of tilt and decenter, it is necessary to measure the astigmatism. When Eq. (1) is satisfied the rms astigmatism in waves at 633 nm is given by

$$\text{Ast} = 2.12\text{E-}5 \times \text{dec(microns)} \times \text{theta(')} \qquad (2)$$

where theta(') is the field angle in arc minutes.

The aim of this proposal is to request that the SM be set at four points around the ZC-point with FOC f/96 images taken at each point. (The WF/PC is not far enough off-axis to show measureable astigmatism arising from tilt/decenter.) Measures of astigmatism in these images will then permit calculation of the actual values of decenter and tilt at each position, hence the SM setting for a collimated OTA can be determined.

Knowledge of the correct SM setting and its uncertainty should help the 2nd-generation SI teams in their optical designs. It will be necessary, of course, to verify that FGS performance at this setting is satisfactory and hopefully better than it is now.

Test Results Needed:

FOC f/96 Stellar images with F486N filter
at each of four (4) SM settings.

Images taken should include some deep exposures which allow positions of the pad centers to be determined. The changes in the pad positions can be used to check the image retrieval analyses.

Nominal changes in tilt and decenter could be as follows:

xdec(mic)	xtilt(")	ydec(mic)	ytilt(")
+/-300	+/-102	0	0
0	0	+/-300	+/-102

These changes ensure coma remains at zero. The actual choice of offsets will be determined after the astigmatism in the ZC-position is known.

Changes to Flight or Ground System:

No changes are necessary, pending evaluation of test results. The calculated ZC-point would be the starting point for the offsets given.

Existing Data or Already Planned Test:

None, pending completion of the proposal to locate the ZC-point.

Desired Time for Execution:

If this request is approved, it is expected that a specific plan can be prepared within 10 days for suomission to STScI. We anticipate that the plan could be executed by late Sept or early October.

Prerequisites to Execution:

Analysis of the "coma sweep" data.

Estimate of Time Required:

It is estimated that 5 orbits will be needed to take the desired images. One Mode 1 acquisition would be required, with one orbit for each of the SM settings.

Proposal Status:

As noted above, a specific proposal can be ready within 10 days of approval of this request. The SMS defining the FOC images taken for desorption monitoring purposes or the SMS for the focus sweep can serve as starting points for this proposal.

Analysis of Results:

The images taken will be analyzed by Chris Burrows and independently by Dan Schroeder. Chris will use his image retrieval software to determine the astigmatism present in the images; Dan will measure pad locations in the images and apply his algorithm to find the residual astimagtism. These analyses and the comparison of the results should be completed within two weeks after the images are obtained.

Attachment 3

REPORT ON THE PC FOCUS SWEEP OF OCTOBER, 1991

EDWARD J. GROTH
November 1, 1991

ABSTRACT

In order to better characterize the HST and PC optics and to decide on a final HST secondary mirror focus position, a PC focus sweep was carried out on October 16 and 17, 1991. This report describes the reduction and analysis of the images resulting from this sweep. Good data were obtained at all secondary mirror positions allowing the construction of accurate PSFs and encircled energy curves. Within an 0.1 arcsecond radius, the encircled energy fraction at $\lambda = 487$ nm has a maximum of 0.165 ± 0.001 at 12.2 ± 0.3 mm from paraxial focus. The corresponding numbers for $\lambda = 889$ nm are 0.117 ± 0.001 and 14.5 ± 0.1 mm.

1. INTRODUCTION

In the Summer of 1991, the HST Optical Alignment Panel (OAP) was formed by the Project Scientist, Al Boggess, to study and make recommendations for the alignment of the HST secondary mirror. Panel members are listed in Table 1. This action was taken because alignment based on FGS performance was leading to a secondary mirror position that produced substantial coma in HST camera (WFPC and FOC) images. This is due to the fact that small internal misalignments in the FGS optics, interacting with the spherical aberration of the primary mirror, introduce a degradation that is indistinguishable from coma and can therefore be cancelled out by introducing coma in the telescope optics.

Table 1. OAP Membership

Dan Schroeder, Chair	Beloit College
Pierre Bely	STScI
Chris Burrows	STScI
Chris Ftaclas	HDOS
Ed Groth	Princeton University
Robert Jedrzejewski	STScI/ESA
Keith Kalinowski	GSFC
Ed Nelan	University of Texas
John Wood	GSFC
Bob Woodruff	Ball Aerospace

The OAP met several times in the summer of 1991 and considered existing data from the FGSs and the cameras. The consensus was that we knew the approximate secondary mirror decenter of the "zero coma" position and we knew approximately where the peak encircled energy occurred in the cameras as a function of focus and wavelength. The astigmatism (tilt) was a little more problematical. In any case, plans were formulated to carry out five "sweeps" in which stellar images would be obtained at several secondary mirror positions. These included coma and focus sweeps with the PC, and coma, astigmatism and focus sweeps with the FOC. The goal of these sweeps is to determine as precisely as possible the secondary mirror decenter and tilt which results in an aligned telescope and to determine the focus setting that's optimum for the scientific performance of the HST.

The FOC sweeps are discussed elsewhere. In this report I discuss the PC sweeps. Unfortunately, the coma sweep failed. Apparently, a gyro bias update was performed while the secondary mirror was being moved in decenter and the telescope was in fine lock. This introduced an error in the onboard gyro bias such that the subsequent reacquisitions failed to acquire guide stars. Of the three sets of coma sweep exposures planned, one set was completely blank, one set had the star in the corner of PC7 rather than in PC6, and the third set had the star split between PC8 and PC7. In all cases, the exposures were taken under gyro control. The PC coma sweep data appear to be of marginal utility and have been left unreduced.

The PC focus sweep was a success. All but one of 29 exposures were obtained with no apparent pointing or guiding problems. The one unsuccessful exposure was mispointed by 0.6 arcsec but is otherwise a good exposure. Since it is one of a pair of two exposures, no loss of essential information results from ignoring it. The PC focus sweep was taken with the secondary mirror decentered to the "zero coma" position used in the coma sweep. One of the focus positions was taken with the "fifteenth wave coma" position of the coma sweep. Thus, most of the goals of the PC coma sweep can be recovered. Previous modelling has shown that some coma in the images has negligible effect on the encircled energy function, so the focus sweep is not compromised by including these comatic images.

The determination of the telescope aberrations from these images is discussed elsewhere. In this report, I describe the focus sweep, the reduction of the images, and the calculation of encircled energy curves from the images.

2. OBSERVATIONS

The focus sweep observations were done with the 6.6 V magnitude A5 star SAO 7867, whose equinox 2000.0 coordinates are $13^h\ 40^m\ 40^s.99$, $+76°\ 50'\ 37''.5$. Fortunately, this star had been tested in the Summer of 1990, so accurate exposure times could be estimated.

Table 2 gives a log of the exposures. The start time is approximate (it's actually the value of the keyword FPKTTIME in the image header—the start time is probably a minute or two before the time listed). The focus is listed as millimeters from the paraxial focus. It is assumed that the current focus position is 12.2 millimeters. The column V1 lists the secondary mirror despace in microns relative to the current despace. Positive numbers indicate an increase in secondary mirror to primary mirror distance. The columns V2 and V3 give the secondary mirror decenter in microns relative to the launch position. The current decenter is $(+280, -110)$. All observations were taken at the current secondary mirror tilt which is $(TV2, TV3) = (-77, -54)$ arcsec relative to the launch position. Secondary mirror positions quoted here were taken from *Final SMS 287 Mirror Move Plan (10/7/91)* prepared by Keith Kalinowski.

The target acquisition image was used to update the pointing so that in subsequent exposures the star would be centered on pixel (245,310) in PC6. At this location in PC6, the internal obscuration is centered on the secondary mirror obscuration from the telescope. This location was chosen because it simplifies phase retrieval analysis of the images.

I use the convention that the pixel closest to the center of the WFPC pyramid is (1,1). The second coordinate runs anti-parallel to the column readout shift direction. When images are displayed in this report, (1,1) will be in the lower left with the first coordinate increasing to the right and the second increasing to the top. This yields a direct (as opposed to mirror) image of the sky.

Target acquisition was something of an adventure (this paragraph may be skipped if you're not interested in target acquisition). The procedure for target acquisition in the WFPC is somewhat non-intuitive (at least to me). In the observing proposal, I had specified a `POS TARG` on the acquisition image in order to get the target close to the desired location. I assumed that I would be able to identify the location of the target on the OSS console (it turns out it was (254,290)) and the location where it should be placed, (245,310), and the OSS would send commands to repoint the HST by this delta and then leave it there! Not so. At least three discrepancies between my mental picture of target acquisition and its actual implementation were discovered. In the first place, the OSS takes the `POS TARG` together with its idea of an aperture coordinate system and uses that as the desired location of the target (rather than (245,310) in this case). In other words, you can't specify a starting and ending position. You specify the starting position and the OSS specifies the ending position. (Of course, its ending position is based on the `POS TARG` in the proposal, but also on a detailed model of the coordinate system that doesn't seem to be generally available—i.e. one needs the exact origin and scale to relate `POS TARG` coordinates to pixel

Table 2. PC Focus Sweep Exposure Log

No.	Rootname	UT Start Time	Time (s)	Filter	Focus (mm)	V1 (μ)	V2 (μ)	V3 (μ)	Notes
1	W0R85101T	16-Oct-91 02:11	3	F487N	10.7	−14	+150	−70	Acquisition 1/15 wave coma
2	W0R85102T	16-Oct-91 05:11	2.6	F487N	10.7	−14	+150	−70	1/15 wave coma
3	W0R85103T	16-Oct-91 05:17	26	F487N	10.7	−14	+150	−70	1/15 wave coma
4	W0R85104T	16-Oct-91 05:23	4	F889N	10.7	−14	+150	−70	1/15 wave coma
5	W0R85105T	16-Oct-91 05:29	40	F889N	10.7	−14	+150	−70	1/15 wave coma
6	W0R85106T	16-Oct-91 08:09	2.6	F487N	12.2	0	+240	+20	
7	W0R85107T	16-Oct-91 08:15	26	F487N	12.2	0	+240	+20	
8	W0R85108T	16-Oct-91 08:21	4	F889N	12.2	0	+240	+20	
9	W0R85109T	16-Oct-91 08:27	40	F889N	12.2	0	+240	+20	
10	W0R8510AT	16-Oct-91 11:22	2.6	F487N	13.7	+14	+240	+20	
11	W0R8510BT	16-Oct-91 11:28	26	F487N	13.7	+14	+240	+20	
12	W0R8510CT	16-Oct-91 11:34	4	F889N	13.7	+14	+240	+20	
13	W0R8510DT	16-Oct-91 11:40	40	F889N	13.7	+14	+240	+20	
14	W0R8510ET	16-Oct-91 14:36	2.6	F487N	15.3	+28	+240	+20	
15	W0R8510FT	16-Oct-91 14:42	26	F487N	15.3	+28	+240	+20	Bad pointing
16	W0R8510GT	16-Oct-91 14:48	4	F889N	15.3	+28	+240	+20	
17	W0R8510HT	16-Oct-91 14:54	40	F889N	15.3	+28	+240	+20	
18	W0R8510IT	16-Oct-91 19:25	2.6	F487N	17.2	+46	+240	+20	
19	W0R8510JT	16-Oct-91 19:31	26	F487N	17.2	+46	+240	+20	
20	W0R8510KT	16-Oct-91 19:37	4	F889N	17.2	+46	+240	+20	
21	W0R8510LT	16-Oct-91 19:43	40	F889N	17.2	+46	+240	+20	
22	W0R8510MT	16-Oct-91 22:38	2.6	F487N	20.2	+73	+240	+20	
23	W0R8510NT	16-Oct-91 22:44	26	F487N	20.2	+73	+240	+20	
24	W0R8510OT	16-Oct-91 22:50	4	F889N	20.2	+73	+240	+20	
25	W0R8510PT	16-Oct-91 22:56	40	F889N	20.2	+73	+240	+20	
26	W0R8510QT	17-Oct-91 01:51	2.6	F487N	23.2	+100	+240	+20	
27	W0R8510RT	17-Oct-91 01:57	26	F487N	23.2	+100	+240	+20	
28	W0R8510ST	17-Oct-91 02:03	4	F889N	23.2	+100	+240	+20	
29	W0R8510TT	17-Oct-91 02:09	40	F889N	23.2	+100	+240	+20	

coordinates and these are subject to database updates.) The second problem had to do with a 20 pixel discrepancy between the SPSS database value and the OSS database value for the pixel coordinates used when the aperture is PC6. I believe that this would not have been a problem except for the first problem above. Apparently this 20 pixels feeds into the ending position that the OSS computes. The final problem was my assumption

that once the HST was repointed by a small slew commanded from the OSS, it would stay there. It turns out that I did not put POS TARGs on the exposures after the acquisition exposure. Therefore the SPSS decided that I wanted the target at the center of PC6 for these exposures. So it inserted into the schedule a small slew to repoint the HST such that a star at the POS TARG location would wind up at the center of PC6. The solution to these problems was to manually calculate the slew required to go from (254,290) to (245,310) and then add to this the negative of the slew inserted by the SPSS. It turns out it all worked and Keith Kalinowski and Al Holm deserve special thanks for tracking all this down beforehand.

To return to the main discussion, exposures after the acquisition exposure occur in seven sets at a given secondary mirror position. Each set contains a short and a long exposure in two narrowband colors. Two colors were used to enable quantities to be measured as a function of wavelength. The short/long combination was used to get a well exposed core in the short exposure and a well exposed halo in the long exposure.

3. REDUCTION

All images were processed with the WFPC standard data reduction. This includes A to D correction, DC bias subtraction, AC bias subtraction, dark current subtraction, preflash subtraction, flat field normalization and bad pixel masking. Of these steps, all are well in hand except preflash subtraction and flat fielding.

The problem with preflash subtraction is that there is no record in the header of which shutter blade was illuminated to generate the preflash. Fortunately, this turned out not to be a problem. There is about a one DN (data number) difference between the preflashes on blades A and B in PC6. Since the star occupies only a small part of PC6, the remainder could be examined and the proper shutter blade determined. It turns out that the preflashes alternated regularly between blade A and blade B as expected, with the preflash for exposure number 1 occurring on blade A.

The flat fields were constructed from Earth flat data obtained since the last time the WFPC was warmed up and decontaminated. For the F889N data, flats obtained with the F889N filter were used. For the F487N data, flats obtained with the F517N filter were the closest available. In either case, the flats are estimated to have pixel-to-pixel noise of about 0.5%. In addition, there are large scale gradients across all four chips that are probably about $\pm 2\%$ peak-to-peak. However, the star occupies roughly 140 pixels, so the large scale gradients across the star are expected to be much smaller.

The background level in each exposure was computed by averaging all pixels located in an annulus centered on pixel (245,310) with inner and outer radii of 250 and 350 pixels. The average was computed with an iterative algorithm that rejects pixels which differ from the mean by more than three times the rms. Thus cosmic rays are not a problem in this

computation. The background levels ranged from 0.16 DN to 0.35 DN. Presumably these are due to slight fluctuations in the bias level or more likely, to fluctuations in the lamp intensity during the preflash exposures. The computed background level was subtracted from each image.

A byproduct of the background level calculation is the determination of the rms noise at the background level which turned out to be almost exactly 2.0 DN. This corresponds to 15 electrons. The read noise of the WFPC detectors is 13 electrons. The effective read noise here is a little larger because the bias and preflash frames subtracted from the images, although the average of many frames, are still not noiseless.

The next step was to determine the relative exposure level between the short and long exposures. This should be the exposure time ratio, but the exposure times listed in Table 2 are nominal times. The total DN in an annulus centered on (245,310) with inner and outer radii 6 and 36 pixels was computed for exposures 2 through 9. The inner radius was chosen to safely exclude the saturated pixels in the cores of the long exposures and the outer radius was arbitrarily chosen to exclude the low signal to noise pixels in the halos in the short exposures. The resulting ratios were 10.264, 10.205, 10.184, and 10.265. The adopted ratio is 10.23 ± 0.02.

Each pair of short/long exposures was run through a cosmic ray rejector and picture stacker. This compares pixels across the images, rejects those that are cosmic rays, and outputs either the weighted average of two good pixels, or whichever pixel is not a cosmic ray. Note that the short exposure and its noise are scaled by factor of 10.23. The central 10 pixels or so of each long exposure are saturated, so the center of the stacked image comes entirely from the short exposure. Elsewhere, the weight of the long exposure is so much greater than that of the short exposure that the signal comes almost entirely from the long exposure (except in places where the long exposure had a cosmic ray).

This procedure doesn't work all that well with such a large ratio of exposure times (i.e. the short exposure doesn't constrain cosmic rays in the long exposure very well). So, some extra cosmic ray zapping was performed. Beyond 70 pixels from the center of the star, everything greater than 8 DN (4 sigma) was zapped. Within 70 pixels of the center, cosmic rays were identified "by hand." Typically, there were about a dozen contaminated pixels that had not been detected by the automatic procedure. Pixels zapped this way were replaced by the average in a 3x3 box centered on the zapped pixel.

At this point, the data have been reduced to 15 images. With two exceptions, each image is the stack of a short and a long exposure which gives a dynamic range extending from 2 DN (the background noise level) up to as much as 27,000 DN. The two exceptions are the target acquisition image and the image in F487N at focus 15.3 mm. In the former case, there was no corresponding long exposure and in the latter case, the long exposure was ignored. The short exposure was used by itself in these two cases (with by hand zapping of cosmic rays). The acquisition exposure was scaled by 8.866 ($10.23 \times 2.6/3$) and

the other exposure by 10.23 so all exposures are on a uniform scale.

The noise in these images can be calculated as

$$\sigma = \sqrt{2^2 + \mathrm{DN}/7.5}\,,$$

where the first term in the square root is the effective read noise, the second term is the photon noise, and the factor 7.5 is the gain in electrons per DN. At the centers of the stacked images (where the signal level is greater than about 3600 DN), the image comes from the short exposure. In this case the data have been scaled by the factor $f = 10.23$ and the noise calculation is

$$\sigma = \sqrt{(2f)^2 + f\mathrm{DN}/7.5}\,,$$

which is always less than 2%. Note that this equation applies for the entire F487N image at focus 15.3 mm and it applies to the entire target acquisition image with $f = 8.866$.

The next step is the determination of the star center in each of these exposures. This was done by Gaussian smoothing the exposures and fitting the cores to a two dimensional Gaussian (six parameters: x position, y position, amplitude, x width, y width, and ellipticity) plus a constant background. This procedure worked well except in one case. For reasons which I haven't had time to track down, the y coordinate of the F487N image at focus 20.2 mm seems to be anomalous. A corrected coordinate was estimated by subtracting the (presumed) constant offset between the F889N and F487N exposures from the coordinate for the F889N image at focus 19 mm. The coordinate changed from 311.601 to 311.236 as a result of this procedure. The latter value agrees much better with a visual inspection of the image than does the former. The estimated coordinates are listed in Table 3. The average difference between the coordinates in the corresponding F889N and F487N images is $(-0.867, +0.365)$ with an rms of $(0.198, 0.187)$ (These were computed before the anomalous y coordinate was corrected.) Thus the coordinates listed in Table 3 should be accurate to about 0.14 pixels (1σ). Note that the coordinates increase with focus. Presumably this is due to the change in plate scale with focus which causes the distance between the target star and the guide stars to vary. To see if this is reasonable, note that the total change in coordinates is roughly 2.5 pixels or 0.1 arcseconds. This is for a change in secondary mirror despace of 114 microns. A ray trace shows that the guide stars should shift (relative to the center of the field) by something like 30% of this amount. The observed coordinate shift with focus is not currently understood.

After the centers were determined, the images were resampled into a 256×256 subimage with the center of the star placed in the center of pixel (129,129). The resampling was done with a bi-cubic spline interpolation technique which preserves the total flux. The total DN in each image is listed as the last column in Table 3. The consistency of the total counts provides a check on the photometric accuracy and the overall reduction procedure. The peak-to-peak variation of the seven F487N images is just 1% and that for the F889N images is almost as good at 1.7%. The rms values are 0.3% and 0.6%, respectively. Note that this calculation tests both the accuracy of background subtraction

Table 3. Star Coordinates and DN

Focus (mm)	Filter	x pixels	y pixels	Total DN
10.7	F487N	253.407	290.114	807971
10.7	F487N	243.946	309.774	829155
12.2	F487N	244.083	309.871	829972
13.7	F487N	244.268	310.079	828040
15.3	F487N	244.450	310.356	835559
17.2	F487N	244.707	310.790	830085
20.2	F487N	245.011	311.236	831632
23.2	F487N	245.074	311.918	834965
10.7	F889N	243.414	310.317	756515
12.2	F889N	243.315	310.389	752112
13.7	F889N	243.437	310.536	757169
15.3	F889N	243.571	310.755	755928
17.2	F889N	243.615	311.056	757694
20.2	F889N	243.899	311.598	762523
23.2	F889N	244.219	312.290	765294

as well as the overall photometry. One might expect that the background level is variable at the level of a tenth of a DN or so. This is confirmed by visual inspection of the images. Since 65536 pixels contribute to the total DN listed in Table 3, a peak-to-peak variation of 0.1 DN and 0.2 DN in the mean background level can account for the peak-to-peak variation in the total DN in the F487N and F889N images, respectively. The uncertainty in the background level is the major source of error in the encircled energy values discussed in the next section.

4. ENCIRCLED ENERGIES

Point spread functions (PSFs) and encircled energy functions (EEFs) were computed by an algorithm which sums the values of all pixels whose centers lie within successive annuli centered on pixel (129,129) in the resampled images described in the previous section. The first annulus has radii 0 and 0.25 pixels. All other annuli have radii $0.5n \pm 0.25$ pixels where n is an integer. Some annuli contain no pixels! This is not a problem for the EEFs, but for the PSFs, the widths of the annuli were increased so the first annulus has inner and outer radii 0 and 0.75 pixels and the others have radii $n + 0.25 \pm 0.5$ pixels, where again, n is an integer.

The sum of all annuli up to some given annulus is the encircled energy within the outer radius of the last annulus included in the sum. For small radii, the aperture is not exactly a circle. For example, the first five annuli include pixels arranged as follows:

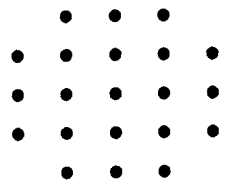

Below, the energy contained within these 21 pixels is listed as the encircled energy within $r = 0''.099$ which corresponds to the outer radius (2.25 pixels) of the fifth annulus, assuming a scale of $0''.044$ per pixel. Similarly, the first ten annuli approximate what would be found in a circular aperture of radius $0''.209$:

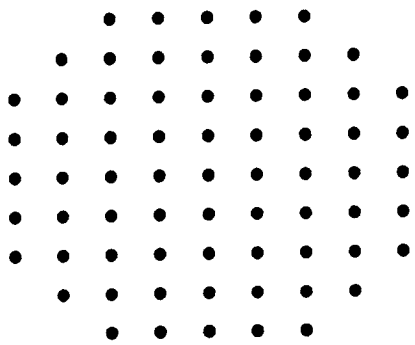

The point is that the encircled energies do not correspond exactly to circular apertures, because the pixel size is an appreciable fraction of the aperture radius. However, for comparing the change in encircled energy as a function of focus, this presents no problem.

The next concern was the overall normalization of the EEFs. After plotting and studying the EEFs, it was decided to normalize the EEFs to unit energy within a radius of $5''.0$. Figure 1 shows all fifteen EEFs. The point of this figure is to show the good agreement among the EEFs at large radii.

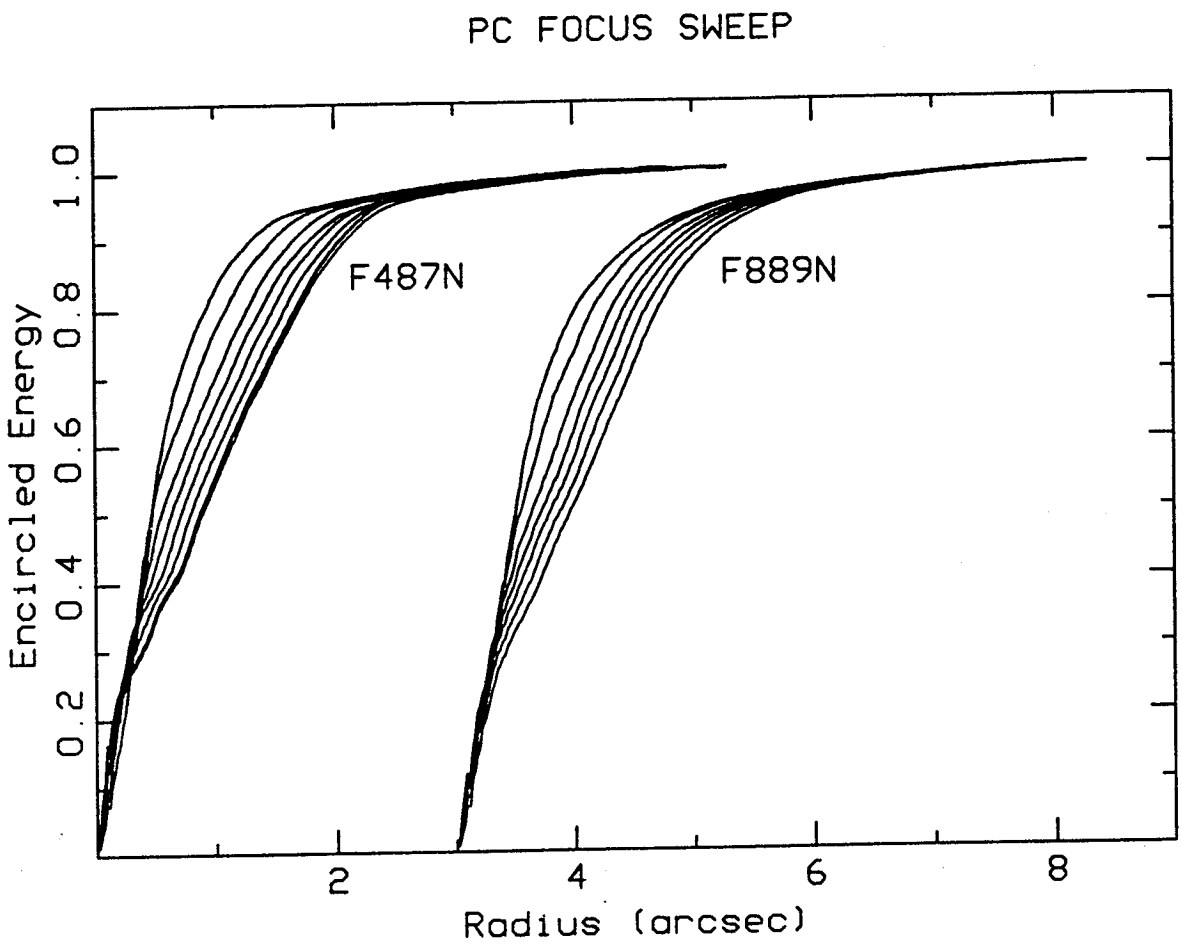

Figure 1. EEFs for all images obtained in the PC focus sweep. F889N EEFs have been shifted to the right by 3″.0.

The full EEFs for the F487N data are plotted in Figure 2. Here there are offsets between the curves, so that each one may be seen clearly. Similarly, the full EEFs for the F889N data are plotted in Figure 3. Figures 4 and 5 show the region within 0″.3 more clearly. The geometrical "edge" of the image occurs at about $r = 2''.4$ for focus 10.7 mm and moves inwards to about $r = 1''.6$ at focus 23.2 mm. The light occuring beyond this geometrical edge is entirely due to diffraction and scattering. Presumably, this light would be out there even if the primary mirror had no spherical aberration.

From the EEFs, values at five selected radii were extracted and are listed in Table 4. The main source of error in these numbers is the uncertainty in the background level. As mentioned above, this amounts to 0.3 and 0.6% rms for the F487N and F889N data, respectively. To these numbers, 0.2% has been arbitrarily added to account for centering uncertainties and any other source of uncertainty. The adopted errors are then 0.5 and 0.8%. The agreement between the values for the target acquisition image and the F487N

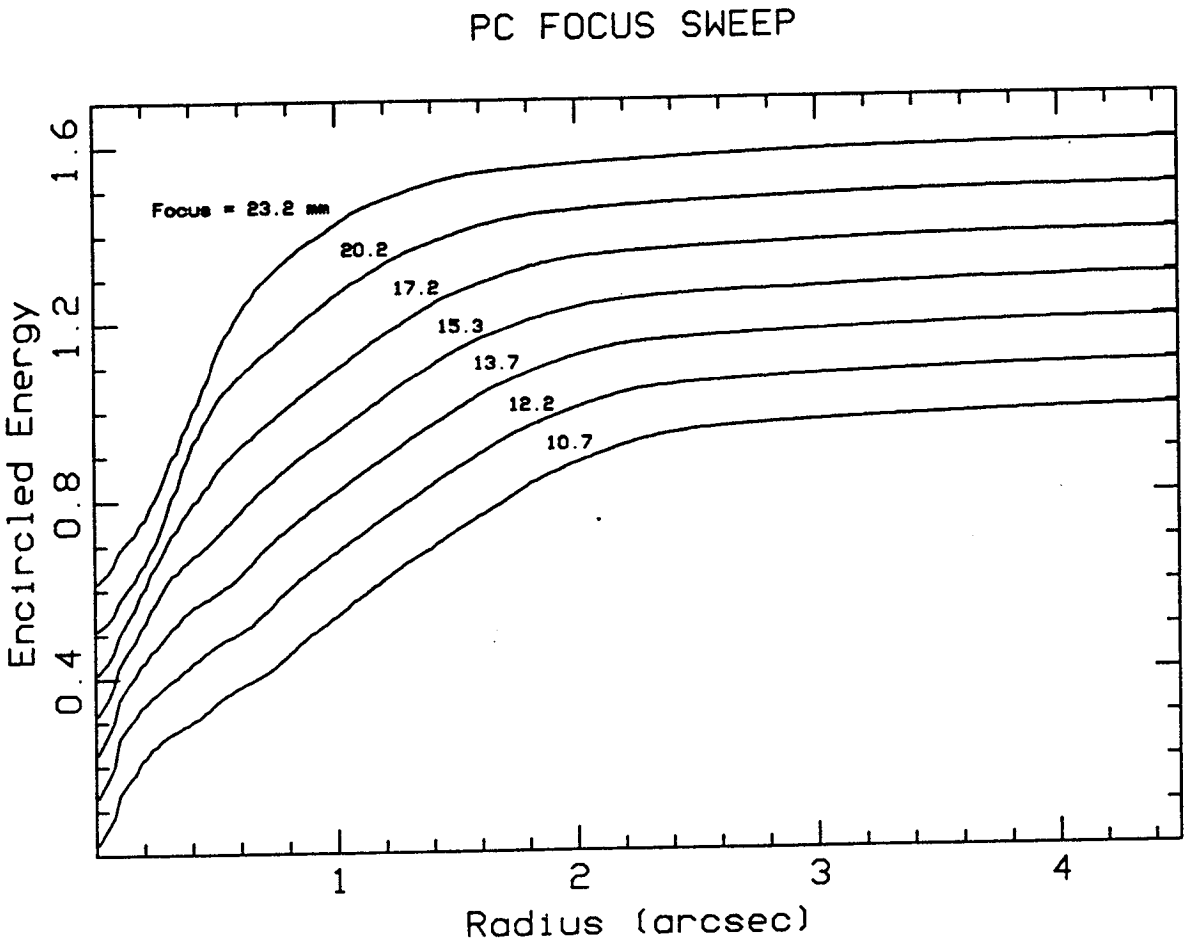

Figure 2. EEFs for the F487N PC focus sweep data. EEFs for successive focus settings are shifted up by 0.1.

image at focus 10.7 mm (which should be identical except for the small difference in the location of the star on the detector) supports these estimates.

The data in Table 4 are plotted in Figure 6. Of most interest are the encircled energies for an aperture radius of 0″.1 as this is the radius on which the focus setting is based. Data for this radius are plotted in Figure 7 along with cubic spline interpolated curves. The curves have structure which is similar to structure seen in curves based on modelling.

In order to determine the focus at the maximum encircled energy, three estimates were made: First, the peak of a parabola passing through the two highest points on the curve and the point at the next lower focus setting was determined. Second, the peak of a parabola passing through the two highest points on the curve and the point at the next higher focus setting was determined. Finally, the peak of the cubic spline was determined. For F487N, these procedures gave focus settings at the peak of 12.5, 11.7, and 12.4 mm.

Table 4. Encircled Energy versus Radius and Focus

Focus (mm)	Filter	Radius 0″.099	0″.209	0″.297	0″.495	1″.001
10.7	F487N	0.1369	0.2240	0.2729	0.3458	0.5494
10.7	F487N	0.1373	0.2213	0.2671	0.3395	0.5385
12.2	F487N	0.1640	0.2407	0.2859	0.3715	0.5834
13.7	F487N	0.1530	0.2388	0.2991	0.3889	0.6173
15.3	F487N	0.1272	0.2273	0.3146	0.4165	0.6533
17.2	F487N	0.0973	0.2064	0.3021	0.4570	0.6935
20.2	F487N	0.0738	0.1604	0.2706	0.5134	0.7640
23.2	F487N	0.0864	0.1614	0.2652	0.5157	0.8242
10.7	F889N	0.0832	0.1645	0.2234	0.3202	0.5062
12.2	F889N	0.1014	0.1917	0.2496	0.3439	0.5361
13.7	F889N	0.1155	0.2085	0.2689	0.3671	0.5711
15.3	F889N	0.1156	0.2160	0.2821	0.3890	0.6112
17.2	F889N	0.1067	0.2119	0.2911	0.4145	0.6611
20.2	F889N	0.0969	0.1852	0.2793	0.4559	0.7272
23.2	F889N	0.0680	0.1529	0.2603	0.4785	0.7863

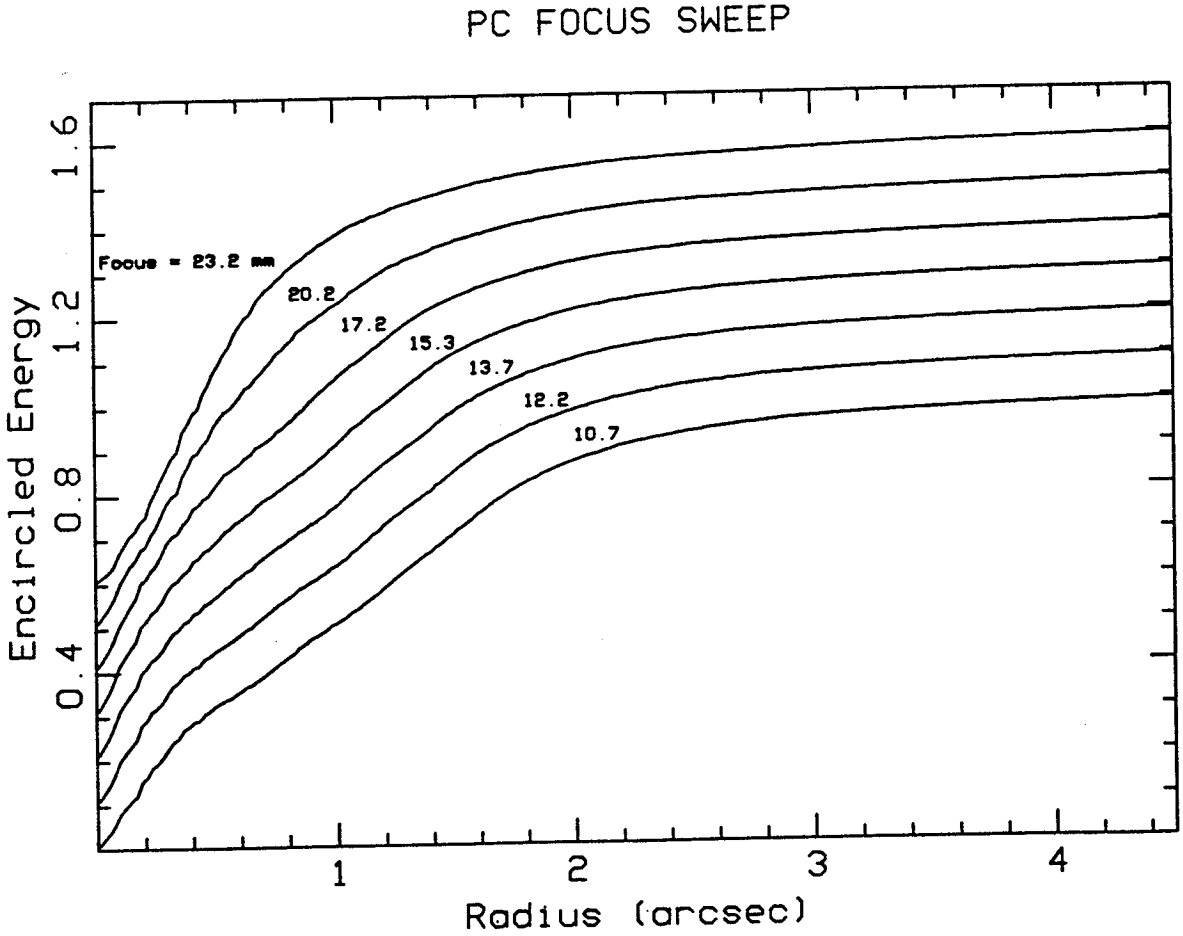

Figure 3. EEFs for the F889N PC focus sweep data. EEFs for successive focus settings are shifted up by 0.1.

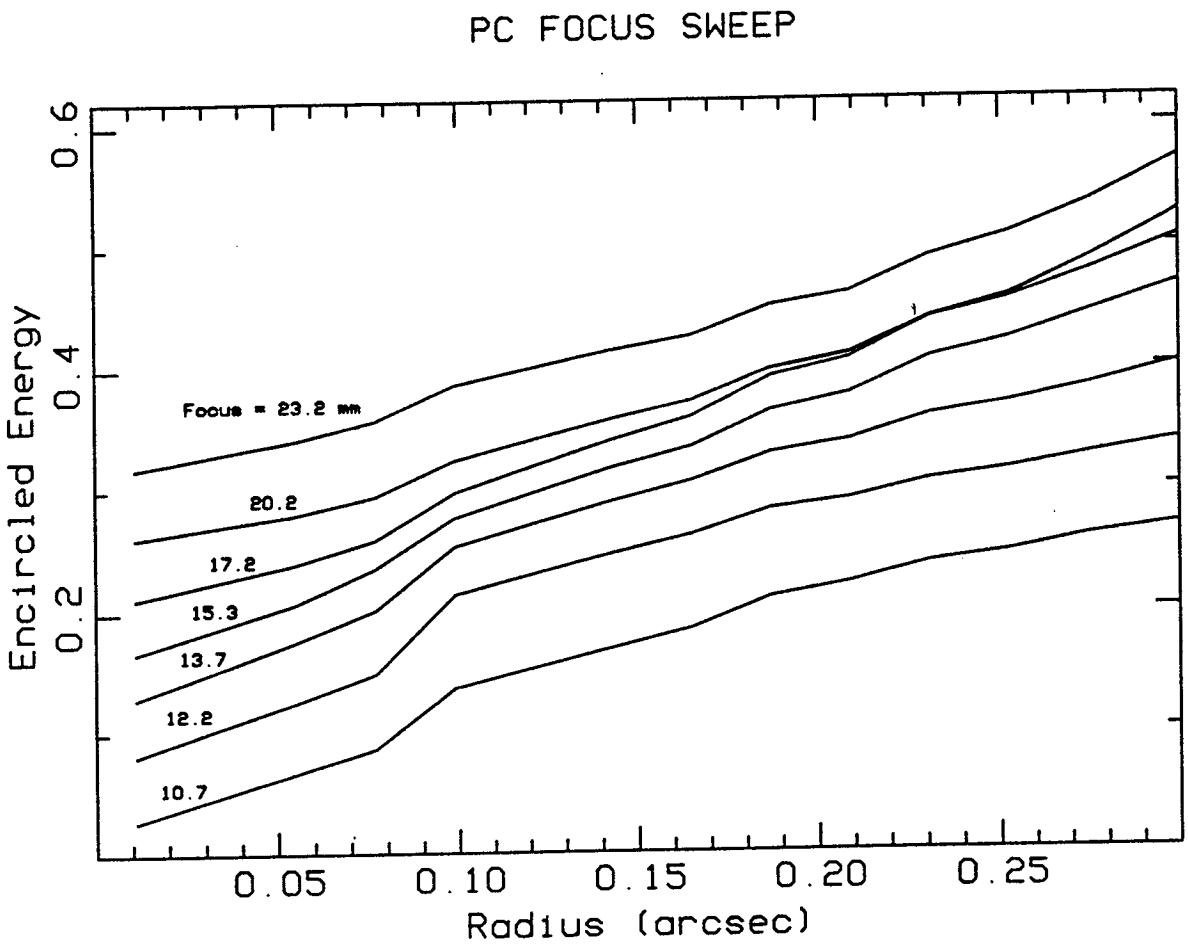

Figure 4. EEFs for the F487N PC focus sweep data. This plot shows the behavior at small radii. EEFs for successive focus settings are shifted up by 0.05.

For F487N, one concludes that the peak of the encircled energy function occurs at focus 12.2 ± 0.3 mm. In all cases, the values of the peak encircled energy were in very good agreement at 0.165 ± 0.001. For F889, the three procedures gave focus settings of 14.5, 14.5, and 14.4 mm, and one concludes the peak occurs at 14.5 ± 0.1 mm from paraxial focus. Here again, the peak values were all in agreement at 0.117 ± 0.001 peak encircled energy fraction.

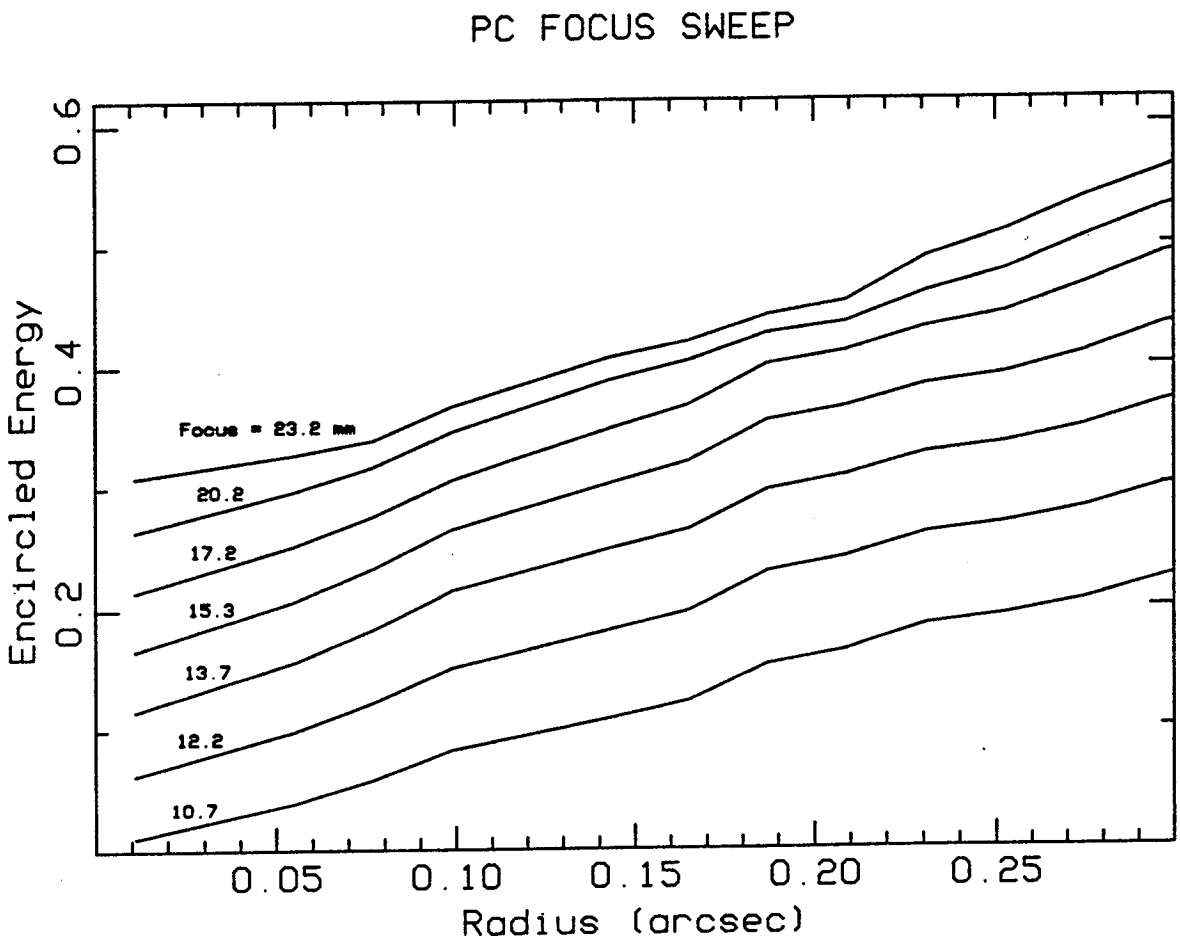

Figure 5. EEFs for the F889N PC focus sweep data. This plot shows the behavior at small radii. EEFs for successive focus settings are shifted up by 0.05.

5. POINT SPREAD FUNCTIONS

For completeness, the azimuthally averaged point spread functions for the focus sweep images are shown in Figures 8 (F487N data) and 9 (F889N data). These functions were computed as described in the previous sections.

In addition, the images themselves are shown in Figures 10 through 24. Each image is displayed at four different stretches: 0 to 1/3, 1/15, 1/75, and 1/375 the peak value.

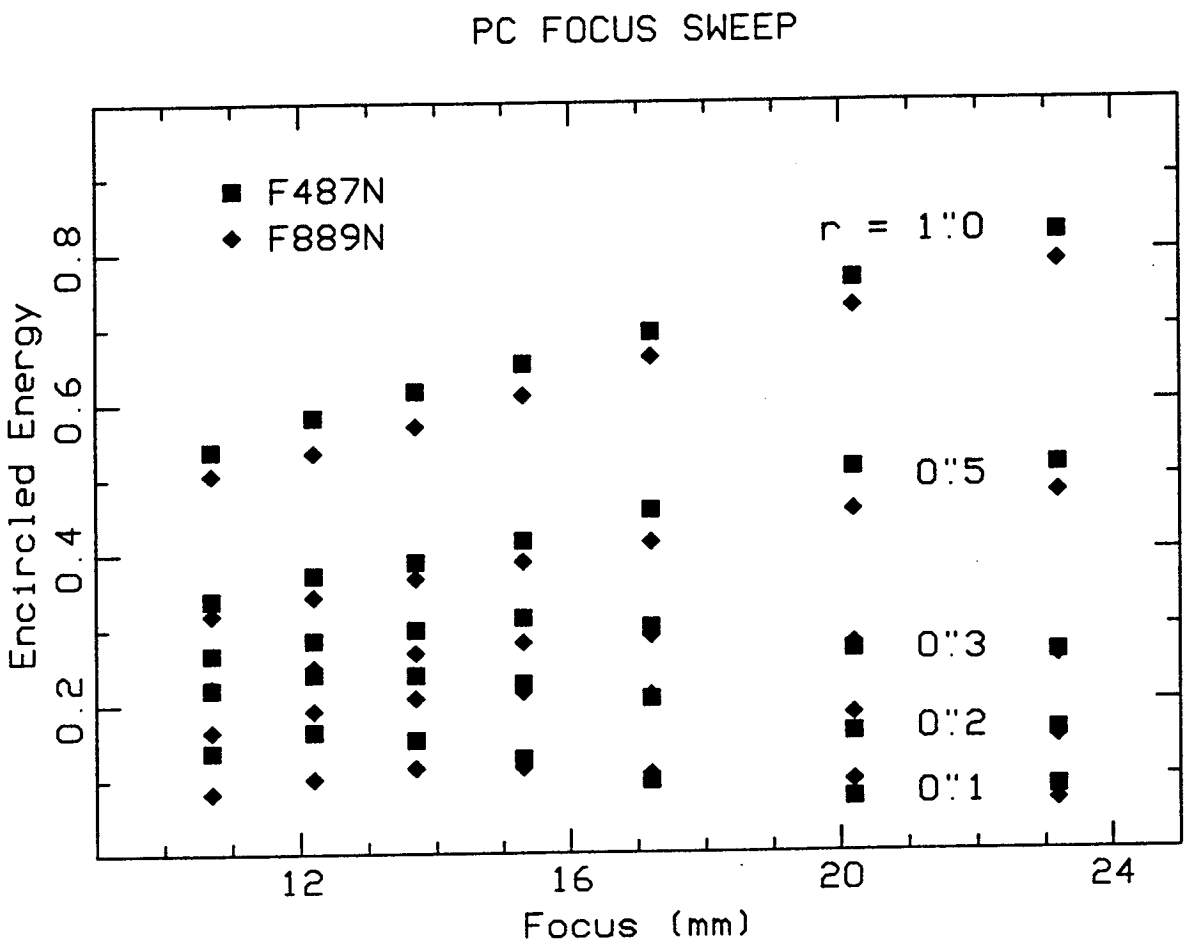

Figure 6. Encircled energy versus focus setting and aperture radius. Error bars are smaller than the points. The data plotted here are listed in Table 4.

6. CONCLUSION

Most WFPC science occurs at visible to near IR wavelengths, so focus settings between 12.2 and 14.5 mm from paraxial focus would be optimum for WFPC science. Of course, the focus setting must optimize the science of the entire observatory and UV science is optimized at smaller focus settings.

The implementation of the focus sweep required the efforts of many people: I wish to acknowledge and thank the members of the OAP, Peg Stanley and her planning and scheduling staff, Al Holm and his staff at the OSS, the staff at the support center at GSFC, and surely many others, for making this endeavor a success.

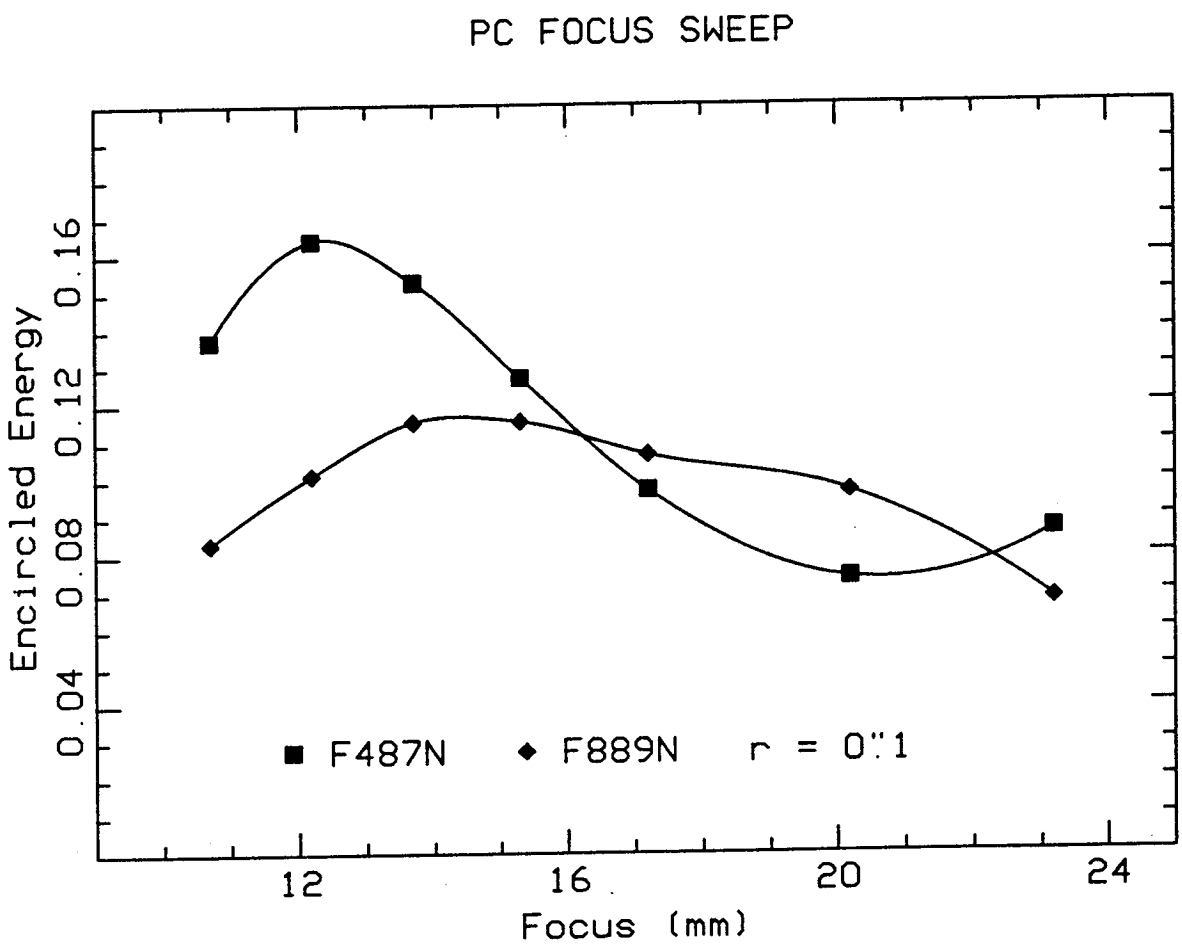

Figure 7. Encircled energy versus focus for an aperture radius of 0″.1. Error bars are smaller than the points. The curves are a cubic spline forced to pass through the points.

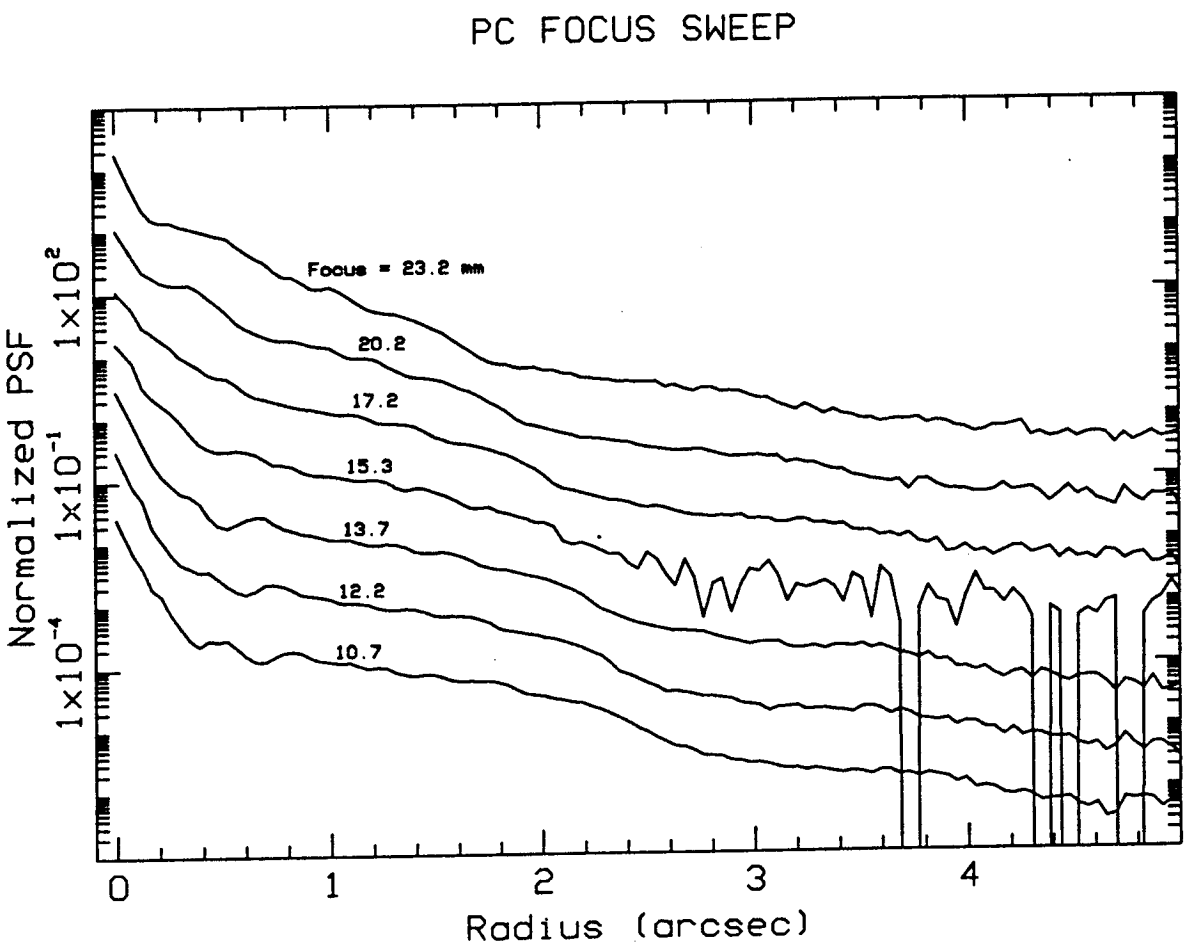

Figure 8. Point spread functions for the F487N PC focus sweep data. Curves for successive focus settings have been multiplied by a factor of 10. The PSF at focus 15.3 mm is noisy at large radii because the long exposure could not be used. Bumps and wiggles at small radii are not noise but real structure in the PSFs.

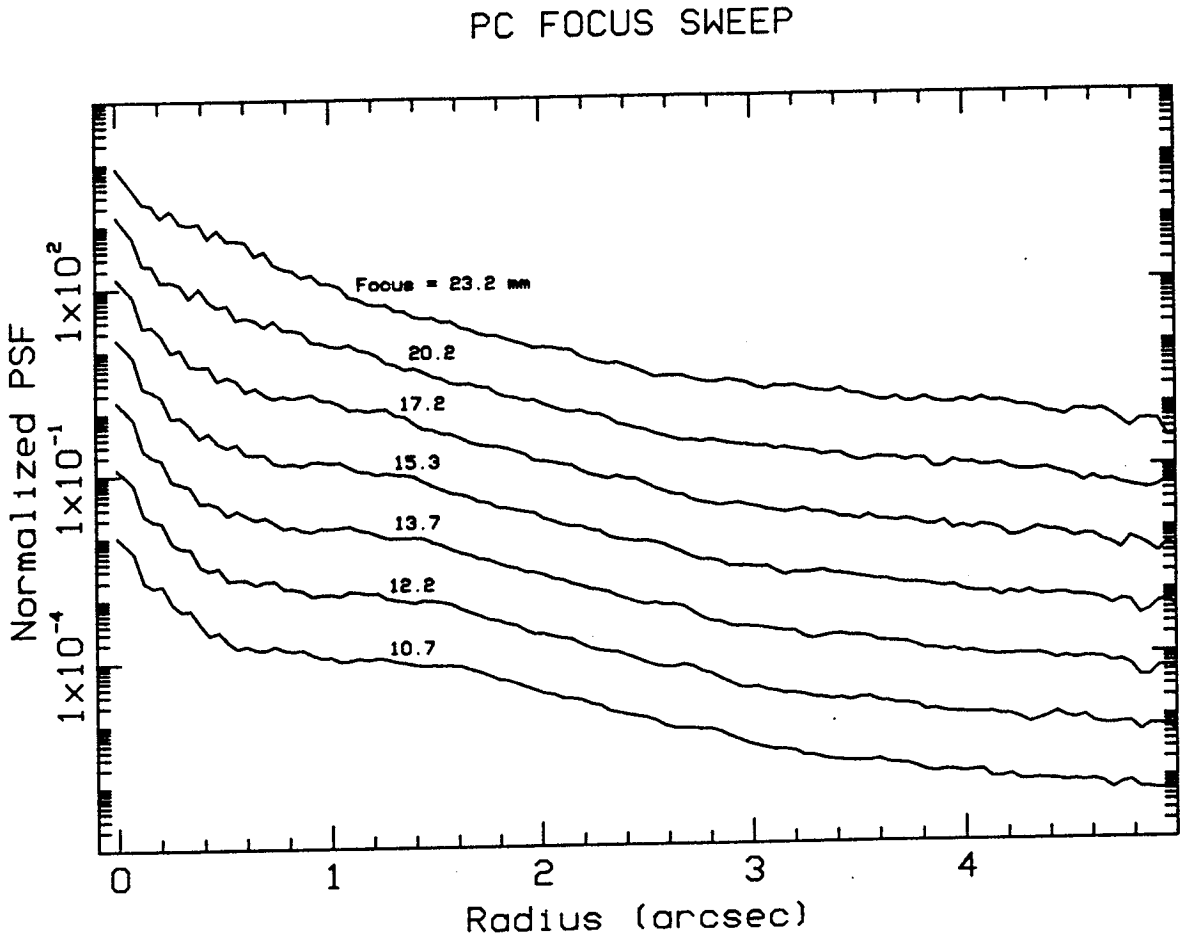

Figure 9. Point spread functions for the F889N PC focus sweep data. Curves for successive focus settings have been multiplied by a factor of 10. Bumps and wiggles at small radii are not noise but real structure in the PSFs.

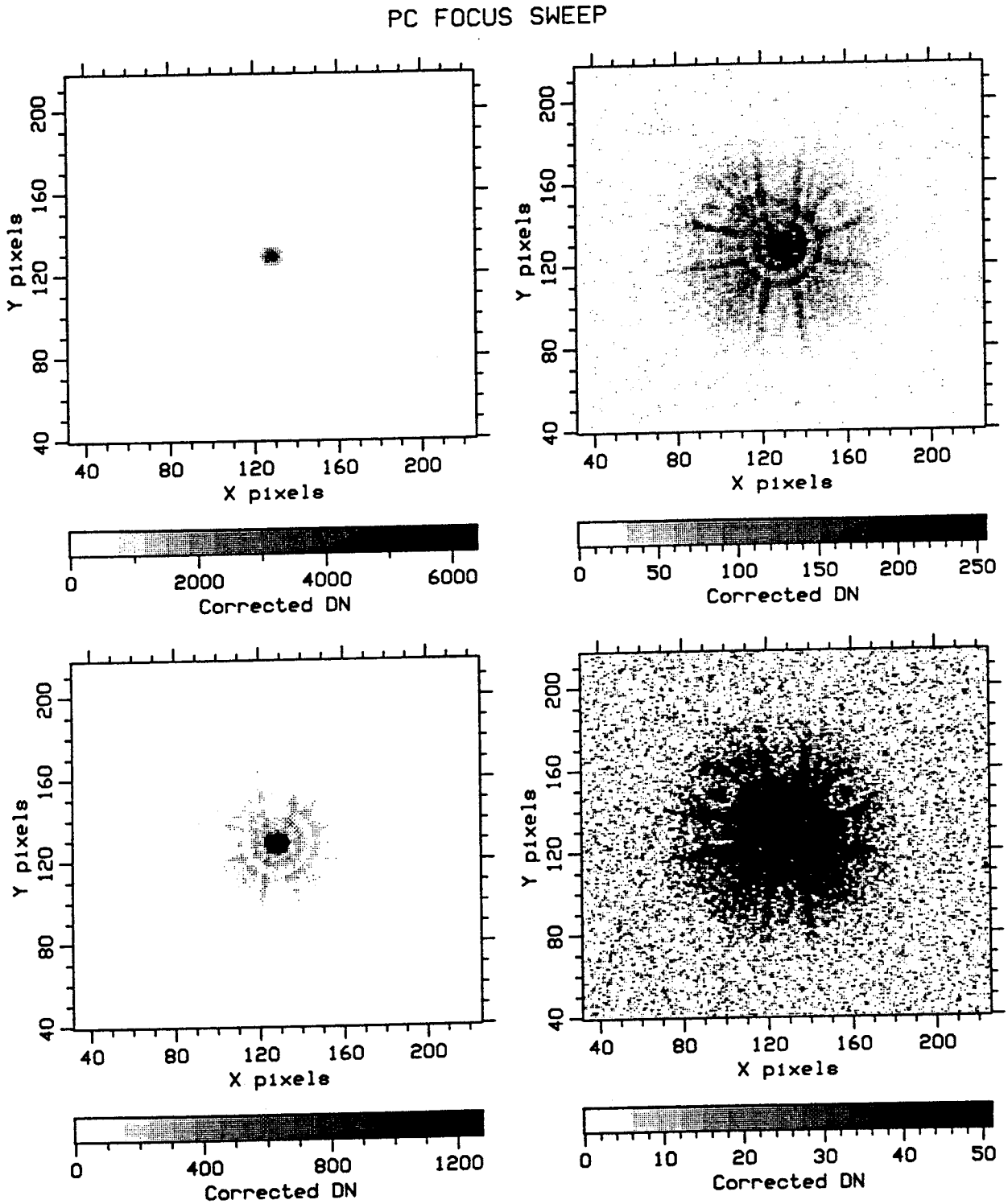

Figure 10. The PC focus sweep F487N target acquisition image shown at four stretches. It is noisy at the deepest stretch, because there was no long exposure taken during target acquisiton.

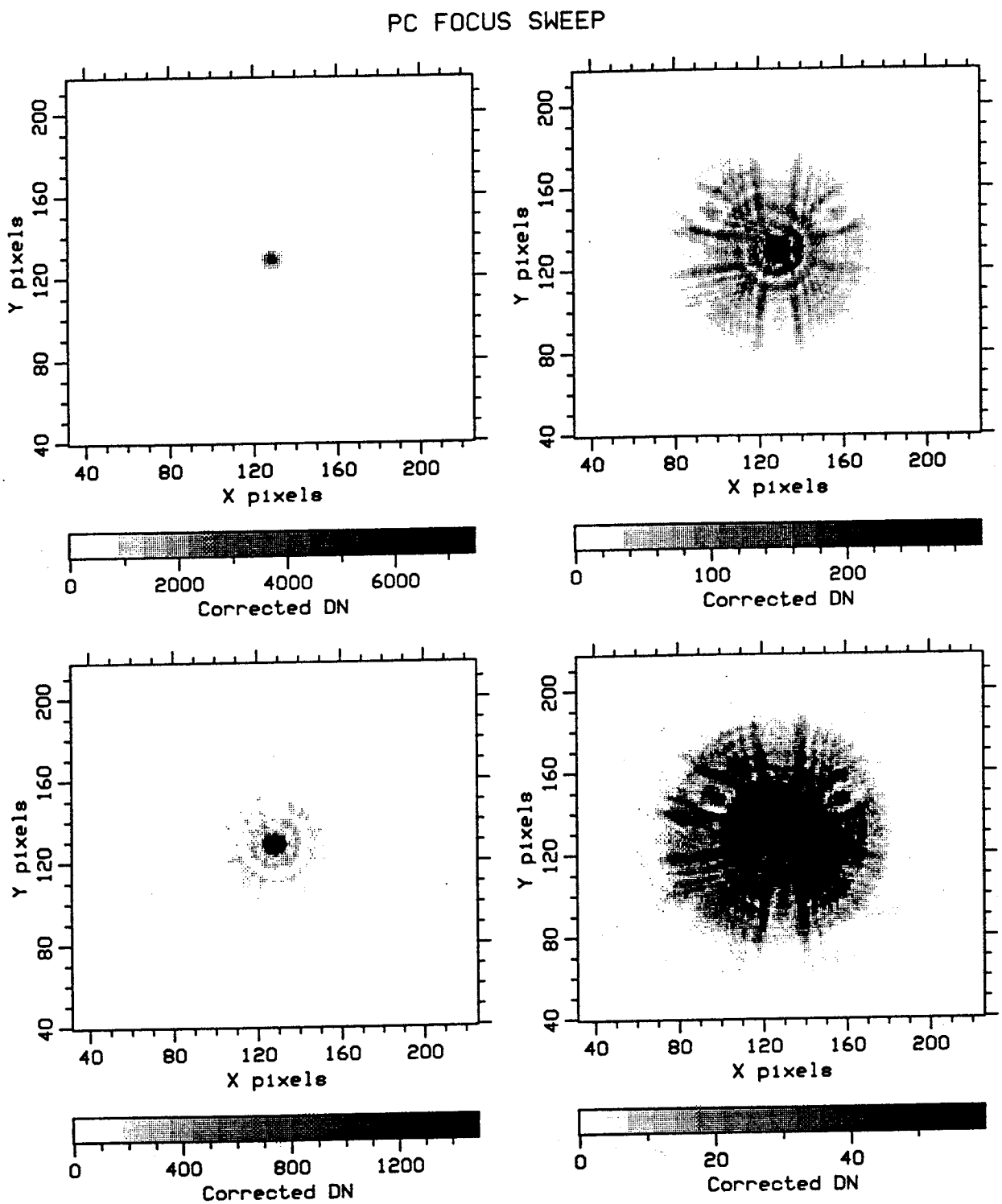

Figure 11. The PC focus sweep F487N image for focus 10.7 mm shown at four stretches.

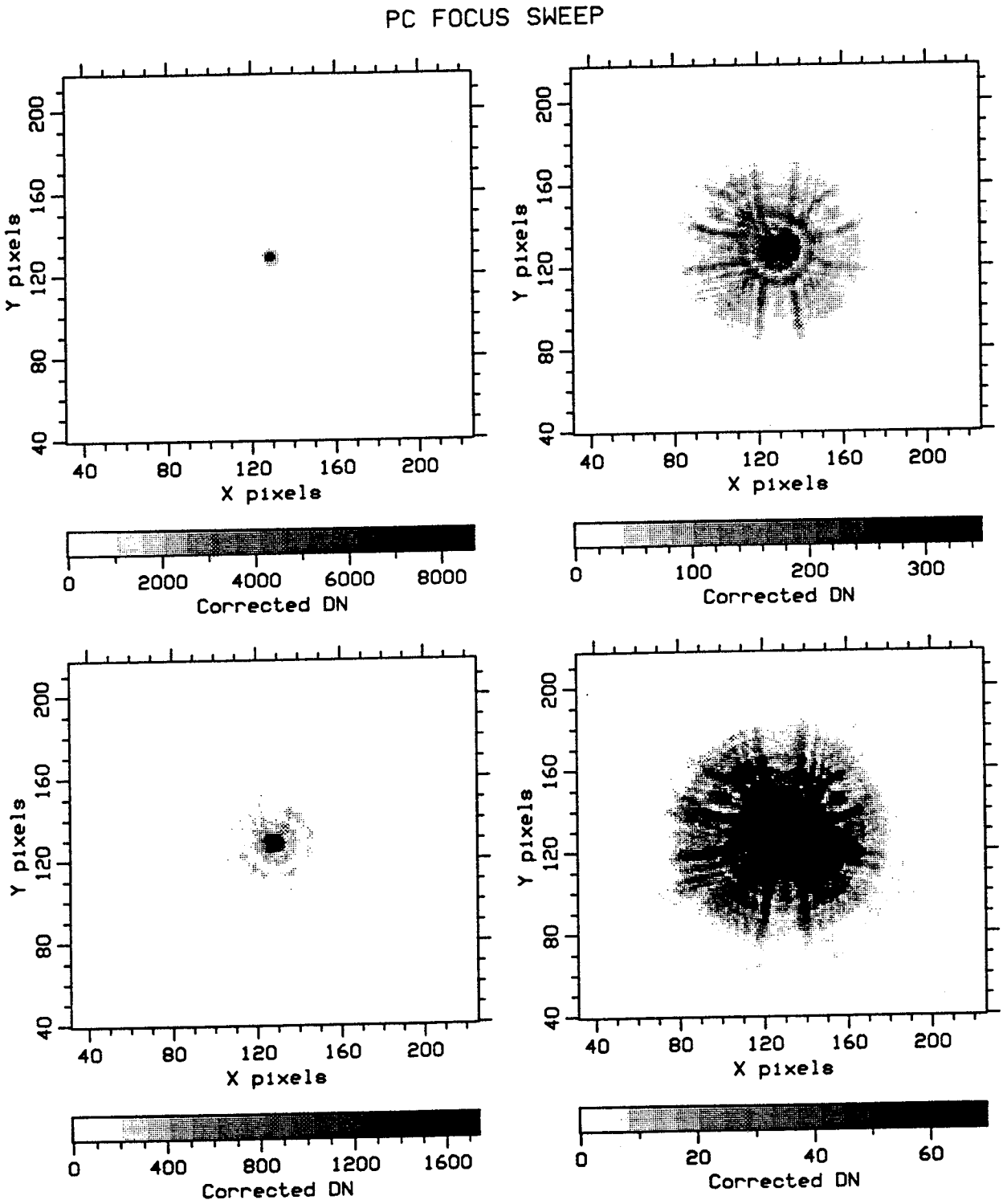

Figure 12. The PC focus sweep F487N image for focus 12.2 mm shown at four stretches.

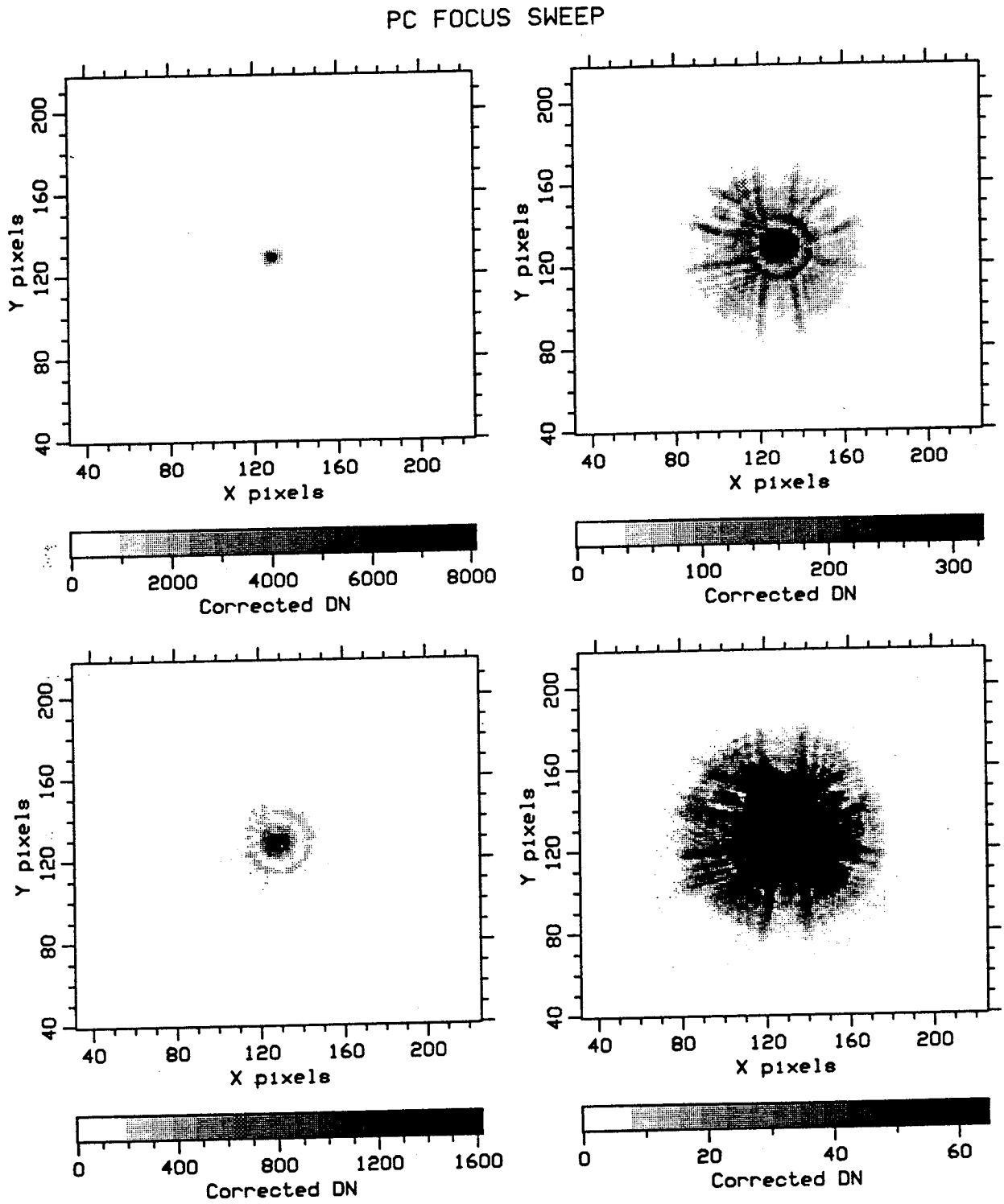

Figure 13. The PC focus sweep F487N image for focus 13.7 mm shown at four stretches.

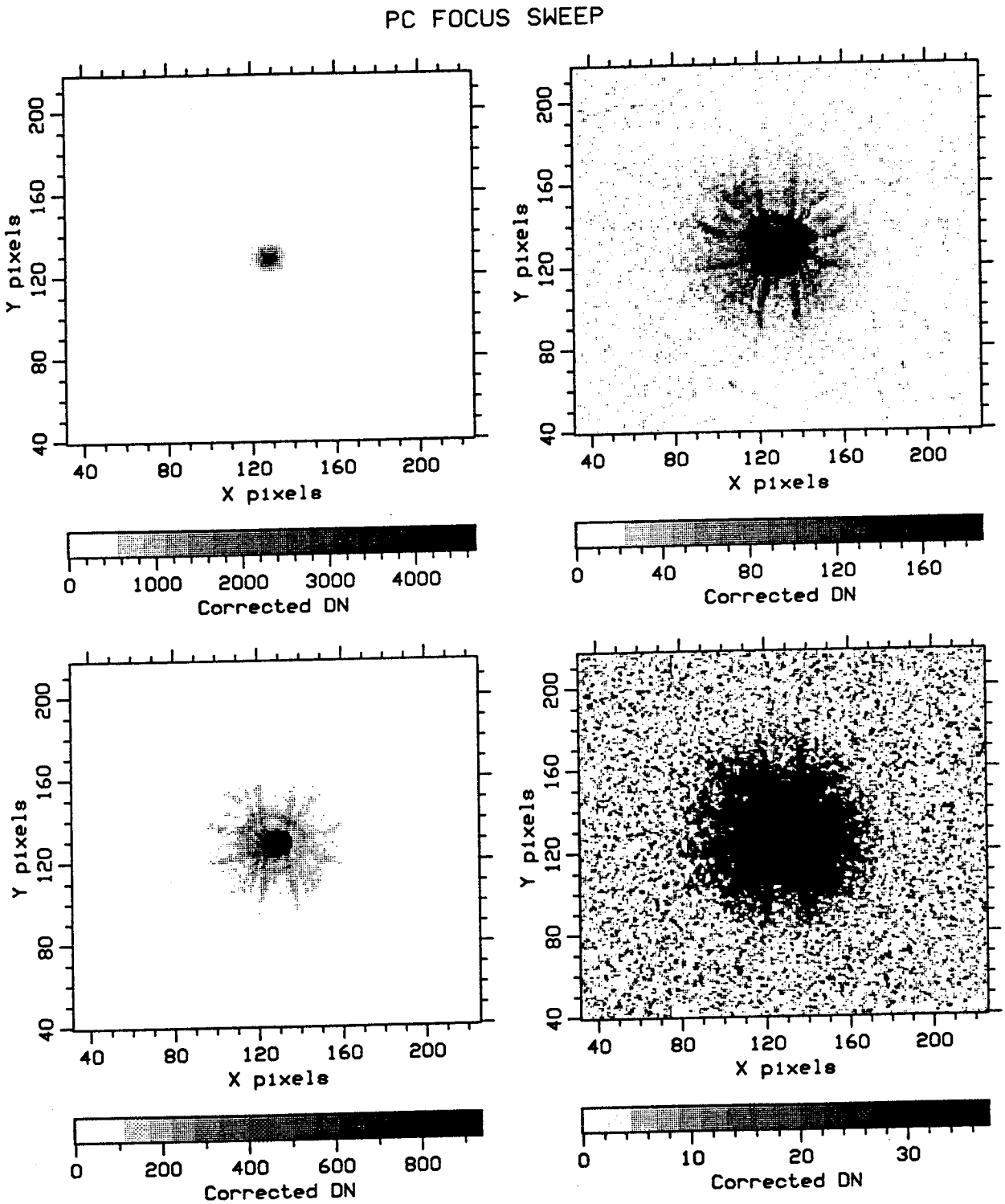

Figure 14. The PC focus sweep F487N image for focus 15.3 mm shown at four stretches. It is noisy at the deepest stretch, because the long exposure at this focus setting was mispointed and was not used.

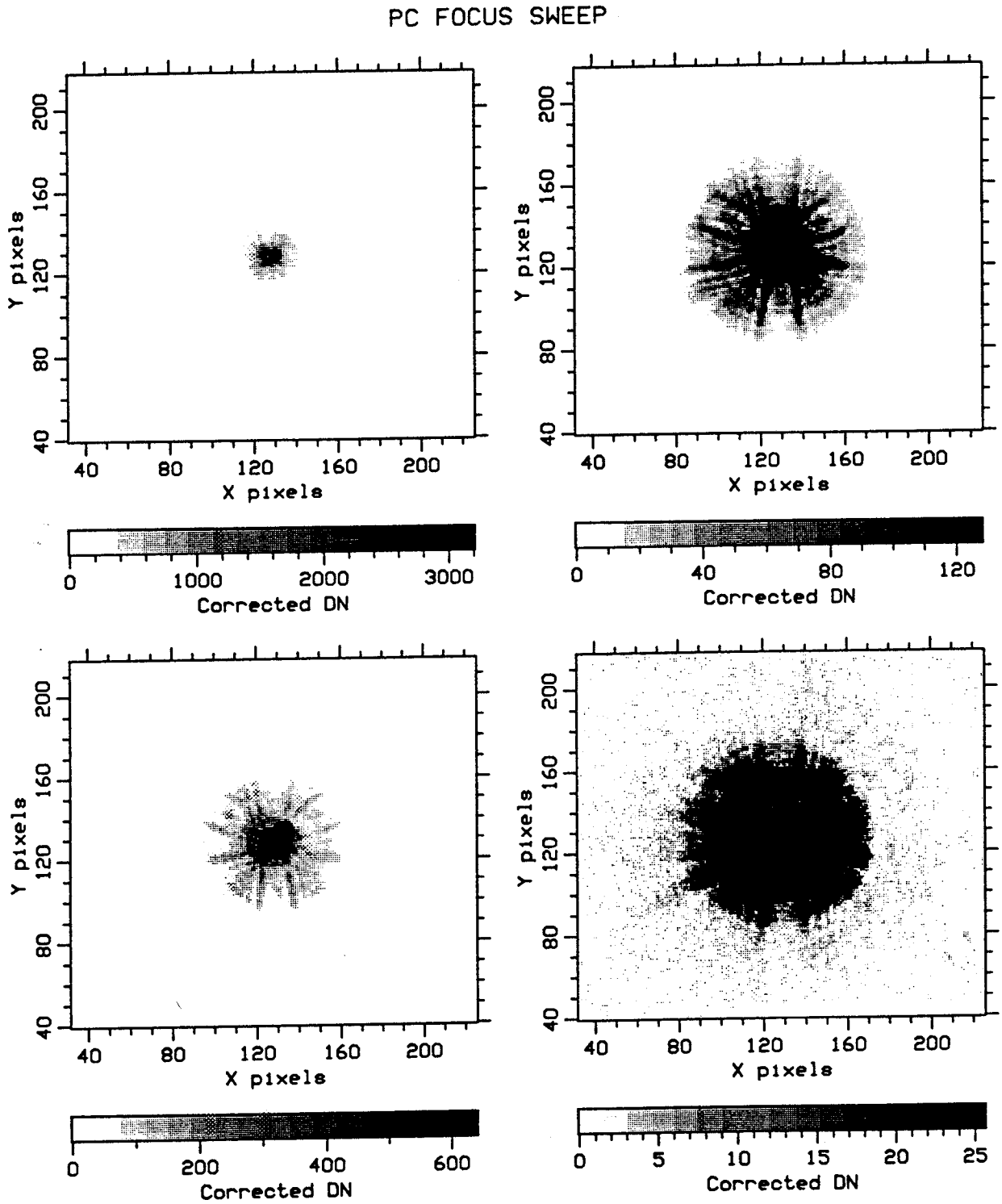

Figure 15. The PC focus sweep F487N image for focus 17.2 mm shown at four stretches.

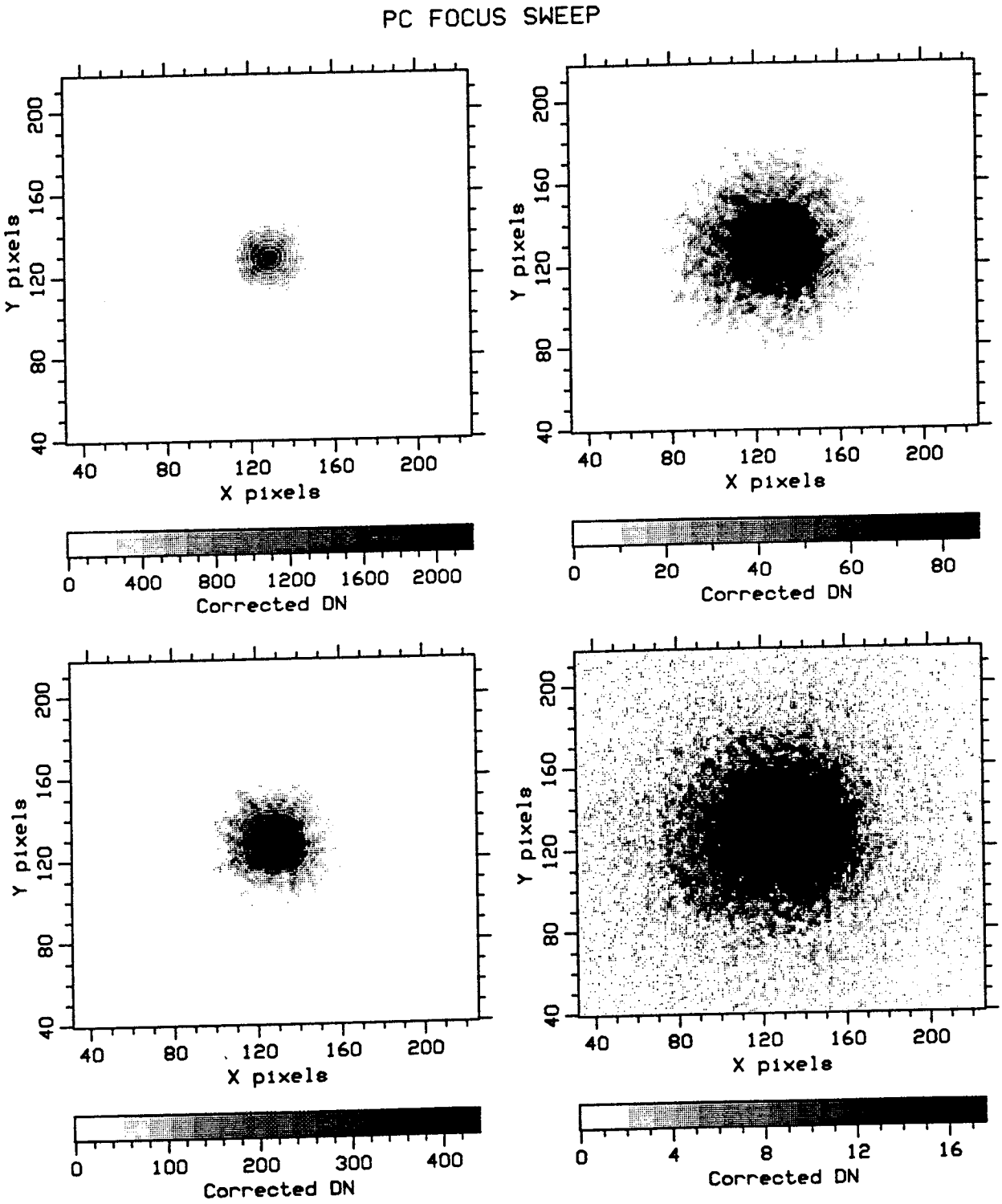

Figure 24. The PC focus sweep F889N image for focus 23.2 mm shown at four stretches.

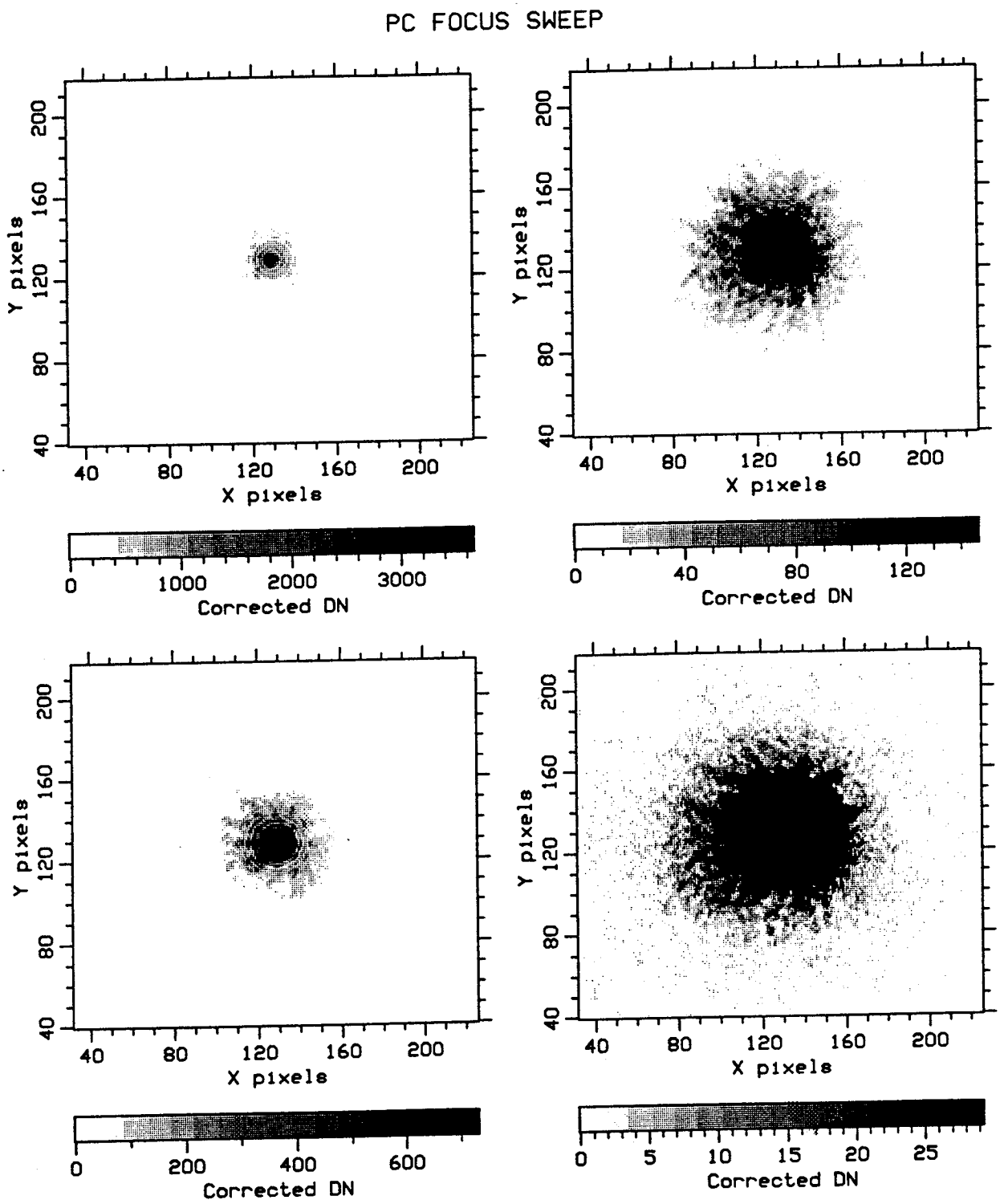

Figure 23. The PC focus sweep F889N image for focus 20.2 mm shown at four stretches.

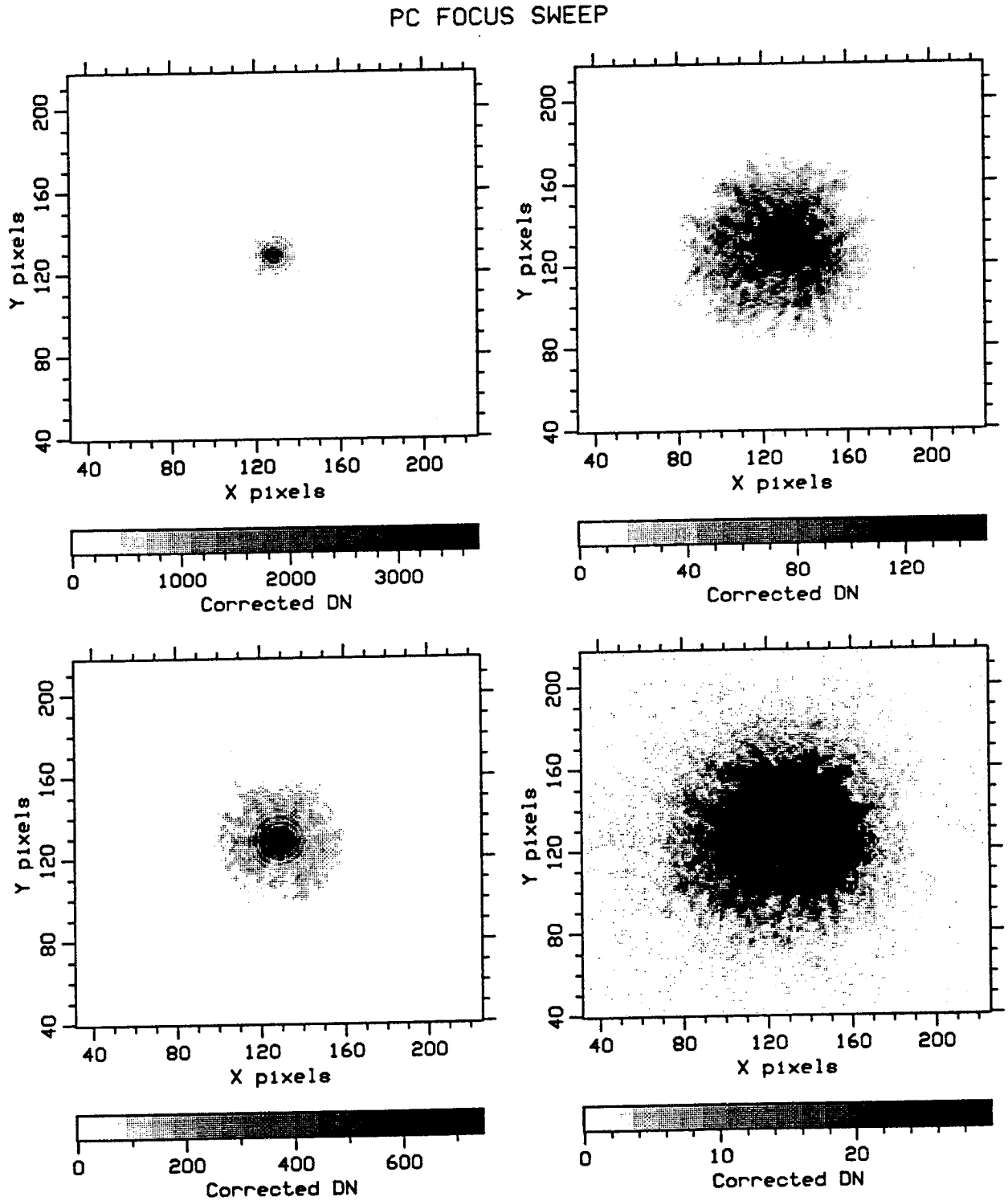

Figure 22. The PC focus sweep F889N image for focus 17.2 mm shown at four stretches.

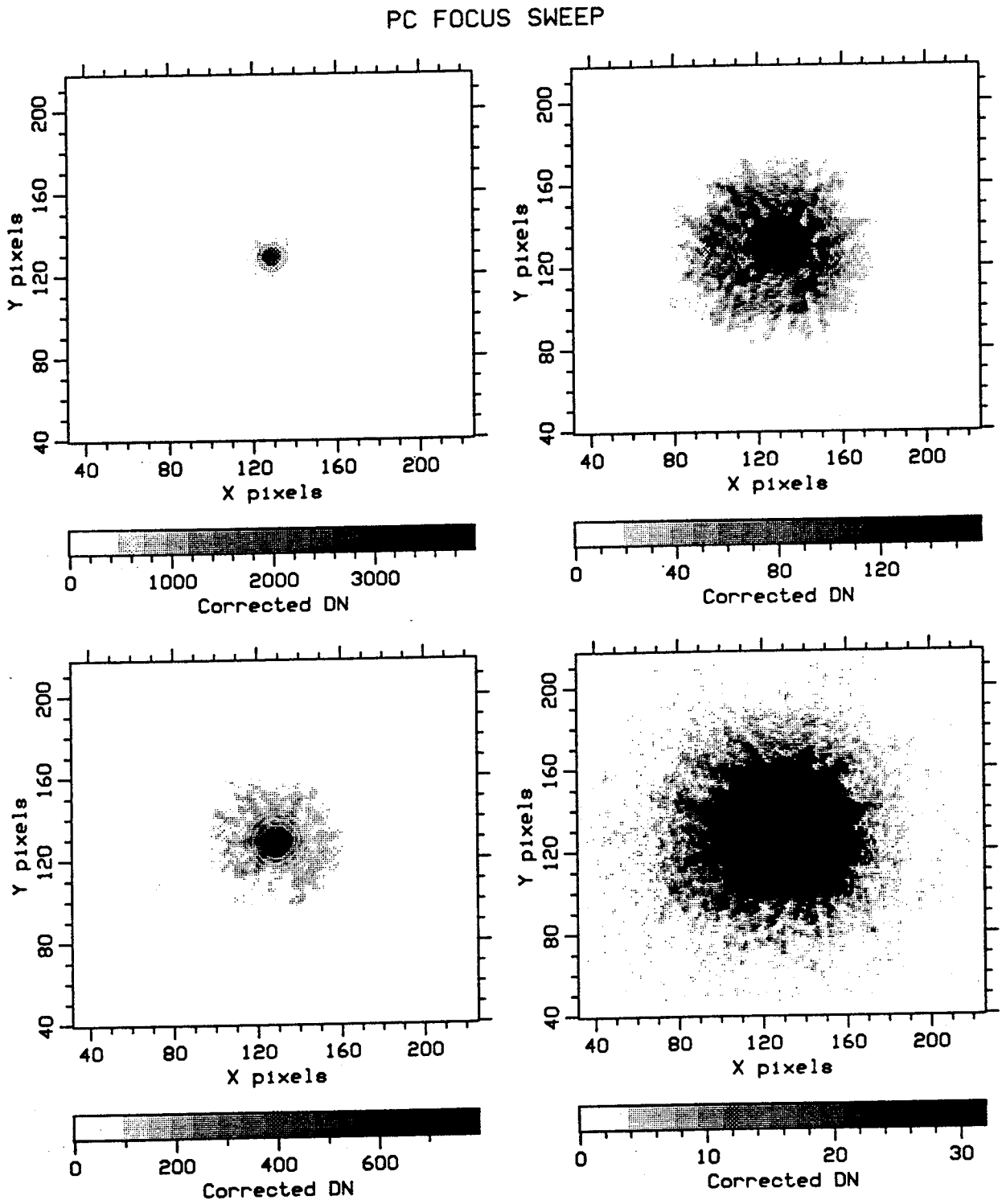

Figure 21. The PC focus sweep F889N image for focus 15.3 mm shown at four stretches.

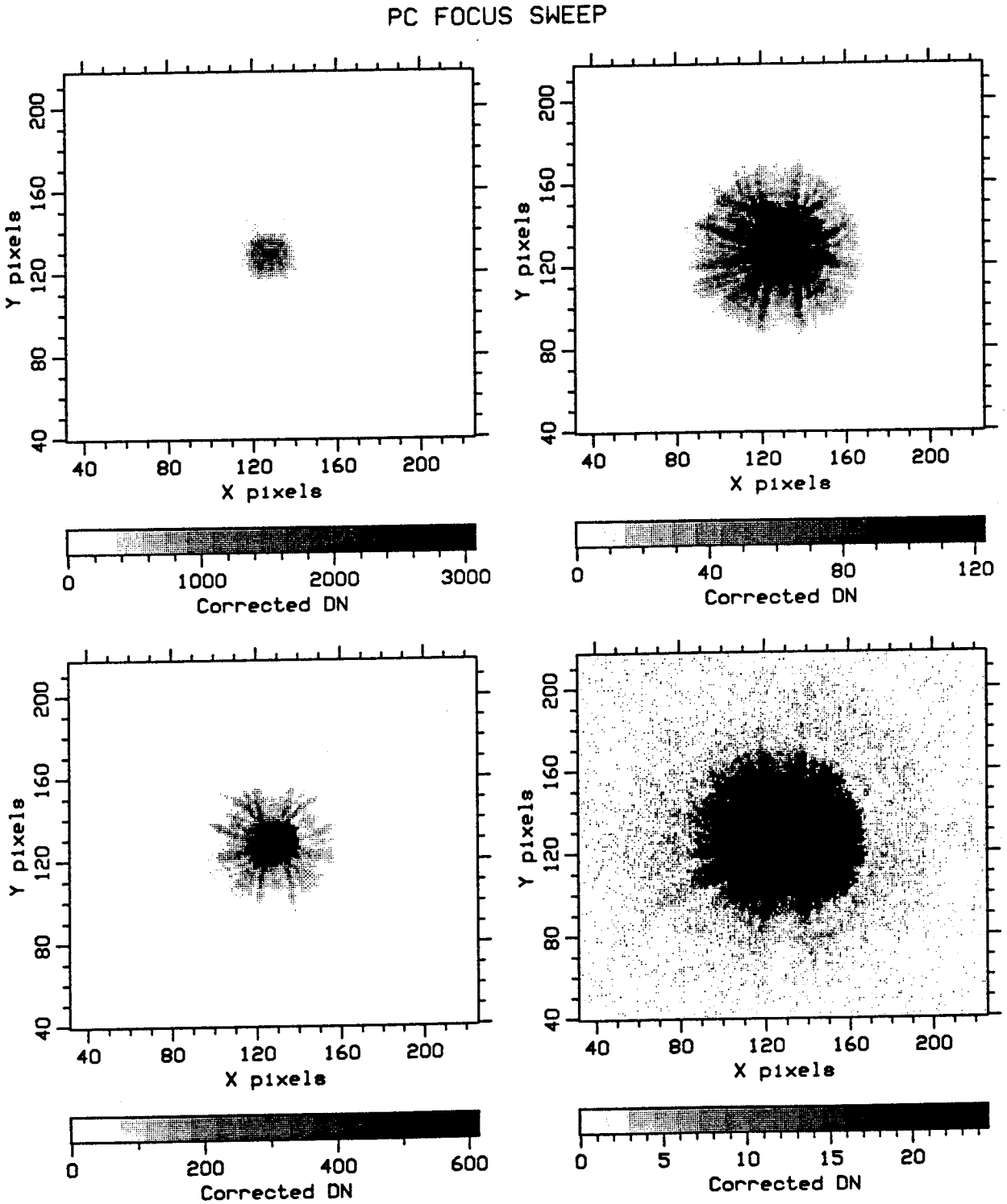

Figure 16. The PC focus sweep F487N image for focus 20.2 mm shown at four stretches.

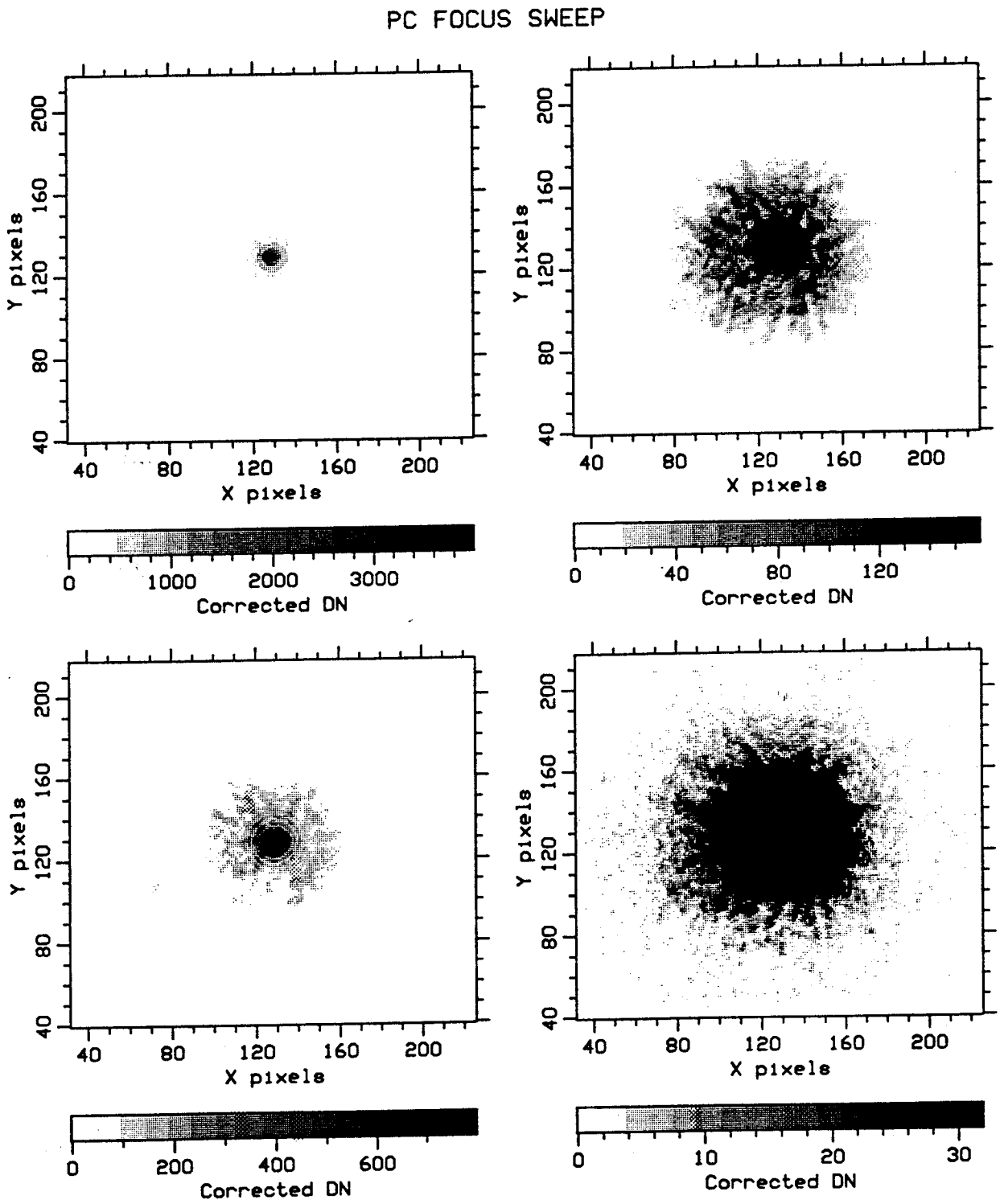

Figure 21. The PC focus sweep F889N image for focus 15.3 mm shown at four stretches.

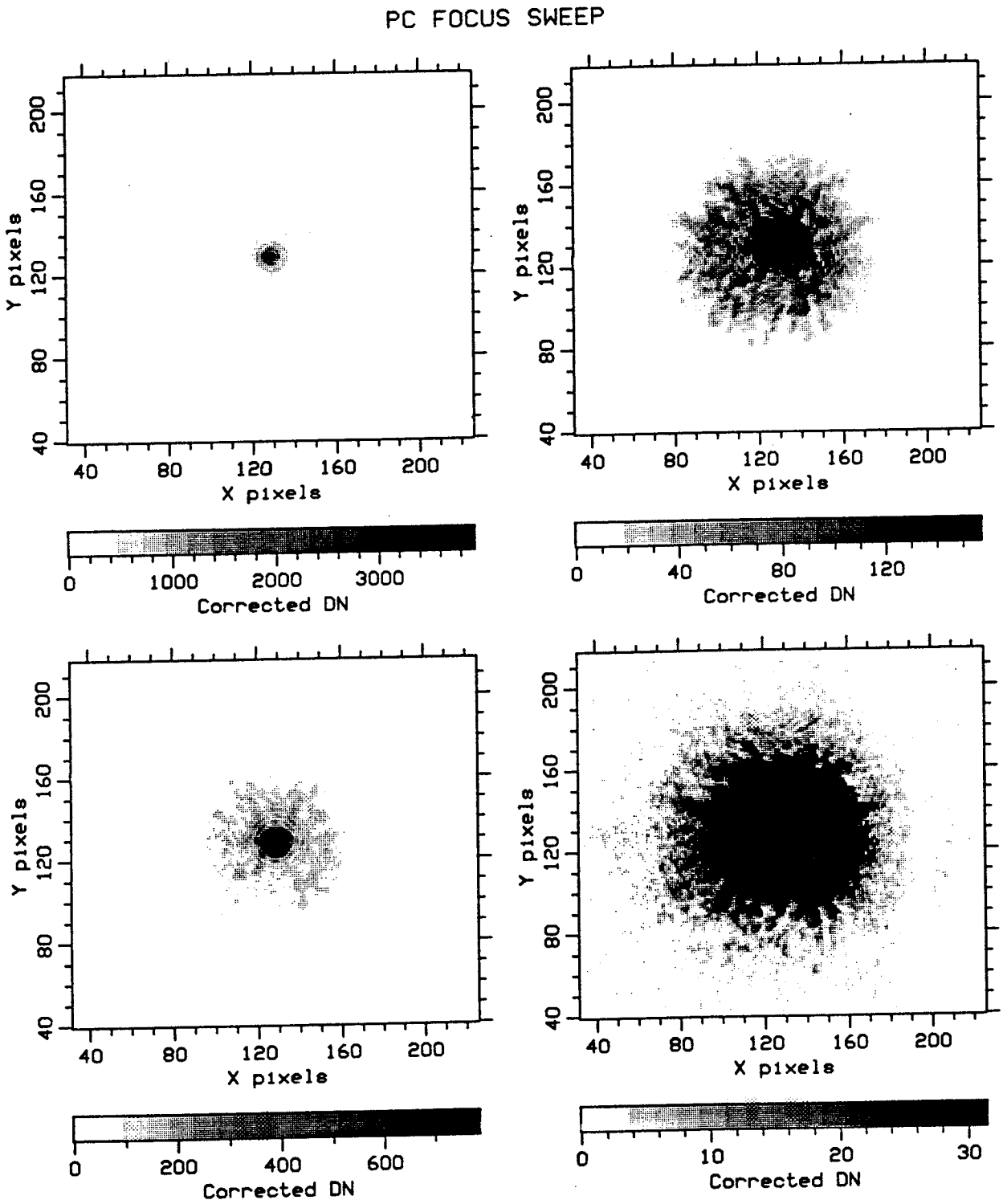

Figure 20. The PC focus sweep F889N image for focus 13.7 mm shown at four stretches.

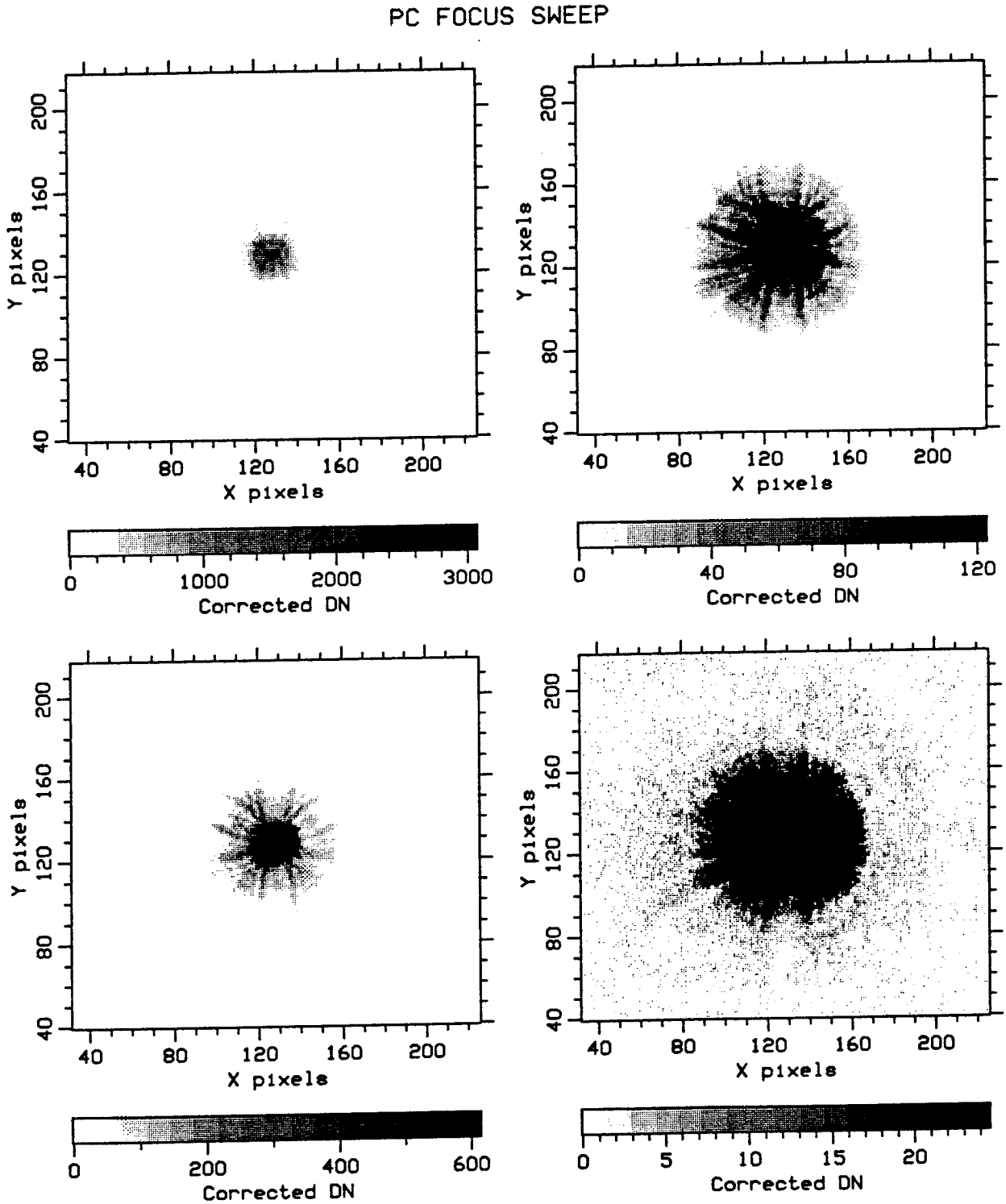

Figure 16. The PC focus sweep F487N image for focus 20.2 mm shown at four stretches.

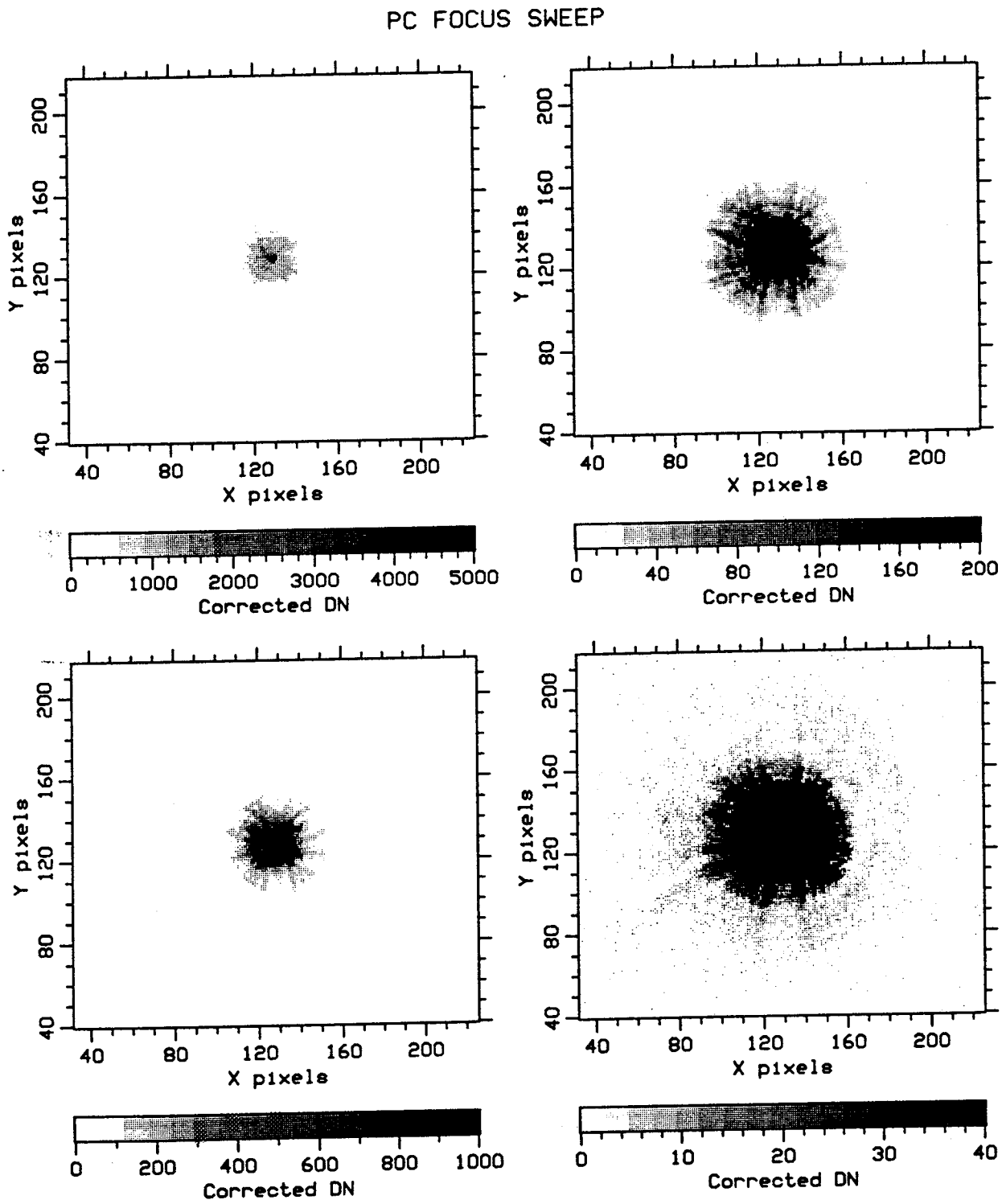

Figure 17. The PC focus sweep F487N image for focus 23.2 mm shown at four stretches.

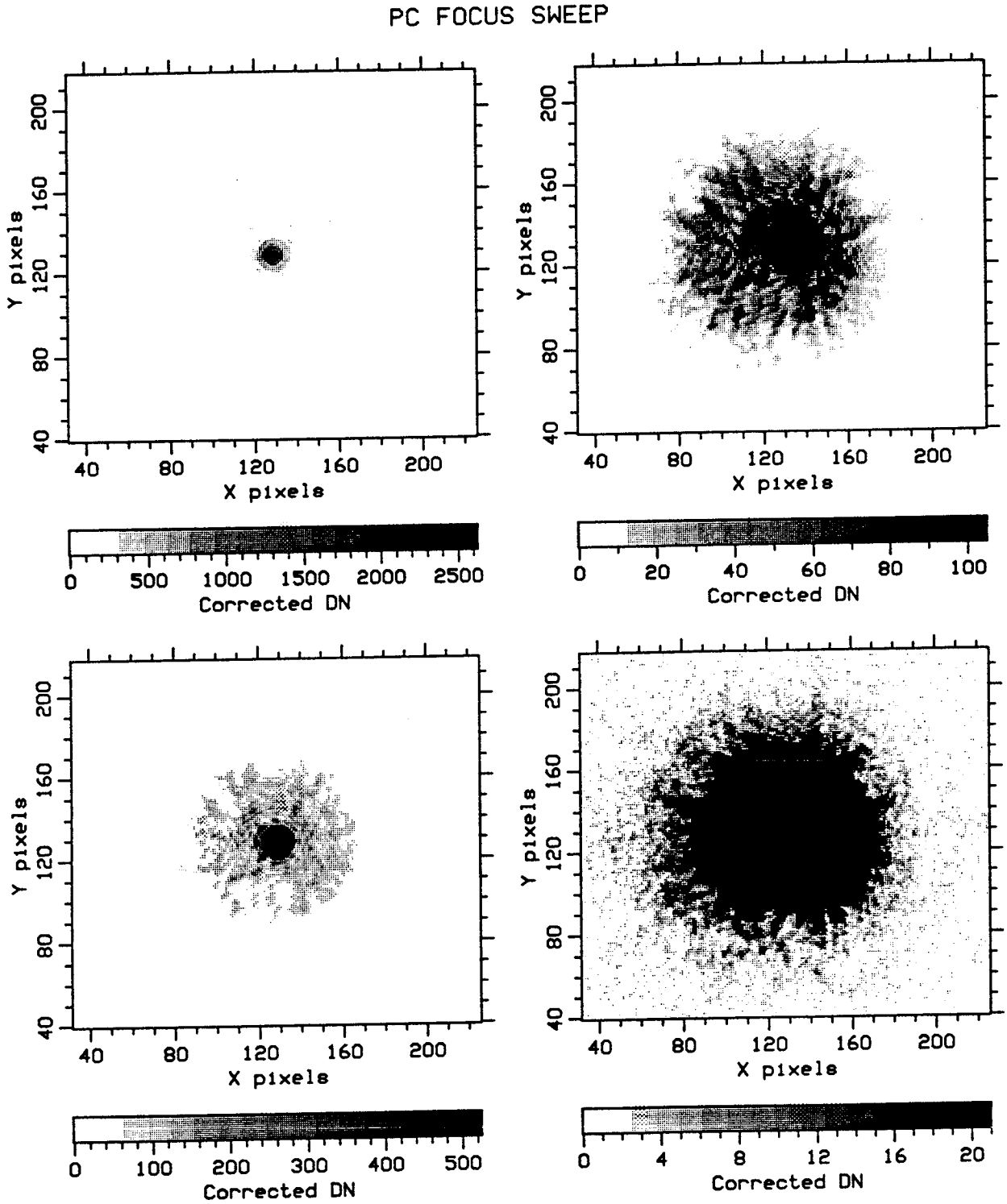

Figure 18. The PC focus sweep F889N image for focus 10.7 mm shown at four stretches.

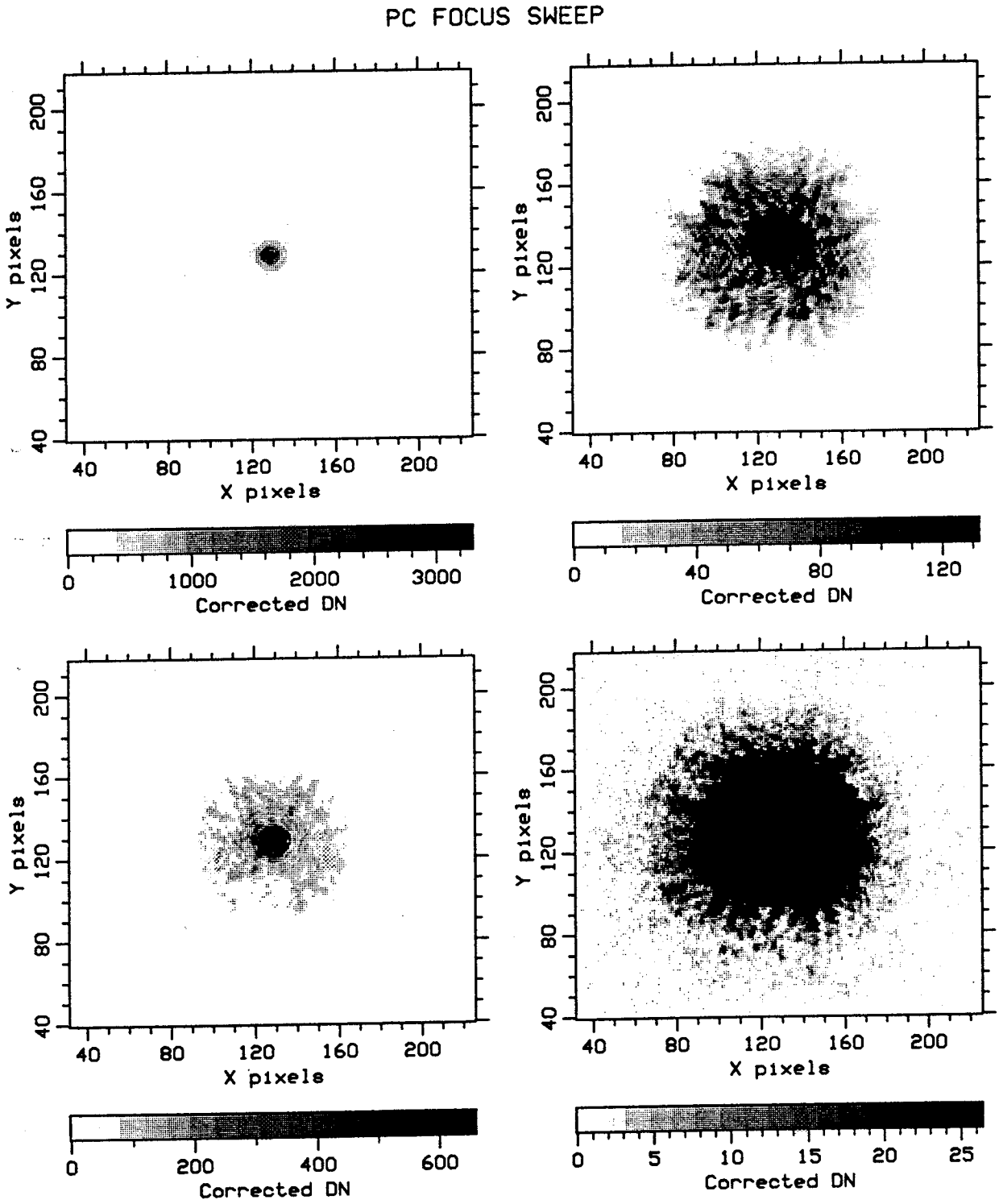

Figure 19. The PC focus sweep F889N image for focus 12.2 mm shown at four stretches.

Attachment 4

The FOC Focus Sweep 1991

Robert Jedrzejewski, STScI

The rationale for performing a focus sweep has been described in the proposal to the Telescope Time Steering Committee (Attachment 2B in this Report). To summarize: there was a need for a definitive calibration of the optimum secondary mirror despace setting in the post-desorption era of HST Operations that would also allow determination of the relation between the pad positions and the encircled energy curves. The data from the August 1990 sweep was not deep enough and suffered from frequent losses of lock so that it was not suitable for this type of analysis.

Selecting a suitable target for the program is something of a balancing act due to the photon-counting nature of the FOC. Unlike using, for example, the WFPC, one cannot ensure linearity by merely changing the exposure time as the FOC non-linearity is dependent on the count RATE rather than the total counts in the exposure. The only means available to change the flux from a given source is to choose the filters appropriately and make use of the neutral density filters to allow good signal-to-noise ratio in both the pads and the core. Since the count-rate requirements are quite strict, it is essential to use spectrophotometric standards that allow prediction of the expected count rate to about 10% or so.

The goals for this program were twofold: to investigate the dependence of encircled energy on secondary mirror despace position for the visible and ultraviolet wavelengths and to tie the encircled energy curves to measurements of the positions of images of the mirror pads - the former are predictable from diffraction theory while the latter are predictable from ray-tracing.

The visible filter used is the F486N, a narrow band filter centered on the wavelength 486nm, while the F120M filter (medium band centered on 120nm) serves for the ultraviolet.

In practice, this means that one F486N exposure is required that is not saturated in the core (allowing a measurement of encircled energy within 0.1" unaffected by non-linearity), one that gives good signal-to-noise ratio in the pads at F486N (to allow measurement of pad positions) and one that gives good signal-to-noise ratio in the core at F120M (for encircled energy - the pads are not visible at F120M). The optimum count rate for a linear PSF core region is 0.5-1 count/pixel/second in the brightest pixel, which which

would mean that to obtain good signal/noise ratio in the pad region would require an exposure time of several tens of thousands of seconds. Using neutral density filters in the 'core' exposure and removing them for a subsequent 'pad' exposure allows the acquisition of both types of data in a reasonable time. For F120M, there are no conflicting requirements but time is saved by selecting a target which can be used for both the F486N and F120M exposures. Fortunately, most spectrophotometric standards are very blue objects, so many have plenty of flux in the ultraviolet. The target that fulfilled all the requirements of predicted count rates with and without neutral density filters with F486N and for F120M (with ND's if necessary), as well as having good guide stars available for the duration of the program, was AGK+81D266, a V=11.92 mag O star.

Table 1: PREDICTED COUNT RATES

	Filters	*rate (/s)*
AGK+81D266	F486N	852
	F486N+F2ND	141
	F120M+F4ND	124

The central count rate for a star observed with the F/96 channel is about 1-2% of the count rate integrated over the star. In the region of the pads, the count rate is about 0.1-0.5% of that in the central pixel.

OBSERVATION STRATEGY

For the core region, sufficient signal-to-noise ratio for encircled energy analysis can be obtained in about 3-400 seconds. To guard against losses of lock shortening the exposure to less than 100 seconds, typical FOC exposures are 900 seconds. For the wings, the count rate per pixel with F486N filter alone is about 0.01-0.04 count/sec/pixel, so again a 900-sec exposure will give 9-40 counts/pixel, which should be enough to determine the position of the pad centers. For the UV exposures, as well as measuring the encircled energy,

it was desired to evaluate the core shape to look for asymmetries (the familiar FOC UV "boomerang") and see how they move with secondary despace. For this reason, 2 900-second exposures were taken with F120M+F4ND.

THE DATA

The FOC focus sweep proposal was run on October 18-19 1991 (days 91.291 and 91.292). Data were taken at each of 6 different secondary mirror positions, all in mm from the nominal position: -3.5, -2.0, -0.5, +1.0, +2.5 and +4.1. Negative positions have the secondary mirror closer to the primary mirror than positive ones. This is to be compared with the August 1990 sweep, which had secondary mirror positions ranging from -5.5mm to +5.5mm. After an initial Mode I Target Acquisition, consisting of a single 900-s F486N image that allows subsequent centering of the star in the FOC field, there were 4 exposures at each mirror setting: 900-s F486N, 900-s F486N+F2ND, 2x900-s F120M. These exposures typically took 2 orbits to execute. The secondary mirror was then moved during the subsequent occultation to the next despace position. The observations had to be split into two sessions as the target visibility was typically only a few hours in each day. All data were taken in fine lock, and the secondary mirror position was in the nominal 'zero coma' position (different from the usual mirror position by a decenter only). A catalogue of the observations is given in Table 2.

Here the column SM refers to the Secondary Mirror position relative to nominal, the column ACTUAL/PLAN refers to the exposure time. All FOC exposures are normally cut short from 900.0 to 895.875 seconds. Negative exposure times indicate where the take data flag came up and then went down within 15 seconds, the smallest time resolution for the UDL file. 'TRK' refers to the tracking mode - Fine lock in this case, and PEAK is the peak count/pixel in the brightest pixel. The F486N images have a PEAK value that is totally dependent on the FOC linearity performance and does not reflect what the peak counts would be if the FOC were linear.

Exposure X0RF0205T was affected by V1 excursions, although lock was not actually lost. The image shows a faint 'double' image of the star, but this did not affect the encircled energy measurements significantly.

The data was processed by the PODPS pipeline in the standard way — the images were flipped in the X-direction (to convert to the same par-

Table 2:

NAME	*SM*	*FORMAT*	*FILTERS*	*ACTUAL/PLAN*	*TRK*	*PEAK*
x0rf0201t	0	512X1024(Z)	F486N	350.250/600.0	F	74
x0rf0202t	-3.5	512X512	F486N	895.875/900.0	F	2537
x0rf0203t		512X512	F486N,F2ND	810.375/900.0	F	907
x0rf0204t		512X512	F120M,F4ND	895.875/900.0	F	390
x0rf0205t		512X512	F120M,F4ND	895.875/900.0	F	272
x0rf0206t	-2.0	512X512	F486N	895.875/900.0	F	2561
x0rf0207t		512X512	F486N,F2ND	895.875/900.0	F	1209
x0rf0208t		512X512	F120M,F4ND	895.875/900.0	F	548
x0rf0209t		512X512	F120M,F4ND	831.375/900.0	F	472
x0rf020at	-0.5	512X512	F486N	895.875/900.0	F	2397
x0rf020bt		512X512	F486N,F2ND	813.375/900.0	F	1684
x0rf020ct		512X512	F120M,F4ND	703/250/900.0	F	384
x0rf020dt		512X512	F120M,F4ND	895.875/900.0	F	429
x0rf0101t	0	512X1024(Z)	F486N	-268.250/600.0	F	107
x0rf0102t	+1.0	512X512	F486N	895.875/900.0	F	2197
x0rf0103t		512X512	F486N,F2ND	-195.875/900.0	F	1056
x0rf0104t		512X512	F120M,F4ND	895.875/900.0	F	236
x0rf0105t		512X512	F120M,F4ND	789.375/900.0	F	239
x0rf0106t	+2.5	512X512	F486N	895.875/900.0	F	2423
x0rf0107t		512X512	F486N,F2ND	595.375/900.0	F	851
x0rf0108t		512X512	F120M,F4ND	895.875/900.0	F	173
x0rf0109t		512X512	F120M,F4ND	743.375/900.0	F	128
x0rf010at	+4.1	512X512	F486N	895.875/900.0	F	1185
x0rf010bt		512X512	F486N,F2ND	806.375/900.0	F	505
x0rf010ct		512X512	F120M,F4ND	895.875/900.0	F	252
x0rf010dt		512X512	F120M,F4ND	700.250/900.0	F	185

ity as the sky), flatfielded and then geometrically corrected to ensure that pixels have the same size and separation — the pixel size after geometrical correction is 0.02237 ± 0.00005 arcsec/pixel. This is different from images supplied for pad position analysis, but for the purposes of this analysis it is not necessary to be consistent. The geometrical correction does apply a small amount of smoothing, but not enough to affect the results of this analysis significantly.

Images were provided for analysis by other members of the Panel (D. Schroeder, C. Burrows) — they were not flipped with respect to the sky and were geometrically corrected to a different resulting plate scale (consistent with all other sets of FOC data delivered for this type of analysis). The results are documented elsewhere in this report.

Encircled energy profiles were determined using a fairly simple-minded approach. After identifying the brightest pixel as the center of the PSF, each pixel was binned according to distance from the center, with a bin width of 1 pixel. The mean intensity is then calculated as the sum of the flux within the bin divided by the number of pixels. The encircled energy is then the cumulative sum of these annular averages.

These values are not corrected for background — typically a 900-s FOC exposure has about 0.5-1 count/pixel of background. At the edge of the PSF the contribution of the PSF is only a few tenths of a count/pixel, so accurate subtraction of the background is essential. This is accomplished by plotting the intensity profile and encircled energy profile for the image for different values of assumed background. If the assumed background is too high, the intensity profile will cut off at some radius (where the 'true' PSF contribution is equal to the difference between the adopted background value and the 'true' one) and the encircled energy profile will reach a maximum at the same radius and decline outside that as negative flux is added to the cumulative sum.

If, instead, the adopted background is too low, the PSF intensity profile will flatten out to a constant value (equal to the difference between the true background and the adopted one) and the encircled energy profile will never approach an asymptotic limit but instead increase quadratically with radial distance. The correct background will give an intensity profile that falls off steadily into the noise, while the encircled energy profile will increase to an asymptotic limit (the total flux from the star). In practice, to achieve reliable background values, it was necessary to plot the profiles out to a

radial distance of 5 arcseconds (i.e. almost to the edge of the FOC field) and then the background was measurable to about 0.01 counts (i.e. an accuracy of about 1%).

For the F120M exposures, where there were two images for each focus position, the images were analyzed separately and the encircled energy curves averaged. The agreement between the curves was very good.

The resulting encircled energy curves are presented in Figures 1-4.

Figure 1 shows the encircled energy curves interior to 0.5 arcseconds radius for the observations with F486N (+F2ND) filter. This shows the difficulty of trying to develop a criterion for choosing a focus position that maximizes the encircled energy - the curves cross over each other so that the position that gives the greatest encircled energy within 0.5 arcsec (+4.1mm) is the worst for an aperture radius of 0.1 arcsec or less. For 0.5 arcsec radius, the encircled energy is between 39% and 49%, with the curves ordered by despace value.

The criterion we have been using for setting the focus is to maximize the encircled energy within 0.1 arcsecond radius. Using this criterion, it can be seen that the curve at position +1.0mm gives the largest encircled energy within 0.1 arcsec, but that at -0.5mm is better for radii smaller than 0.08 arcsec. Figure 2 shows that there is very little to choose between the encircled energy at -0.5 and +1.0mm for apertures containing up to 20% of the light, and it is therefore clear that the current default nominal position is optimal for FOC observations at F486N, with a margin of about $\pm 0.5mm$ that would not seriously degrade the imaging performance (although the degree to which deconvolution experiments would be affected by such a difference in focus position between a science observation and a PSF observation is not known).

The behaviour at 120nm wavelength is somewhat different. The encircled energy is never as high as it is at 486nm at any aperture size, and the encircled energy within 0.1 arcsec peaks at a smaller value of despace (i.e. more negative). This is understood from optics theory — the peak in the encircled energy curve for a given aperture size has a short wavelength limit (the ray-trace limit) and a long-wavelength limit (the diffraction limit). As the wavelength changes the encircled energy peak shift from one peak to the other.

For F120M data, the -2.0mm and -0.5mm curves are almost identical for aperture radii less than 0.1 arcsec, so clearly the best value is in between these two values. Again the encircled energy values within 0.5 arcsec are

ordered by despace, but now the values are between 34% and 44% of the total. The adopted value for the 'best' focus at 120nm is -1.0mm, with an uncertainty of 0.5mm.

The only value that is consistent with both of these values is -0.5mm — this would be the 'best' despace value for the secondary mirror for FOC observations. However, 0.0mm is not unacceptable, and as has been reported by Ed Groth, -0.5mm is starting to move away from the WFPC best focus.

Desorption tends to make the effective despace value go more negative with time. Over the past few months, the effective despace value has been firmly on the + side, and only now reached zero. Over the rest of the life of HST, desorption will move the effective despace value to the - side, but the total amount of further desorption left to run is probably only on the order of 0.5mm, so any additional desorption corrections are probably unwarranted.

Finally, the core asymmetry that we see in far-UV images taken with the FOC were also apparent in these images, despite being taken in the 'zero coma' position. It became clear from modelling that no combination of tilt and decenter could give such a core asymmetry, so the observation that moving to the zero coma position was unable to improve the image quality was no surprise.

Figure Captions

1. Curves of encircled energy vs. aperture radius for the 6 focus positions for the F486N filter.

2. The variation of encircled energy with focus position for 4 different aperture sizes for the F486N filter.

3. Same as 1, except for the F120M filter.

4. Same as 2, except for the F120M filter.

Fig. 1

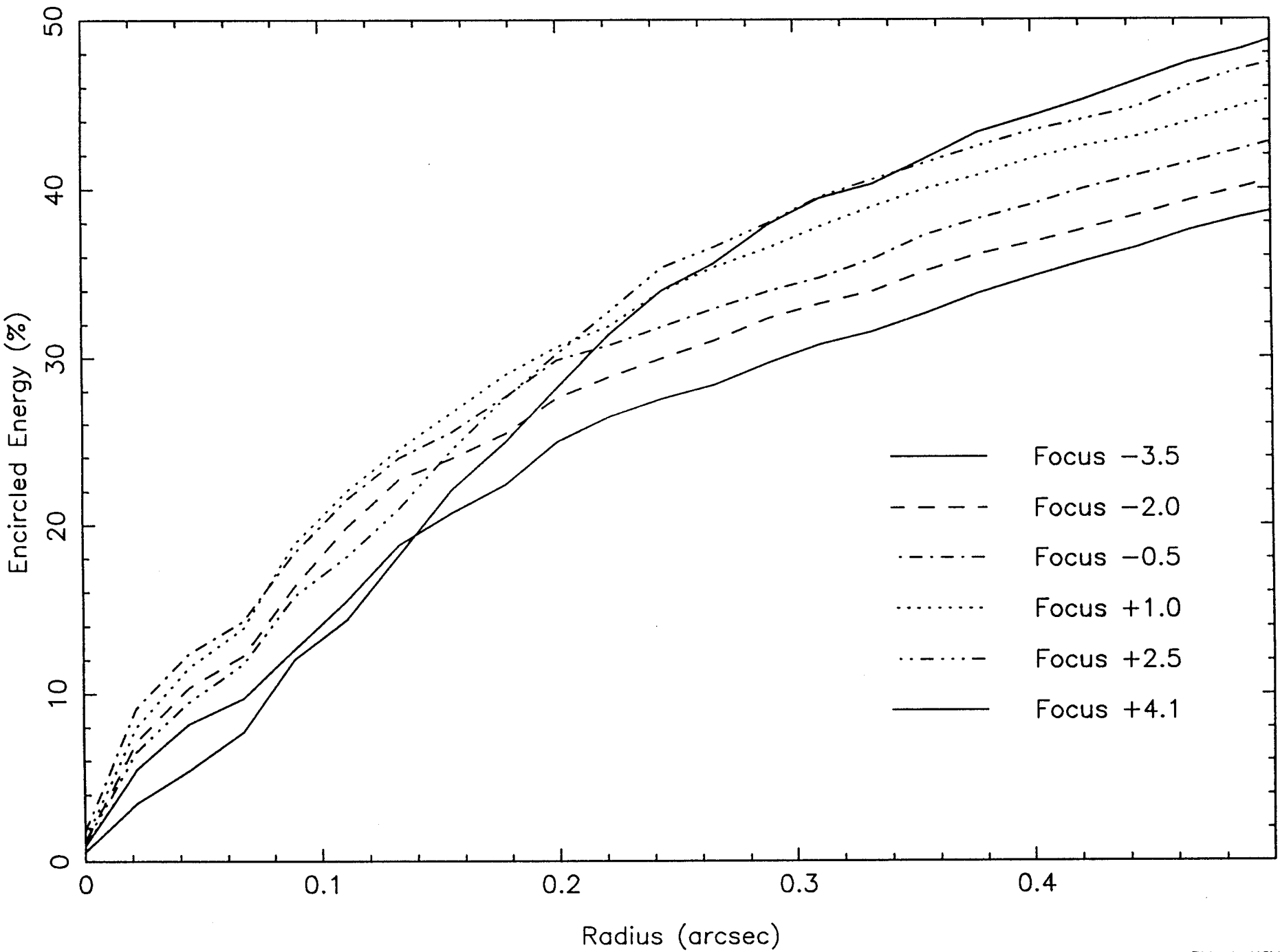
Encircled Energy vs. Focus Position for FOC+F486N
Encircled Energy (%)
0
10
20
30
40
50
0
0.1
0.2
0.3
0.4
Radius (arcsec)
Focus −3.5
Focus −2.0
Focus −0.5
Focus +1.0
Focus +2.5
Focus +4.1
RIJ 1-NOV-1991 15:54

Fig. 2

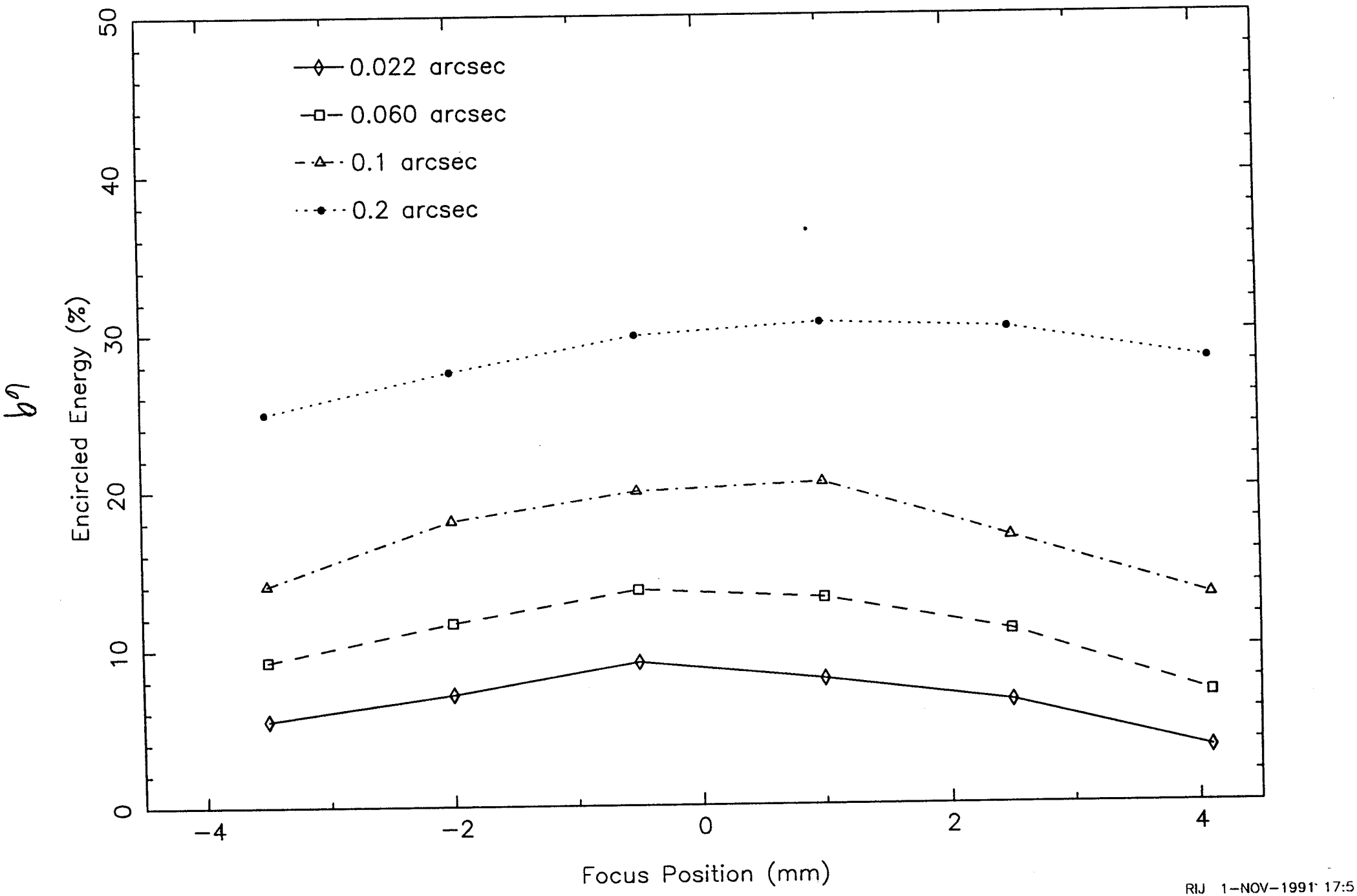
Encircled Energy vs. Focus Position for FOC+F486N
0.022 arcsec
0.060 arcsec
0.1 arcsec
0.2 arcsec
Encircled Energy (%)
0
10
20
30
40
50
−4
−2
0
2
4
Focus Position (mm)
RIJ 1-NOV-1991 17:5

Fig. 3

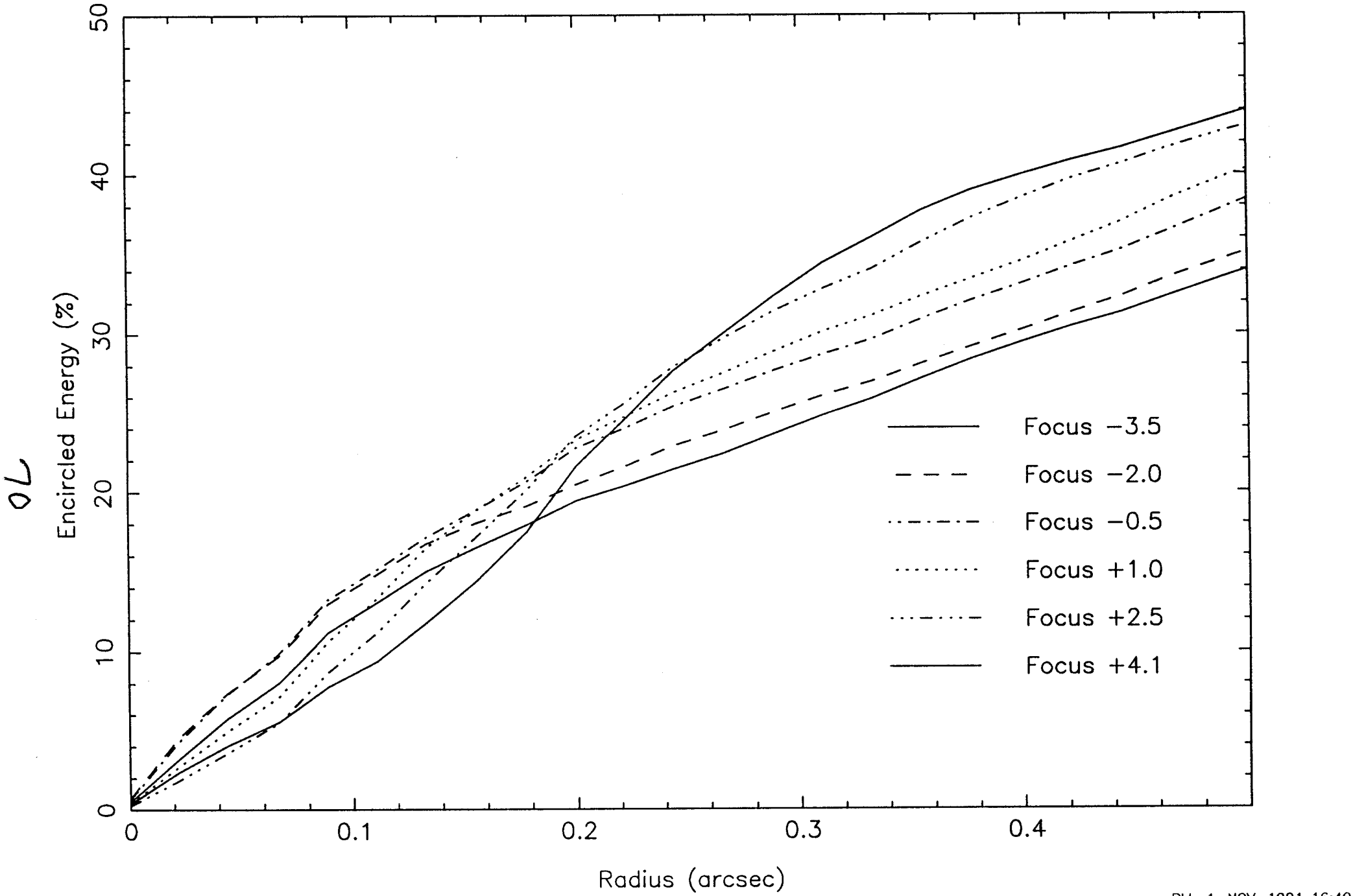
Encircled Energy vs. Focus Position for FOC+F120M
Encircled Energy (%)
0
10
20
30
40
50
0
0.1
0.2
0.3
0.4
Radius (arcsec)
Focus −3.5
Focus −2.0
Focus −0.5
Focus +1.0
Focus +2.5
Focus +4.1
RIJ 1-NOV-1991 16:40

Fig. 4

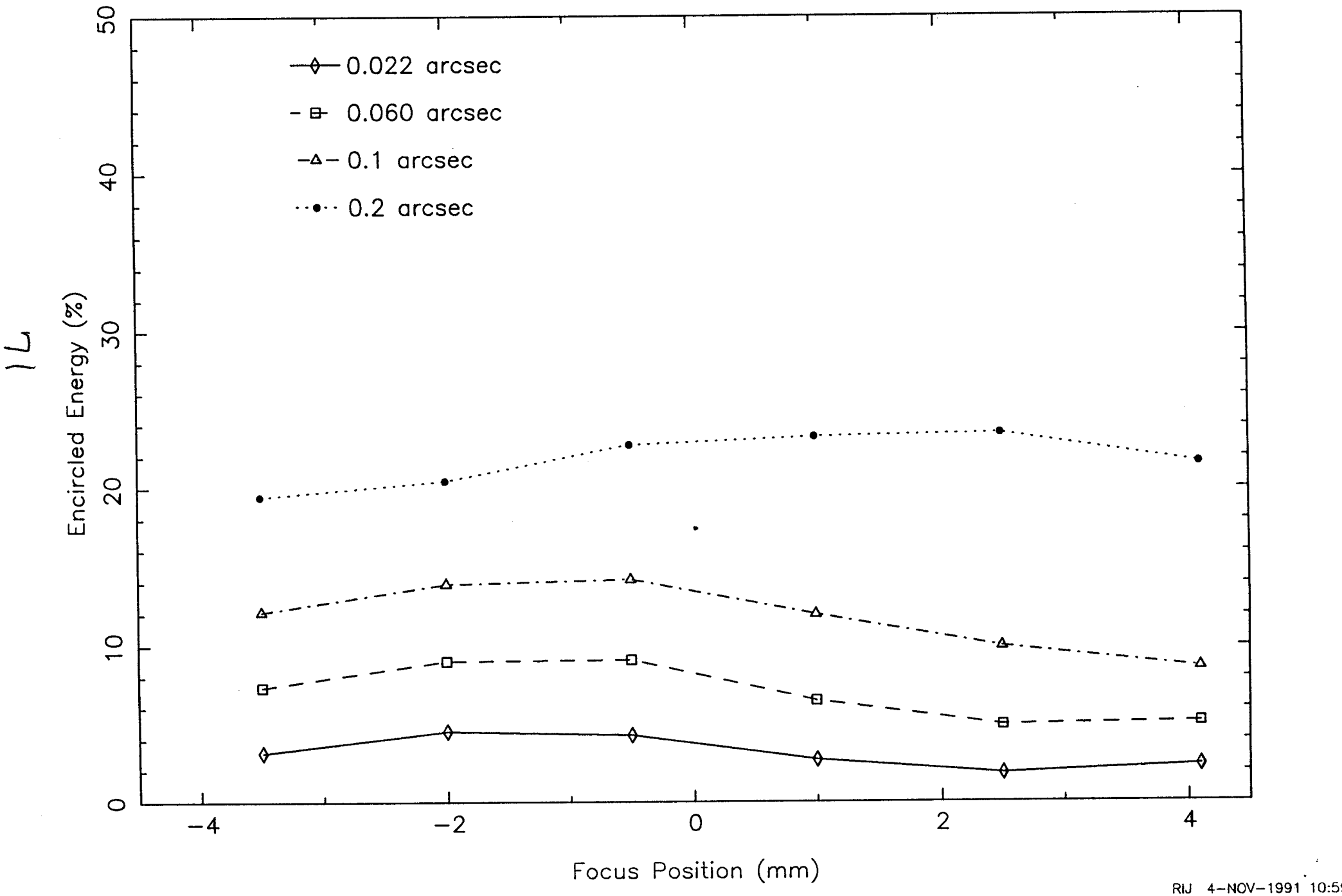
Encircled Energy vs. Focus Position for FOC+F120M
0.022 arcsec
0.060 arcsec
0.1 arcsec
0.2 arcsec
Encircled Energy (%)
0
10
20
30
40
50
−4
−2
0
2
4
Focus Position (mm)
RIJ 4-NOV-1991 10:59

DESORPTION MONITORING

Included among the many OV and SV activities was monitoring of the shrinkage of the graphite-epoxy OTA structure and periodic despace of the secondary mirror (SM) to hold the focus constant within a mm or so. The wavefront sensors (WFS) would provide the data for this program. Because of the spherical aberration (SA), confirmed shortly after launch, and the resulting frenetic activity during the summer of 1990, desorption monitoring was given a low priority. During this time it also became apparent that the WFSs were not able to function as expected because of the large SA, and their use was largely abandoned.

Following a focus sweep in August 1990, a "best focus" position was agreed to and the question of how to monitor the desorption then became important. The method adopted for this purpose is called the "pad method"; the theory behind this method is described in some detail in Attachment A titled OTA PAD POSITIONS IN ABERRATED IMAGES. Basically it involves measures of the distance of each pad feature in an FOC f/96 image from the image peak. The average of these three distances is the "radius of the pad circle", denoted by <r>; via the algorithm in Attachment A this is converted into a distance from paraxial focus (PF) to the OTA focal surface. The analysis in Attachment A shows that <r> depends only on focus for a given amount of spherical aberration and is unaffected by the presence of coma or astigmatism.

It is important to note that the algorithm in Attachment A was based on SA for a primary mirror conic constant K = -1.0135. The current best estimate is K = -1.0139; this changes the absolute scale but not the deltas between different images. The algorithm adjusted to the current value of K is shown in Fig. 1.

Desorption monitoring using the pad method has been a continuing effort since August 1990, with the first images used selected from ones taken by the FOC for other purposes. A program was put in place in late 1990 to get deep FOC images at 486 nm, exposed to bring out the pad features, specifically for desorption monitoring.

The results of this monitoring program are shown in Fig. 2. By definition, the SM position on 16 Aug 1990 is taken as the zero-point, with offsets from that position plotted in the graph. The best-fit exponential curve, supplied by Chris Burrows, is based on data available through September 1991. The latest point, from an image taken in late November, fits this curve within the uncertainty of the measurements of <r>. This uncertainty, about +/- 0.8 pixels for a single image, gives an uncertainty in del SM of +/- 3 microns.

Periodic offsets of the SM made to counteract the desorption were as follows:

20 microns (26 Oct 90)
25 microns (22 Feb 91)
15 microns (11 April 91)

Since the final corrective move in early April, the SM position has steadily approached the August 90 setting of approximately 12.1 mm from paraxial focus. Measures during the fall of 1991 indicate a rate of desorption of about 1.5 microns/month during that time period, with approximately 5 microns total additional shrinkage remaining according to Burrows' curve.

The calibration of the distance from paraxial focus to the OTA focus (dPF) was done during the FOC focus sweep on 18 October 1991. Results from measures on these images are shown in Fig. 3, with the SM position at the start of the sweep defined as zero. Although no image was taken at del SM = 0 during the focus sweep, an FOC image was taken at this position during the coma sweep one month earlier; this value, after adjustment for desorption, is included in Fig. 3. The best-fit straight line through the data gives del SM = 0 equivalent to dPF = 12.2 mm on 18 October 91, with an uncertainty of +/- 0.3 mm based on the estimated uncertainty in <r> given above. The value from this calibration and the value from Burrows' curve adjusted for the 60 micron offset differ by 0.2 mm. These values agree within the stated uncertainties.

Dan Schroeder
20 January 1992

Fig. 1. Pad images

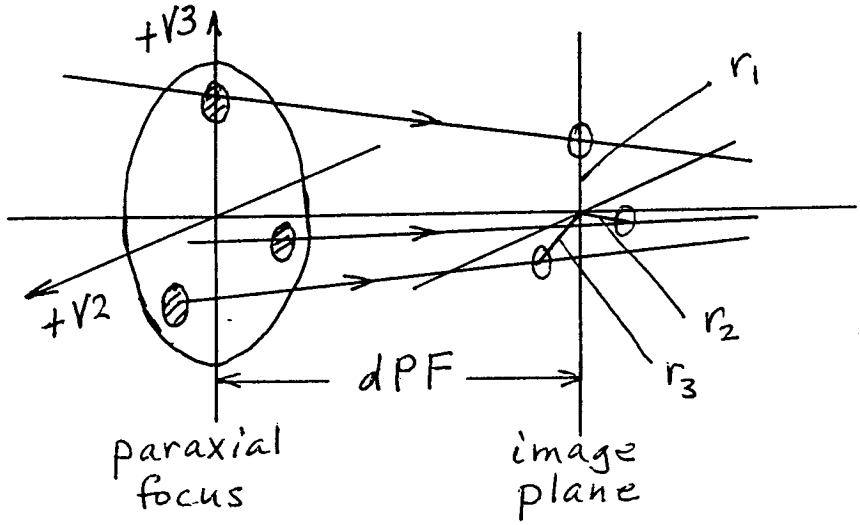

Define ⟨r⟩ = average distance from pad centers to image peak.

Given K = -1.0139 for primary mirror, ray trace analysis of rays from the pad centers gives the following relation:

⟨r⟩(microns) = 596.5 - 1.998 dSM(microns)

where dSM is the distance of the secondary mirror from its nominal position which places paraxial focus (PF) at the OTA focal surface.

For the camera, in pixels, we get

⟨r⟩ = 87.57 - 0.2933 dSM(microns) FOC f/96
= 87.57 - 2.677 dPF(mm)

Fig. 2

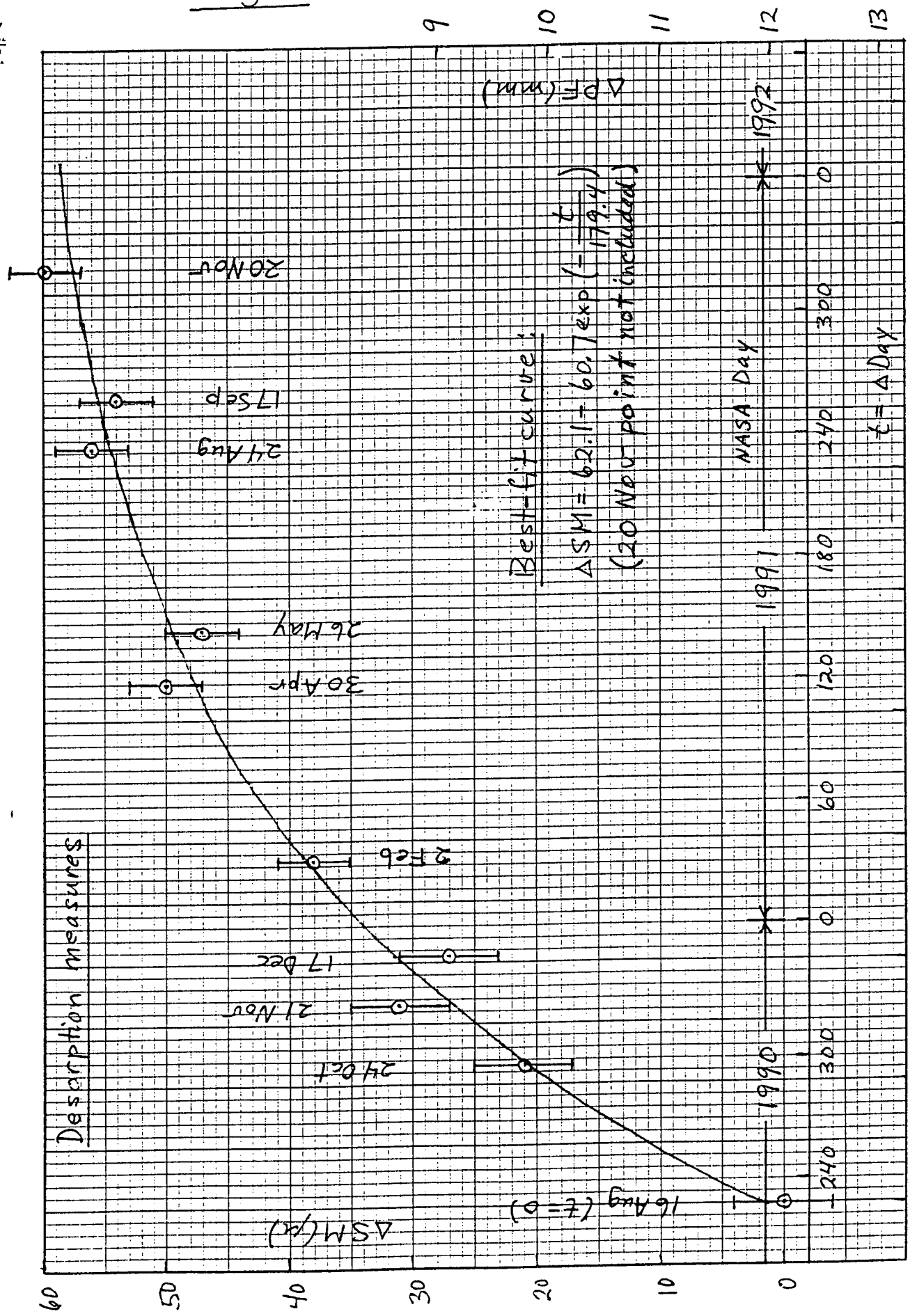
ΔSM(cm)
60
50
40
30
20
10
0
Description measures
16 Aug (t=0)
24 Oct
21 Nov
17 Dec
Δ Feb
26 May
30 Apr
24 Aug
17 Sep
20 Nov
1990
1991
1992
NASA Day
0
60
120
180
240
300
0
120
240
300
0
180
240
300
360
420
480
540
t = ΔDay
ΔPF (mm)
9
10
11
12
13
Best-fit curve:
ΔSM = 62.1 + 60.7 exp (− t / 179.4)
(20 Nov point not included)

Fig. 3

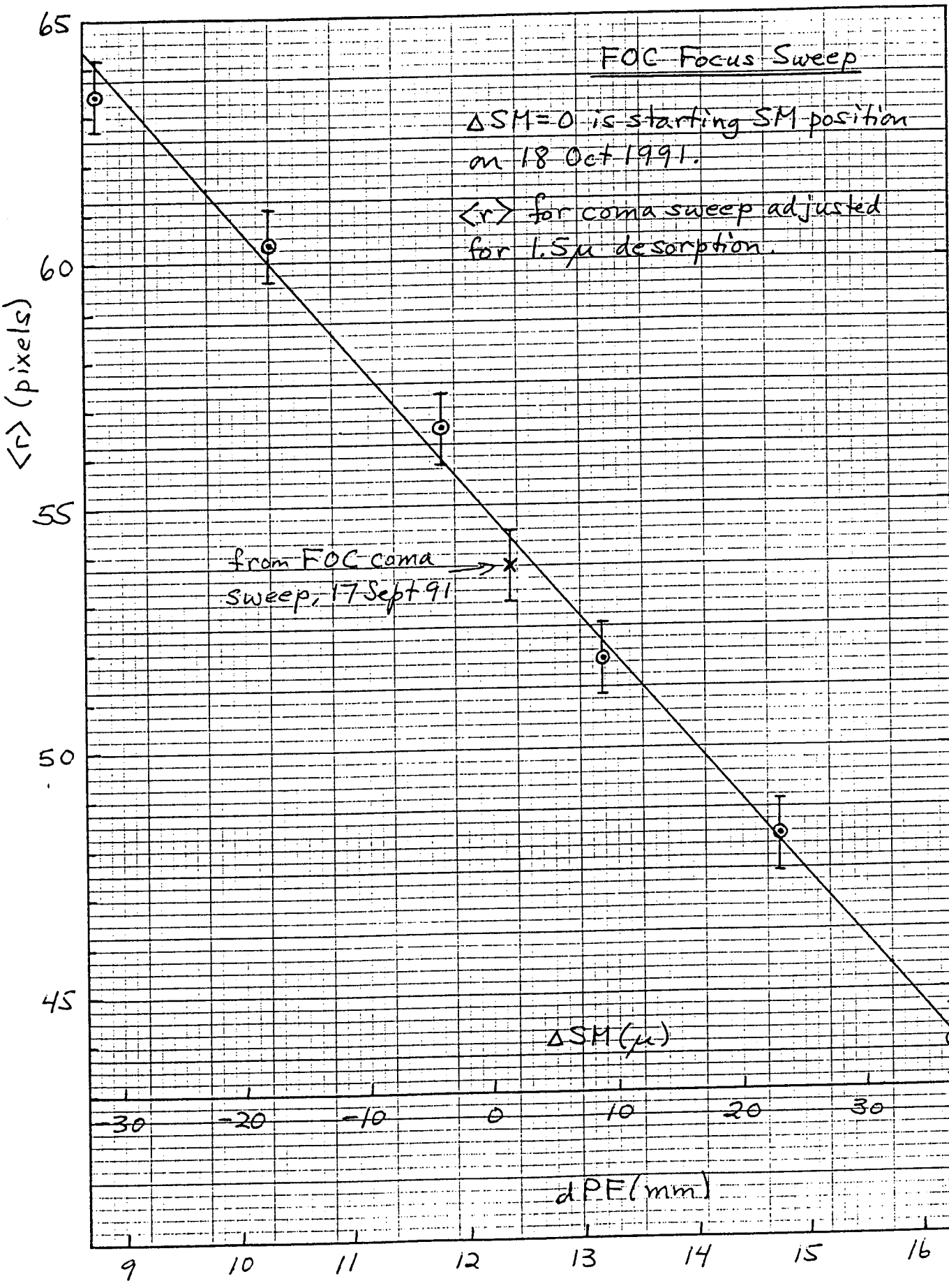
FOC Focus Sweep
ΔSM=0 is starting SM position on 18 Oct 1991.
⟨r⟩ for coma sweep adjusted for 1.5μ desorption.
from FOC coma sweep, 17 Sept 91
⟨r⟩ (pixels)
65
60
55
50
45
ΔSM (μ)
-30
-20
-10
0
10
20
30
dPE (mm)
9
10
11
12
13
14
15
16

Attachment A

OTA PAD POSITIONS IN ABERRATED IMAGES

INTRODUCTION

The OTA entrance pupil, as shown in Fig. 1, has three pads whose radial positions from the image peak in the image plane are related to the distance from paraxial focus (dPF). The relation between the pad radii, measured from the center of the pad features in the image to the image peak, and dPF is set by the spherical aberration (SA) in the OTA. An example of an FOC f/96 image showing the pad features is shown in Fig. 2. It is worth noting that a pad feature is analogous to the Fresnel bright spot formed behind an obstacle in a light beam.

In this note I will derive the relation between pad radii and dPF for an image with SA only, as well as the relation for the changes in these radii when coma and astigmatism are present. The latter aberrations are present when the secondary mirror (SM) is tilted and/or decentered from its aligned position. In each case I will compare the calculated radii for given dPF's with measures made on model images with known dPF's and aberrations. I will also present some results on measures of FOC images taken for desorption monitoring purposes.

ABERRATED IMAGE WITH SA ONLY

In this section I derive the relation between the pad radii r and dPF, with the pad designations as shown in Fig. 1. This is done in two ways, (1) by finding the intersections of rays from the centers of the pads in the image plane for various SM positions by geometric ray tracing, and (2) by locating the pad centers from the normals to an aberrated wavefront with 3rd-order SA only. In both cases I assume the primary mirror conic constant K1 = -1.0135, hence the zero-peak SA coefficient A_4 = 6.82 waves at 633 nm, or 4.317 microns OPD.

For the ray tracing approach I take the nominal as-built parameters of the OTA: R1 = -11041.7 mm, K2 = -1.496, R2 = -1358.065 mm, PM-SM separation = -4906.889 mm, SM-PF distance = 6407.017 mm. The actual and fractional coordinates of the pad centers, taken from Fig. 1, follow.

pad	R(mm)	ρ	ρ^3	
1	1064.34	0.88695	0.69775	
2	1065.17	0.88764	0.69938	
3	1069.54	0.89128	0.70802	$\bar{\rho}$ = 0.88862

Ray traces were done for the field point on the OTA axis. I take this field point because the FOC corrects for the inherent astigmatism in the Ritchey-Chretien design, hence any distortion in the r_i's due to astigmatism is absent. The distance of a ray from the image peak is also converted to equivalent FOC f/96 pixels as follows: The OTA scale is 3.581 sec/mm and the FOC scale is 0.0244 sec/pixel, hence the FOC scale projected on the f/24 focal plane is 146.8 pixels/mm or 6.812 microns/pixel. The results from ray traces in the following table are given in both microns and pixels.

With dSM = displacement of the SM from its nominal location, the ray trace results follow. dSM and dPF are in mm.

dSM	pad	r(mic)	r(pix)	dPF
0.00	1	574.1	84.25	0.00
	2	574.4	84.30	
	3	581.1	85.28	
0.10	1	374.8	55.00	-10.972
	2	375.1	55.05	
	3	380.7	55.88	
0.20	1	175.5	25.75	-21.915
	2	175.8	25.80	
	3	180.4	26.84	

The relations between the pad radii and dPF follow directly from the data in this table. Expressed in pixels,

$$\begin{aligned} r_1 &= 84.25 - 0.2925\ \mathrm{dSM(mic)} = 84.25 - 2.669\ \mathrm{dPF(mm)} \\ r_2 &= 84.30 - 0.2925\ \text{"} = 84.30 - 2.669\ \text{"} \\ r_3 &= 85.28 - 0.2940\ \text{"} = 85.28 - 2.683\ \text{"} \end{aligned} \qquad (1)$$

$$\langle r \rangle = 84.61 - 0.2930\ \mathrm{dSM(mic)} = 84.61 - 2.674\ \mathrm{dPF(mm)}\ . \qquad (2)$$

Note that r_1 and r_2 are each about 0.3 pix less than $\langle r \rangle$, while r_3 is about 0.6 pix greater than $\langle r \rangle$. These numbers are used to adjust $\langle r \rangle$ when coma and/or astigmatism are extracted from real images.

An alternative approach, though basically equivalent, starts with the OPD on the wavefront. Assuming SA3 only, the wavefront error is

$$\mathrm{OPD} = G = \lambda A_4 \rho^4,$$

and the corresponding change in slope of a ray due to the aberration is

$$\varphi = \frac{dG}{dR} = \frac{dG}{d\rho}\frac{d\rho}{dR} = \frac{\lambda}{a} \cdot 4A_4\rho^3, \qquad (3)$$

where $a = R/\rho = 1200$ mm. The transverse SA (TSA) is then

$$\mathrm{TSA} = f\varphi = 2F\lambda \cdot 4A_4\rho^3, \qquad (4)$$

where f = OTA focal length and F = 24.

With the aid of the diagrams in Fig. 3,

$$\begin{aligned} r &= \mathrm{TSA} - \delta \\ &= 8F\lambda A_4\rho^3 - \mathrm{dPF}(\rho/2F)\ . \end{aligned} \qquad (5)$$

Substituting the appropriate numbers from above gives, in pixels,

$$r_1 = 84.90 - 2.713\ dPF(mm)$$
$$r_2 = 85.10 - 2.715\ "$$
$$r_3 = 86.15 - 2.726\ " \qquad (6)$$

$$\langle r \rangle = 85.38 - 2.718\ dPF(mm)\ . \qquad (7)$$

Note that $r_1 \cong \langle r \rangle - 0.4$, $r_2 \cong \langle r \rangle - 0.2$, and $r_3 \cong \langle r \rangle + 0.6$ over the range of interest for dPF. These adjusted radii are used when extracting aberrations from model images.

Comparison of equations (1) and (2) derived from ray traces with (6) and (7) shows small, but expected, differences. Aberration calculations on the OTA show (1) the presence of a small amount of 5th-order SA (SA5) of opposite sign to SA3, and (2) SA3 which increases slowly as the PM-SM separation is increased. The first of these effects accounts for the difference at dPF = 0; the second is responsible for the difference in slopes. Equations (1) and (2) are used when dealing with real images, while (6) and (7) are used with model images.

MEASURES ON MODEL IMAGES

Verification that dPF can be found from measures of $\langle r \rangle$ and application of (7) was done with computed diffraction images using the OTA pupil with pads (but without spider) at various dPF. The measurements were made by displaying the model image using IDL, "stretching" the image to bring out the pad features and using the cursor to find the center of each pad and the image peak. The results on a number of images are summarized in the table to follow. As shown below, the addition of coma to a spherically aberrated image does not change $\langle r \rangle$ within the errors of measurement. All measures of $\langle r \rangle$ are in FOC pixels.

C_x	C_y	$\langle r \rangle$(dPF=12)	$\langle r \rangle$(dPF=15)
0	0	52.7	44.7
0.5	0	53.1	44.5
-0.5	0	53.2	44.4
0	0.5	52.6	44.5
0	-0.5	52.5	44.0
	$\langle\langle r \rangle\rangle$	52.8	44.4
	$\langle r \rangle$(by (7))	52.8	44.6

A single image at dPF = 10 gave $\langle r \rangle$ = 58.3 measured versus 58.2 by (7).

An examination of the results for images with SA3 only indicates that there is an uncertainty of about +/- 0.3 pix in each measured r_i, and therefore also in $\langle r \rangle$. This corresponds to d(dPF) = +/- 0.1 mm. The uncertainties on measures of real images are certainly larger than this because of S/N considerations, but d(dPF) = +/- 0.3 mm should be attainable. This corresponds to d(dSM) = +/- 3 microns.

The procedure for finding the pad center as described above may have a systematic error associated with it. Because of SA3 on the wavefront, rays from the inner and outer edges of the pad are not located the same distances from the ray from the pad center. The point midway between these inner and outer rays is displaced radially outward from the ray which comes from the pad center. My analysis shows that this difference is about 1.27 pixels or an equivalent shift in dPF of 0.47 mm.

If this shift is present, then measures of $\langle r \rangle$ based on the pad centers should be decreased by 1.27 pixels before applying (7). It is clear from looking at the results in the above table that this introduces significant differences between measured $\langle r \rangle$'s and calculated ones. It appears, therefore, that there is a compensating factor which puts the center of the pad, as perceived in a displayed image, close to the position of the ray from the pad center. I surmise that this is due to the general decrease in intensity radially outward, hence the outer part of a pad feature is less bright and the apparent center is moved inward. I have not tried to quantify this supposition, but the agreement between measures of $\langle r \rangle$ on model images and those computed from (7) indicates the expected systematic shift is not a significant factor.

MEASURES ON FOC IMAGES

Chris Burrows and Dan Schroeder have independent measures of one common FOC image taken on Day 033. My results are derived from $\langle r \rangle$ provided by Glen Mackie at UW-Madison. CB analyzed this image using TIM and applied the pad center method as well. Results are given in the following table with dPF for the pad method calculated using (2).

Person	$\langle r \rangle$	dPF(mm)	method
DS	60.7	8.8	pad center
CB	59.7	9.2	" "
CB		8.4	TIM

The TIM software computes the focus shift from diffraction focus (dDF), in this case -13.64 mm (-1.391 waves rms at 547 nm). The PF-DF separation is 22.06 mm, hence dPF = 8.4 mm. I consider these measures to be in reasonable agreement.

It is clear from measures on both real and model images that the method of using pad centers to find $\langle r \rangle$ and dPF is a simple and reasonably accurate one for finding the position of paraxial focus relative to the nominal image plane.

ADDITION OF COMA AND ASTIGMATISM

The presence of coma and astigmatism in the spherically aberrated OTA wavefront causes the centers of the pads in the diffraction image to shift both radially and azimuthally. Measures of these shifts in pad locations can be used to determine the amount of coma and astigmatism present - a poor man's method of image inversion.

The additional wavefront error is given by

$$G = \lambda\left[\rho^3(C_x \sin\theta + C_y \cos\theta) + \rho^2(A_x \cos 2\theta + A_y \sin 2\theta)\right], \tag{8}$$

where θ is measured CW from the y-axis. The aberration coefficients are zero-peak values in waves.

Following the procedure above gives the change in ray angle, both radially and in azimuth. The results are

$$\varphi_\rho = \frac{\partial G}{\partial R} = \frac{\lambda}{a}\left[3\rho^2(C_x \sin\theta + C_y \cos\theta) + 2\rho(A_x \cos 2\theta + A_y \sin 2\theta)\right], \tag{9}$$

$$\varphi_\theta = \frac{1}{R}\frac{\partial G}{\partial \theta} = \frac{\lambda}{a}\left[\rho^2(C_x \cos\theta - C_y \sin\theta) + 2\rho(-A_x \sin 2\theta + A_y \cos 2\theta)\right]. \tag{10}$$

The corresponding transverse aberrations in radius and azimuth are

$$TA_\rho = f\varphi_\rho = 2F\lambda\,[\text{ from (9) }] = dr$$
$$= B_2(C_x \sin\theta + C_y \cos\theta) + B_1(A_x \cos 2\theta + A_y \sin 2\theta), \tag{11}$$

$$TA_\theta = f\varphi_\theta = 2F\lambda\,[\text{ from (10) }] = \langle r\rangle d\theta$$
$$= (B_2/3)(C_x \cos\theta - C_y \sin\theta) + B_1(-A_x \sin 2\theta + A_y \cos 2\theta), \tag{12}$$

where $B_2 = 6F\lambda\rho^2$, $B_1 = 4F\lambda\rho$. Note that the radial changes in pad location do not depend on $\langle r\rangle$, but the azimuthal changes do.

Substituting for ρ and θ at each pad position, with λ = 633 nm, gives the transverse aberrations in the following table.

pad	TA_ρ = dr(mic)
1	$71.7C_y + 53.9A_x$
2	$71.8(0.852C_x - 0.523C_y) - 53.9(0.453A_x + 0.891A_y)$
3	$72.4(-0.856C_x - 0.517C_y) - 54.2(0.465A_x - 0.885A_y)$

	$TA_\theta = \langle r\rangle d\theta$ (mic)
1	$23.9C_x + 53.9A_y$
2	$23.9(-0.523C_x - 0.852C_y) + 53.9(0.891A_x - 0.453A_y)$
3	$24.1(-0.517C_x + 0.856C_y) - 54.2(0.885A_x + 0.465A_y)$.

Summing separately the radial and angular changes gives

$$S(dr) = -0.8C_x - 3.3C_y + 4.3A_x - 0.06A_y ,$$

$$S(\langle r\rangle d\theta) = -1.1C_x + 0.3C_y + 0.06A_x + 4.3A_y .$$

Given the uncertainties in measuring these changes, the sums are effectively zero unless the aberrations are large. If, for example, $C_y = 1$, then S(dr) = -3.3 mic and $\langle r\rangle$ changes by less than 0.2 FOC pixels, or less than the uncertainty in $\langle r\rangle$. It is worth noting that for pads with constant ρ at 120-deg intervals, the sums are zero.

COMA EQUATIONS FOR ZERO ASTIGMATISM

If the astigmatism is zero, only the radial equations are needed to find the coma coefficients. Converting dr to pixels, the inverted equations are

$$C_x = 0.055(dr_2 - dr_3), \quad C_y = 0.095\ dr_1 = -0.091(dr_2 + dr_3) . \qquad (13)$$

To get rms error in Zernike terms, multiply the C's by 0.12.

Each dr = r' - r, where r' is the measured radius when coma is present and r is the radius in the absence of coma. As noted above, r_1 and r_2 are smaller than $\langle r\rangle$, while r_3 is greater than $\langle r\rangle$. For real images the adjustments following (2) are used; for model images the adjustments following (7) are used.

We now give results for a number of model images with different input C's and constant SA. Two outputs are given: (1) r' is measured from where the image center would be in the absence of coma, (2) r' is measured from the actual image peak. The shift in x or y from the

center used in (1) is approximately 1.6 times C_x or C_y , respectively, in pixels. The outputs are calculated using (13).

	Input		Output(1)		Output(2)	
dPF	C_x	C_y	C_x	C_y	C_x	C_y
12	0	0	0.03	0.06	0.03	0.06
	0.5	0	0.63	0.05	0.56	0.05
	-0.5	0	-0.48	0.02	-0.41	0.02
	0	0.5	0.03	0.57	0.03	0.50
	0	-0.5	0.04	-0.57	0.04	-0.50
15	0	0	0.04	-0.01	0.04	-0.01
	0.5	0	0.61	-0.04	0.56	-0.05
	-0.5	0	-0.46	-0.05	-0.41	-0.05
	0	0.5	0.02	0.54	0.03	0.47
	0	-0.5	0.04	-0.53	0.04	-0.47

Some systematic trends in the results are evident from the table: (a) dif = output - input for C is always positive, with $\langle dif \rangle_x = 0.05$, (b) $\langle dif \rangle_y = 0.02$ for dPF = 12, = -0.02 for dPF = 15, (c) outputs based on measures from the actual image peaks are, overall, somewhat closer to the input values. The reasons for these trends are not understood, but may be a function of the "stretch" given to bring out the pad features.

A look at the uncertainties in the measures shows that, in most cases, output = input. Given that the uncertainty in each measured r is +/- 0.3 pix, the uncertainty in each dr is approximately +/- 0.6 pix, and from (13) the uncertainties in C_x and C_y are about +/- 0.06. In rms terms this translates to an uncertainty of about +/- 0.007 or $\lambda/140$.

The fact that measures of r' from the actual image peak gives good measures of the coma coefficients is very important because these are the only measures which can be obtained on real images. For model images the center in the absence of coma is known; for real images it is unknown. The results above demonstrate clearly, I believe, that the algorithm given by (13) will work when applied to the actual image peak for images with coma but no astigmatism.

ASTIGMATISM EQUATIONS FOR ZERO COMA

If coma is zero, then again only the radial equations are needed to find the astigmatism coefficients. With dr in pixels, the inverted equations are

$$A_x = 0.126\ dr_1 = -0.137(dr_2 + dr_3), \quad A_y = -0.071(dr_2 - dr_3) \ . \quad (14)$$

To get rms in Zernike terms, multiply the A's by 0.43.

This algorithm has been applied to model images and gives satisfactory results. Given the same uncertainty in dr from above, the uncertainty in each A is about +/- 0.08, or +/- 0.034 or $\lambda/30$ in rms terms. This is significantly larger than in the case of coma, and indicates that the extraction of astigmatism coefficients using (14) is much less practical than finding coma coefficients using (13), especially for aberrations at a low level. For a tilted/decentered SM the coma generally dominates the astigmatism for random choices of tilt and center, hence the assumption that (13) is applicable, while (14) is not, is warranted.

GENERAL EQUATIONS

If both coma and astigmatism are present in an image, both the radial and angular changes must be measured and the full set of inverted equations must be used. This has been done and applied to model images with satisfactory results. However, the application to real images is not practical because the image center in the absence of coma is required in this case, and is not known apriori. This center is needed in order to find the $d\Theta$, values of which are quite sensitive to the location of the chosen image peak.

MEASURES ON FOC IMAGES

Chris Burrows and Dan Schroeder have independent measures of pad radii on one common FOC image taken on Day 033 (see $\langle r \rangle$ results above). Here I give the full set of measurements and the calculated coma results assuming the astigmatism is zero. It is worth noting that different display software was used to measure r'. CB has also measured a Day 084 FOC image taken at the Day 066 SM position, and these results are also shown.

Person	pad	r'	r	dr	C_x	C_y
CB D033	1	54.1	59.4	-5.3	-0.22	-0.50
	2	60.0	59.4	0.6		-0.47
	3	64.9	60.3	4.6		
	$\langle r \rangle$ = 59.7					
DS D033	1	55.5	60.4	-4.9	-0.09	-0.47
	2	62.0	60.4	1.6		-0.45
	3	64.6	61.3	3.3		
	$\langle r \rangle$ = 60.7					
CB D084	1	57.4	54.1	3.3	0.84	0.31
	2	60.1	54.1	6.0		0.30
	3	45.7	55.0	-9.3		
	$\langle r \rangle$ = 54.4					

The results for the D033 image are in good agreement in y, but less so in x. What is noteworthy is the difference between the D084 image and the D033 images - the coma on both axes has changed signs with the total coma in the D084 image, taken at the Day 066 SM position, significantly larger. These results show clearly that a zero-coma position is located at an SM position between that of the above images, and closer to the D033 position.

CONCLUSIONS

The pads on the OTA pupil provide a convenient benchmark for (1) the distance of the image plane from paraxial focus and (2) the amount of coma in the image due to SM tilt/decenter. Measures of the former provide the data for monitoring desorption of the OTA structure, while measures of the latter will help in the alignment of the SM to the PM.

Dan Schroeder
7 August 1991

DRAFT by T. Facey 90.9.1

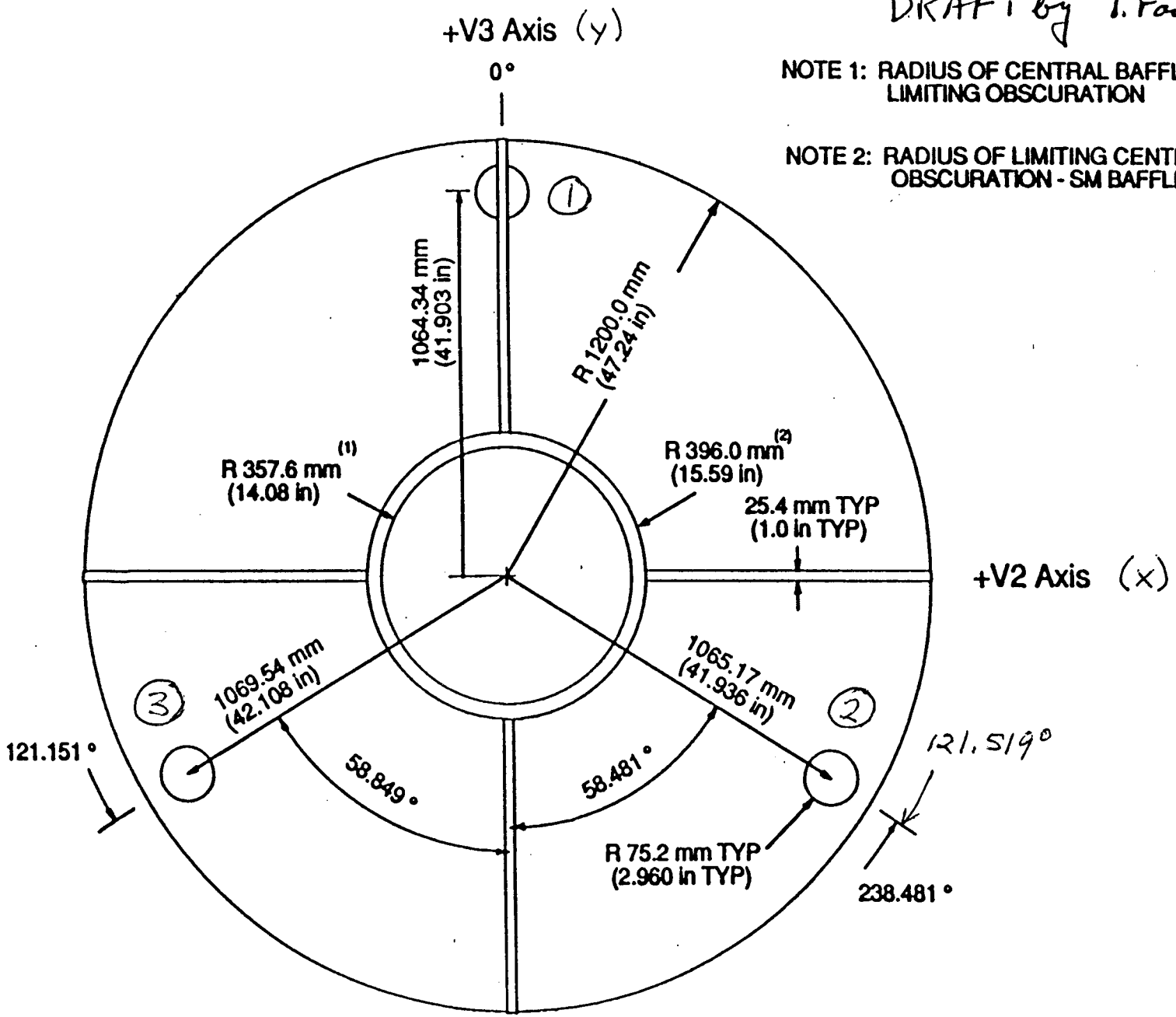

LOCATION AND SIZE OF FEATURES IN OTA ENTRANCE PUPIL

Fig. 1

[mackie.foc]f486n_d033_sum12_gcf

Fig. 2

FOC foc=+10 Day 033 sum 1,2

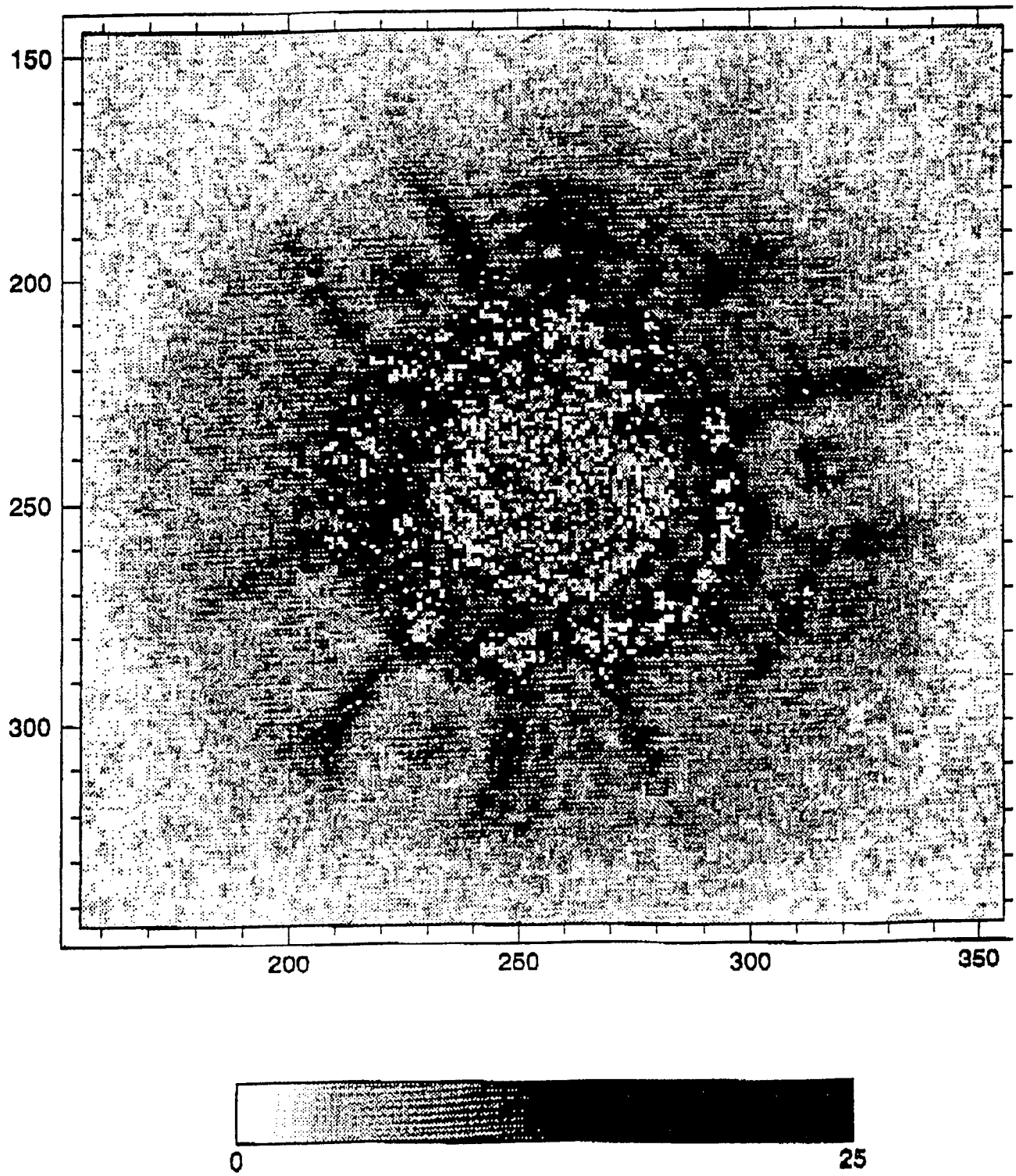

Fig. 3

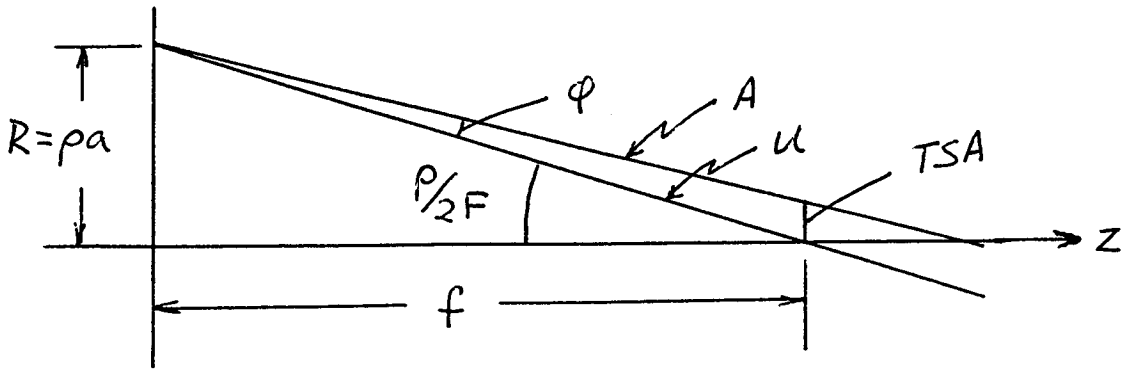

A = aberrated ray
u = unaberrated ray

$\varphi << \frac{\rho}{2F}$